CRANFIELD UNIVERSITY

EDWARD CARNELL

REGIONAL AND NATIONAL SCALE CALIBRATIONS OF HYPERSPECTRAL GAMMA-RAY SIGNALS FOR SOIL MONITORING

SCHOOL OF APPLIED SCIENCES

MSc THESIS
Academic Year: 2012 - 2013

Supervisors: Dr. R. Corstanje and Dr. T. Mayr
July 2013

CRANFIELD UNIVERSITY

SCHOOL OF APPLIED SCIENCES

MSc THESIS

Academic Year 2012 - 2013

EDWARD CARNELL

REGIONAL AND NATIONAL SCALE CALIBRATIONS OF HYPERSPECTRAL GAMMA-RAY SIGNALS FOR SOIL MONITORING

Supervisors: Dr. R. Corstanje and Dr. T. Mayr

July 2013

Abstract

There is an increasing demand for accurate, timely soil information to ensure the sustainable management of our limited land resources. This information is crucial for effective environmental modelling, essential for adapting to climatic changes and ensuring global food security. Traditionally, soil information has been attained through conventional soil sampling and laboratory analyses, which are time consuming and expensive. Consequently, soil maps typically lack the fine-scale spatial and temporal resolution required for computer simulations, soil monitoring and land management. Increasingly, this fine-scale information is being attained through the use of proximal and remote sensors, which generally rely on indirect, surrogate indicators of soil variability, such as electrical conductivity. In this study, the potential of γ-ray spectroscopy as a soil-monitoring tool is assessed. The underlying principle of γ-ray spectroscopy is that long-lived terrestrial radionuclides act as environmental tracers, reflecting changes in the mineralogical and textural composition of soil. Airborne radiometric surveys proved to be valuable tools for geological mapping and have led to the development of ground-based (proximal) sensors for soil sensing. A recent study by Viscarra Rossel *et al.* (2007) demonstrated that robust predictions of topsoil characteristics could be made through multivariate calibrations of proximal γ-ray signals, at the within-field scale. Adopting this chemometric approach, this study assesses whether similar predictions could be made at coarser scales, using a laboratory-based spectrum analyser. The results show that at a regional scale, fair predictions of cation-exchange capacity (CEC) can be made, despite changes in parent material, land use and topography. However, more tenuous results were found at the national scale, which suggests that local relationships between γ-ray activity and soil properties (such as soil texture) may not necessarily hold at coarse scales. The findings indicate that radiometric baselines vary between soil types and host geologies, which subsequently mask localised variations in physical and chemical soil properties.

Keywords: γ-ray spectroscopy; proximal soil sensing; partial least squares regression; airborne radiometrics.

Acknowledgements

Firstly, I would like to thank my supervisors Dr. Ron Corstanje and Dr. Thomas Mayr for their continuous support and diligent supervision throughout this study. I greatly appreciate the time they invested in me and the expertise they passed on. I would also like to thank Prof. Guy Kirk for his helpful advice and guidance during my time at Cranfield. I would also like thank Richard Andrews for assembling the γ-ray spectrum analyser and helping with its calibration. Lastly, I am incredibly thankful to The Douglas Bomford Trust and The Felix Cobbold Trust for funding this piece of research, without their financial support this study would have not been possible.

Table of Contents

List of Figures

List of Tables

Chapter 3 – Regional Scale Determination of CEC

Chapter 4 - National Scale Calibrations of γ-ray signals for England and Wales

Appendices

List of Equations

Notation and Acronyms.

Notation

$\lvert e_i \rvert$	Absolute residual
adj γ_i	Adjusted γ-ray counts for the ith channel to account for variations in mass between samples
$\overline{m}$	Average sample mass
${}^{bg}\gamma_i$	Background sensor response for the ith channel, where background refers to the absence of a soil sample
γ	Gamma
γ_i	Gamma-ray counts for the ith channel
d	Line gradient
X	Matrix of independent variables
T	Matrix of latent variables of X
U	Matrix of latent variables of Y
W	Matrix of PLSR loading weights
P	Matrix of PLSR loadings of X
Q	Matrix of PLSR loadings of Y
B	Matrix of regression parameters
$\bar{y}$	Mean of Y
a	Number of latent variables
n	Number of samples
k	Polynomial degree of Savitzky-Golay filter.
e_i	Residual
e	Residual information in PLSR model of X

f	Residual information in PLSR model of Y
m	Sample mass
F	Savitzky-Golay filter width
α	Smoothing parameter of Loess
$\sigma_{y_{i-n}}$	Standard deviation of Y
$\sum$	Sum of
y_i	The ith observed value
$\widehat{y_i}$	The ith predicted value
γ_{TC}	Total gamma-ray counts
$\mathbf{Y}$	Vector of dependent variables
c	y-intercept, constant

Acronyms

ANOVA	Analysis of variation
CEC	Cation-exchange capacity
CV	Cross-validation
DWT	Discrete wavelet transform
EC	European Commission
EC_a	Apparent electrical conductivity
FSA	Full spectrum analysis
ICP	Inductively Coupled Plasma Emission Spectrometry
KeV	Kiloelectronvolt
Loess	Local regression using weighted linear least squares and a 2nd degree polynomial model
LOOCV	Leave-one-out cross-validation
LV	Latent variable
ME	Mean error
MLR	Multi-linear regression

NF	Number of PLSR factors
NIR	Near infrared (700 – 2500nm)
NSI	National soil inventory
OM	Organic matter
PC	Principle component
PCA	Principle component analysis
PCR	Principle component regression
PLS1	Partial least squares algorithm for one dependent variable
PLSR	Partial least squares regression
R^2	The coefficient of determination
RMSE	Root mean-squared error
RMSECV	Cross-validated root mean-squared error
ROI	Regions of interest
RPD	The ratio of performance to deviation
SD	Standard deviation
SDE	Standard deviation of error
SURE	Steins unbiased risk estimate
TC	Total Counts
Thresh	Wavelet threshold value
UN	United Nations
VNIR	Visible-near infrared (~400-2,500nm)

Units of measurement

"	Inch
Bq	Becquerel (SI unit of radioactivity)
cm	Centimetre
$cmol_c$	Centimole of charge
g	Gram
ha	Hectare
kg	Kilogram
km	Kilometre

l	Litre
m	Metre
M	Molar
mg	Milligram
min	Minute
ml	Millilitre
mm	Millimetre
nm	Nanometre
µm	Micrometre
s	Second

Chemical symbols.

Al	Aluminium
Bi	Bismuth
Ca	Calcium
$CaCO_3$	Calcium carbonate
Cs	Caesium
Fe	Iron
Ge	Germanium
K	Potassium
KCl	Potassium Chloride
Mg	Magnesium
NaI	Sodium Iodide
OC	Organic carbon
P	Phosphorus
$P_{ext.}$	Extractable Phosphorus
$P_{tot.}$	Total Phosphorus
Si	Silicon
Th	Thorium
Tl	Thallium
U	Uranium

Chapter 1 - Introduction

Over the past five decades the world's population has escalated from three billion to over seven billion; during this period, the amount agricultural land has not increased accordingly; rather it has only increased by approximately 9 % (Pretty, 2008; Godfray *et al.,* 2010)**.** This trend is set to continue, with the global population expected to exceed 9 billion by 2050 (UN, 2009) and the amount of arable land per capita set to further decline from about 0.23 ha in 2000 to about 0.15 ha in 2050 (Lal, 1991). Thus to meet the global food demand it is imperative that agricultural productivity is intensified, whilst simultaneously conserving the land for future generations. It is also widely accepted that during this period, global temperatures will also increase, further exacerbating the pressures placed on this limited resource. In order to effectively manage this base resource, modern technologies are required to provide information that will enable better management of site-variability, improve crop yields and optimise the use of finite resources such as water and fertilizers.

During the latter half of the 20th century, economic pressures led to the mechanisation and intensification of agriculture, generating larger fields, which were managed uniformly and without consideration for spatial variation (Stafford, 2000). The view that agricultural land can be treated as a homogenous resource at the 'within-field scale' has been questioned in recent years (Larson and Robert, 1991), leading to the development of precision agriculture. Precision agriculture offers an approach of using information technology to automate site-specific crop management. To be effective, precision agriculture relies on up-to-date, accurate and fine-scale soil information which is currently time consuming and costly to obtain through conventional laboratory analyses. Consequently, quantifying soil variation at the within-field scale required has been impractical and remains one of the biggest restrictions to the adoption of precision agriculture (Sudduth *et al.,* 2010; Adamchuck *et al.,* 2004).

To manage agricultural land effectively, it is essential that mobile sensor systems are developed to map the spatial variability of soil. Apparent electrical conductivity

(EC_a) sensors are at present the only sensors commonly used in agriculture and deliver an indirect measurement of soil variability, by measuring its ability to conduct or resist electrical charge. EC_a sensors provide useful information about within-field soil variability, but cannot be used to make quantitative predictions of specific soil characteristics, since several factors contribute to the EC_a sensor's response. Optical and radiometric sensors potentially offer an alternative, as their spectroscopic response can simultaneously characterise various soil characteristics and provide an affordable and rapid alternative to conventional laboratory analyses (Viscarra Rossel *et al.,* 2006). Proximal gamma (γ)-ray sensors remain in their relative infancy, despite showing promise as a means of predicting within-field variability of soil texture, cation-exchange capacity (CEC) and organic matter (OM) (e.g. Taylor *et al.,* 2010; Viscarra Rossel *et al.,* 2007; Martz and de Jong, 1990). They also have the advantage of other sensor systems, in that they are able to capture information about the soil at depth, with minimal interference from vegetation. With recent advancements in data-processing techniques and instrumentation, this study aims to establish whether γ-ray calibrations can be made for areas greater than the within-field scale and determine which properties are best characterised by γ-ray signal

Chapter 2 - Literature Review & Background

This review introduces the fundamental concepts of soil sensing and in particular describes the development of γ-ray spectroscopy as a surrogate indicator of soil variation. Section 2.1 summarises current soil sensing techniques and introduces the principles of γ-ray spectroscopy in soil sensing. An introduction to the theory of γ-ray spectroscopy is then presented (section 2.2) and is followed by an overview of its application and development in soil monitoring (section 2.3). Section 2.4 provides an executive summary of the statistical methods employed to predict soil characteristics from γ-ray signals, with an introduction to partial least squares regression. A comprehensive comparison between available γ-ray sensors is then given and demonstrates the differences between γ-ray measurements acquired in situ and in the laboratory. The final section of the review (section 2.6) summarises how γ-ray sensors may provide a useful indication of soil status at scales exceeding the 'within-field' scale previously tested and how this study aims to assess this hypothesis.

2.1 Overview of soil sensors

Numerous attempts have been made to develop on-the-go soil sensors, however, the majority of commercially available sensors do not map soil properties directly; rather, they measure indirect responses, such as EC_a (Adamchuk *et al.,* 2004, Taylor J.A. *et al.,* 2010). EC_a sensors are increasingly being used in agriculture, under the assumption that an alteration in a soil's EC_a will correspond to a change in its physical or chemical make-up. The EC_a of soil varies depending on soil texture and the amount of moisture held by soil particles. Conductivity tends to increase as soil becomes heavier in texture (more clay-rich). However, changes in volumetric soil water content and soil salinity also affect EC_a measurements and subsequently this relationship is frequently masked by other factors. In addition, the comparison between sites is difficult, as changes in temperature, humidity and atmospheric electricity also influence EC_a, (Sudduth *et al.,* 2010).

Whilst EC_a sensors are capable of highlighting soil variation within a field, the single sensor response is the result of a culmination of effects and therefore is not necessarily indicative of the variation of a single soil characteristic. Optical and radiometric sensors (e.g. V-NIR, γ-ray) potentially provide a viable alternative to EC_a sensors, with components of their multivariate response being linked to particular aspects of the soil's make-up. Optical and radiometric sensors measure the amount of energy reflected or emitted from a soil surface, over a specific spectral range. These sensors are similarly affected by a combination of factors; however, their response at a certain part of the spectrum can be representative of a particular soil characteristic. Hyperspectral visible and near infrared (V-NIR) sensors are widely reported as being reliable indicators of organic matter (OM) content, amongst others properties (e.g. Shonk *et al.,* 1991; Viscarra Rossel *et al.,* 2006). As with EC_a sensors, V-NIR and NIR sensors are active, meaning they contain both a source and a detector; a light source illuminates the soil and their response in the V-NIR/NIR portion of the spectrum is recorded. Measurements of V-NIR and NIR are influenced by soil geometry and the position and angle of the light source, which means the acquisition of reliable measurements in situ is problematic. To address this limitation, soil has to be de-vegetated and the surface smoothed prior to measurement (Mouazen *et al.,* 2005).

Gamma (γ)-ray spectrometers are radiometric sensors, which have received widespread interest among soil scientists in recent years (e.g. Viscarra Rossel *et al.,* 2007; Loonstra and Van Egmond, 2009), as they can be considered a direct measurement of the mineralogical and textural composition of soil, offering the potential to rapidly and cost-effectively characterise the variation of soil properties (Petersen *et al.,* 2012). Unlike EC_a and infrared sensors, γ-ray sensors are passive, detecting γ-ray radiation emitted from the natural decay of radioactive isotopes in the upper layers of a soil profile. Early applications of γ-ray spectroscopy came from Uranium prospecting and have since extended to geological mapping, mineral deposit detection and in recent years soil mapping (Wilford and Minty, 2007). Recent advancements in data-processing techniques and instrumentation have allowed soil scientists to demonstrate the potential of γ-ray spectroscopy to

quantitatively predict certain soil characteristics (e.g. Van Egmond *et al.,* 2010; Petersen *et al.,* 2012). To date, γ-ray spectroscopy has proven to be a successful indicator of soil texture, Fe, Mg, OM, CEC and plant available P at the within-field scale (e.g. Pracilio *et al.,* 2006; Van Egmond *et al.,* 2008; Viscarra Rossel *et al.,* 2007; Petersen *et al.,* 2012).

2.2 Gamma-ray spectroscopy

Radioactivity is an unaided, spontaneous, reaction of an atom, which transforms the parent nucleus into a daughter product, releasing radiation in the form of alpha (α), beta (β) and gamma (γ) rays (Ward, 1981; IAEA, 2003; Hyvönen *et al.,* 2005). γ -rays comprise part of the decay processes of α and β radiation and are not an independent form of radiation. Unlike α and β radiation however, γ-rays do not carry charge or mass, making them energetic, penetrating and allowing for detection by airborne sensors (Minty, 1997).

Natural radioactivity is ubiquitous in soils, due to the decay of terrestrial radionuclides, synthesised during the creation of the solar system and occurring in the mineral phase of soils or adsorbed onto soil components (Martz and de Jong, 1990; Navas *et al.,* 2002; Vukašinović *et al.,* 2010). Terrestrial radionuclides originate from Earth's liquid outer core, and were transported by liquid magma, during volcanic eruptions, to form igneous rock and subsequently created Earth's crust. Igneous rock accounts for 95% of the Earth's crust and is a major constituent of all soil types (Loonstra and Van Egmond, 2009).

Radioactive decay can be described as a statistical process, in which the number of atoms to disintegrate per unit of time is proportional to atoms present. The decay of a radionuclide is described by its half-life, which is the period of time it takes for a radioactive isotope to decay to half its size. Half-lives vary in time from a millionth of a second to billions of years. The radioisotopes of Potassium (^{40}K) and the decay series of Thorium (^{232}Th and its daughters) and Uranium (^{238}U, ^{235}U and its daughters), are of particular interest to soil scientists as their half-lives are in the order of hundreds of millions of years, are sufficiently abundant in the

environment and are of the intensity to be measured by γ-ray spectroscopy (IAEA, 2003; Anjos *et al.,* 2004).

In addition to naturally occurring radioisotopes, anthropogenic sources of γ-radiation exist in the environment. ^{137}Cs was introduced into the global environment in the 1950s and 60s as a result of nuclear weapons tests and in higher concentrations in Europe and W. Russia following the Chernobyl disaster of 1986. Once ^{137}Cs enters the environment, it becomes fixed to soil colloids and is essentially non-exchangeable in most soils. As ^{137}Cs is largely immobile, it can be a good indication of soil erosional and depositional processes, through its emission of γ-rays at 662 kiloelectronvolts (KeV) (Ritchie and McHenry, 1990).

γ -ray spectrometers typically measure information in the energy range 400 to 3,000 KeV, over 256 or 512 channels. ^{40}K is the only radioisotope of K and decays in one step to ^{40}Ar emitting γ-rays. The decay of the radioactive forms of Th and U do not emit γ-rays directly, but contribute to the γ-ray spectrum through their energetic, γ-emitting daughter products ^{214}Bi and ^{208}Tl respectively (Minty, 1997; Hyvönen *et al.,* 2005). In soil science, the value of γ-ray spectrometry lies principally in the fact that different rock types contain varying amounts of these radioisotopes, as do the soil profiles to which they weather (Viscarra Rossel *et al.,* 2007). Major hosts of K are potassic feldspars and micas, which, when weathered, release K and may produce clay minerals such as illite. Under favourable conditions, K may also be adsorbed in smaller quantities to other clay minerals such as mortmorillonite. Due to similar electron properties, U and Th share many of the same host minerals, such as monazite, xenotime and zircon. The weathering of these minerals often leads to their adsorption to clay colloids and iron oxides (Dickson & Scott, 1997; Hyvönen *et al.,* 2005). This association between radioactive elements and clay minerals has proved to be very useful in the mapping of topsoil clay content and associated characteristics such as CEC (Loonstra, 2010; Taylor *et al.,* 2010).

2.3 Airborne radiometric surveys

The decay of K, Th and U, produce energetic and penetrating gamma-rays capable of penetrating up to 35 cm of rock and several hundreds of metres of air, which allows airborne spectrometers to measure their abundance in the environment. Airborne gamma-radiometric surveys are typically conducted <120 m above ground (Bierwirth *et al.,* 1996a) and use a scintillation detector to measure the degree of γ-rays produced and the energy of each photon. This information can then be processed to determine the source of the isotope based on the energy of the γ-ray photon and its concentration from the number of photons measured. This information is then typically used to produce ternary images of the distribution of K, Th and U, providing a valuable spatial representation of the geochemistry of the upper rock/soil layer. As radioisotopes behave differently during weathering and pedogenesis, depending on their size, weight and valency, the radiometric signal acts as an environmental covariate, indicative of parent material, mineralogy and textural composition. K is a useful indicator for soil mapping, due to its relative solubility during weathering compared to Th and U. The ratio of Th:K has proven to be a useful indication of weathering and soil texture (e.g. Carrier *et al.,* 2006; Bierwirth *et al.,* 1996a).

Airborne radiometric surveys have the potential to assess large areas rapidly (typically 50 m s^{-1}, IAEA, 2003) and in contrast to other remote sensors such as Landsat, interference by vegetation masking is negligible, as γ-ray signals originate from the soil itself (Wilford, 2002). γ-ray spectrometers are therefore suitable for mapping vegetated agricultural and forested areas. With the potential of γ-ray spectroscopy realised through airborne radiometric surveys, ground-based (proximal) γ-ray sensors were developed in the 1990s (Petersen *et al.,* 2012). These proximal γ-ray sensors have a smaller 'footprint' than airborne sensors, making them suitable for precision agriculture as they can detect variations in γ-ray activity within a field. They also are less prone to effects of surface cover and geometry than airborne sensors (Viscarra Rossel *et al.,* 2011).

2.4 Fingerprinting soil characteristics

The comparison between γ-ray spectral signatures and observed soil properties, through statistical analysis is referred to as fingerprinting. The aim of fingerprinting is to model the behaviour between independent variables '**X**' (γ-ray spectra) and a dependent variable '**Y**' (soil characteristic).

There are three main approaches to fingerprinting soil characteristics: the first two approaches use multiple linear regression (MLR) to establish a relationship between **X** and **Y**. In order to do this, the dimensionality of the **X** (γ-ray spectra) needs to be reduced, as MLR requires the number of dependent variables to be less than the number of observations (samples). As most spectrometers measure γ-ray intensities over 256 to 1,024 channels, estimates of γ-ray activity attributed to the decay of K, Th and U need to be established prior to modelling.

The Windows method is the most commonly applied technique to assess the γ-ray activity of K, Th and U. Estimates are made by summing the intensities of three broad regions of interest (ROI) in the spectrum, associated to terrestrial radionuclide activity. Whilst many authors (e.g. Taylor *et al.,* 2002; Petersen *et al.,* 2012) have observed relationships between soil properties and these ROIs, it has been suggested that relevant spectral information is lost by estimating radionuclide activity in this manner (e.g. Mahmood *et al.,* 2011). Consequently, a growing number of studies (e.g. Van Egmond *et al.,* 2008; Mahmood *et al.,* 2011) use a method proposed by Hendriks *et al.* (2001) called Full Spectrum Analysis (FSA); FSA estimates radionuclide activity based on the comparison between an observed γ-ray spectrum and the pure response of the detector system used on a 1 Bq kg^{-1} source of a given radionuclide. Hendriks *et al.* (2001) shows that by utilising more of the spectra, the uncertainty of the estimations is at least a factor of 1.7 lower than the Windows method.

These approximations of radionuclide activity are then used to form a regression of **X** with **Y** that can be expressed by:

$$\mathbf{Y} = \mathbf{XB} + \text{residuals} \qquad \textbf{[Eq. 1]}$$

Where: **Y** is is a $n\times1$ column vector of the dependent variable, $\boldsymbol{X}$ is an $n\times p$ matrix of the estimated γ-ray activity, **B** is a $nx1$ column vector of regression parameters and residuals are the differences between measured and predicted data. MLR however, depends on certain criteria to be effective: the estimates of K, U and Th cannot be collinear and are assumed to be accurate (free from noise).

Viscarra Rossel *et al.* (2007) suggest that these traditional, largely univariate fingerprinting techniques provide an inadequate description of the complex interactions, which give rise to the γ-ray spectrum of a soil profile. They therefore propose a third approach to fingerprinting, which addresses these matters by employing partial least squares regression (PLSR); PLSR was developed to deal with cases of multiple regression that have few observations and are capable of dealing with noisy, highly collinear and numerous **X**-variables (Wold *et al.,* 2001). Unlike the first two methods, the γ-ray activity associated with the decay of K, Th and U is not estimated; rather PLSR is used to find components that capture most of the variation in the γ-ray signal, and which are also useful in predicting **Y**. The following section provides an introduction to the theory of PLSR.

2.4.1 An Introduction to Partial Least Squares Regression

Partial least squares regression (PLSR) is a bilinear regression process developed by Wold *et al.* (1983). Unlike MLR the goal of PLSR is to predict **Y** from **X**, by finding their common structure. PLSR operates in a similar manner to principle component regression (PCR) in that the latent structure of **X** is used to make predictions of **Y**. Both PCR and PLSR minimise the number of independent components of **X**, through the use of latent variables (LVs). In PCR these LVs are selected in order to explain as much of the variation in **X**. However, as some of these LVs of **X**, may not be relevant to explaining the variation of **Y**, PLSR utilises both **X** and **Y** into the calculation of the LVs, in order to optimise the covariance between the LVs and **Y**. It achieves this by modifying the direction of each LV, so that the covariance between it and the **Y** vector is maximised. The general form of PLSR can be expressed by:

$$\mathbf{X} = \mathbf{T}\mathbf{P}^T + e$$

$$\mathbf{Y} = \mathbf{U}\mathbf{Q}^{T} + \boldsymbol{f} \qquad \textbf{[Eq. 2]}$$

Where: **X** and **Y** have the same meaning as Eq. 1; **T** and **U** are matrices of $n \times a$ latent variables (scores), where $a \leq n$; **P** and **Q** are matrices (of size $n \times p$ and $n \times 1$ respectively) of coefficients that relate **T** to the predictor and predicted variables respectively (loadings) and e and f represent the residual information remaining after a LVs. The **B** coefficients for the general MLR model (Eq. 1), can then be computed using **P** and **Q** from Equation 2 and **W**, which is an $n \times a$ matrix of PLSR weights:

$$\mathbf{B} = \mathbf{W}(\mathbf{P}^{T}\mathbf{W})^{-1}\mathbf{Q}^{T} \qquad \textbf{[Eq. 3]}$$

The assessment of how many LVs to include (a) is critical to model construction, as too many LVs can result in 'over-fitting'. Over-fitting refers to an excessive number of LVs, which can lead to a perfect association between **X** and **Y** but will fail to predict on new data. To prevent over-fitting, PLS models are commonly subjected to cross-validation (CV), such as leave-one–out CV (LOOCV). A model that is verified by LOOCV is run n times using $n - 1$ samples, leaving out each sample in turn. The PLS model is then used to predict the left-out sample. The squared residuals of the independent predictions are then typically accumulated, in order to calculate the root mean-squared error of prediction (e.g. Viscarra Rossel *et al.,* 2007), expressed by:

$$\textbf{RMSECV} = \sqrt{\frac{\sum_{i=1}^{n}(\hat{y}_i - y_i)^2}{n}} \qquad \textbf{[Eq. 4]}$$

Where: y_i is the observed (laboratory analysed) value of sample i and $\hat{y}_i$ is the predicted 'left out' value. The number of LVs is then selected by the model, which produces the lowest RMSECV. The model can then be subsequently used to predict from new spectra, either to predict unknown **Y** values or verify model performance.

Another important stage of PLSR analysis is interpreting the importance each **X**-variable (γ-ray energy channel) has in the prediction of **Y**; this is done by plotting **P**

(**X** loadings). Loading plots show the contribution each energy channel has in the prediction of **Y**, positive loadings signify a positive correlation to **Y** and equally negative loadings, a negative correlation. Loading plots can also be a useful diagnostic tool to verify the correct number of LVs is selected; when over-fitting occurs, the loading plots will typically resemble random noise and be of higher frequency than the original spectra. Figure 1 illustrates the difference between clear, noise free loading weights (factor #1) and a factor (#2) containing a high degree of noise.

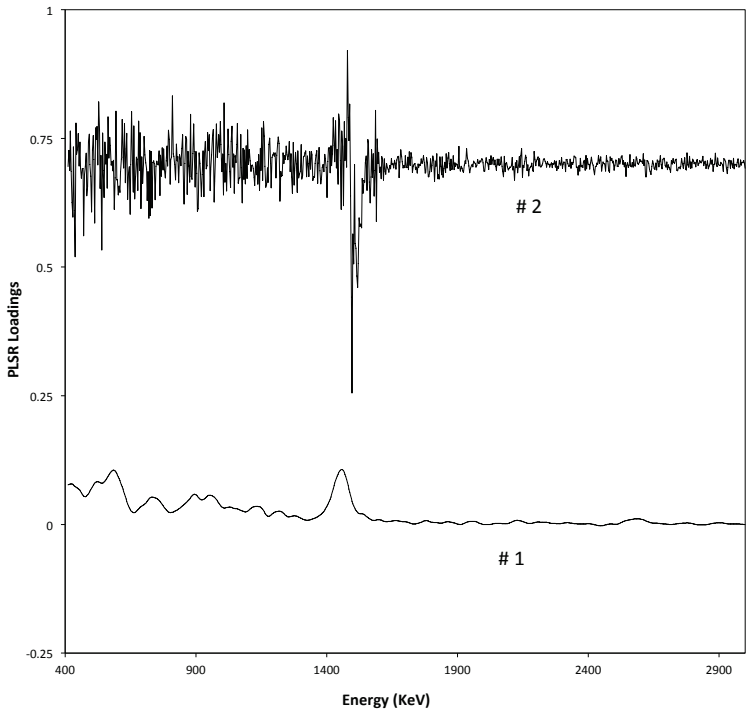

Figure 1 – Example PLSR loading weights plot (offset for clarity). Factor #1 shows an example of a noise free PLSR loading weight and factor #2 contains a high degree of noise, indicative of over-fitting.

PLSR has been used in a number of soil sensing applications using VNIR sensors (Viscarra Rossel *et al.,* 2006), but remains in its relative infancy for γ-ray studies, having only been applied to assess soil at the field level (Viscarra Rossel *et al.,* 2007, Van Egmond *et al.,* 2010). Initial applications of PLSR have shown promising results: Van Egmond *et al.* (2010) compared PLSR with the FSA method and found it outperformed FSA (based on higher R^2 values), in addition to removing the

reliance on standard spectrum responses required for FSA. They note however, that PLSR appears to be less 'automated' than the previous methods, requiring significant amounts of pre-processing to uncover the relationships to soil properties (e.g. Viscarra Rossel *et al.,* 2007; Van Egmond *et al.,* 2010).

2.5 Choice of sensor

Laboratory based spectrum analysers are capable of acquiring γ-ray responses for spatially detached soils, providing a spectra comparable to those measured by in-situ sensors (Petersen *et al.,* 2012), but eliminating environmental 'noise', which can make the comparison of sites challenging. As far as the author is aware fingerprinting of soil characteristics through γ-ray spectroscopy has only previously been performed using in-situ proximal and remote sensors. Proximal sensors such as the 'Mole' (Soil Company, Groningen, the Netherlands) are typically attached to a quad-bike or tractor, to obtain frequent signals that are representative of a study area. As the spectra are gathered in-situ, environmental conditions such as precipitation, water content and background noise can influence the signal response and thus the quality of predictions (Loonstra and Egmond, 2009). The water content of a soil also has a bearing on the γ-ray response, as increased water content can result in the attenuation of γ-rays; Hendriks (2002 cited by Loonstra and Van Egmond, 2009) estimated this loss to be as high as 16 % between a dry and saturated sandy soil, using a Monte Carlo simulation. The fluctuation of Radon gas (a daughter product of ^{238}U) with precipitation, may also contribute to the spectral noise for in-situ measurements (Horng and Jiang, 2004; Loonstra and Van Egmond, 2009). Typically lab based spectrum analysers are lead-shielded to minimise background noise and produce a signal that is characteristic of the soil of interest.

Laboratory based γ-ray sensors typically have spectral resolutions finer than those of portable γ-ray spectrometers or airborne surveys. The RT-50 laboratory spectrum analyser (Georadis, Czech Republic) for example, measures the γ-ray spectrum over 1,024 channels in comparison to in-situ sensors such as the 256 channel GR320 (Exploranium Radiation Detection Systems, Toronto, Canada) or

the Soil Company's 512 channel detector, 'The Mole' (The Soil Company, Groningen). A spectrometer with a high spectral resolution (such as the RT-50) is more adept at differentiating between spectral peaks of a similar energy. The channel width of the RT-50 is <3 KeV, while the GR320 used by Viscarra Rossel *et al.* (2007), has a channel width of 11.7 KeV, which ought to make the differentiation between significant peaks and noise easier to interpret. Petersen *et al.* (2012) compared average responses of a laboratory based germanium (Ge) detector to an in-situ NaI detector in the regions of interest Th, K and U, the results were comparable to one another with R^2s of 0.91, 0.87 and 0.76 respectively. They suggest the lower U correlation may be attributed to low U concentrations in their samples, coupled with an increase in statistical noise. Their results therefore infer that the difference in acquisition methods appears to be minimal, with the responses of a lab-based analyser being similar to an in-situ sensor, under stable environmental conditions.

2.6 Study Aims

γ-ray signals have shown to correlate with certain soil properties at the within-field scale (e.g. Loonstra and Van Egmond, 2009; Viscarra Rossel *et al.,* 2007), however few studies have looked at whether these relationships hold at coarser scales. As far as the author is aware fingerprinting of soils through chemometric analyses has only been achieved at the within field to farm scale. If γ-ray spectroscopy is to become widely adopted and commercially available, models need to be extended beyond the current site-specific calibrations.

This study therefore aims to establish whether γ-ray signals can be an effective indicator of soil status at scales exceeding those already tested. Using a similar approach to Viscarra Rossel *et al.* (2007), calibrations of full, laboratory-acquired γ-ray signals will be made, in order to assess whether γ-ray sensors are an effective tool for soil monitoring at the region and national scale. As the γ-ray responses are to be measured in the laboratory, environmental influences on the γ-ray signal will be eliminated, thus enabling cross-site predictions to be made. In

order to establish at what scale γ-ray spectroscopy stops being effective, two separate studies will be made at the regional and national scale.

Study hypothesis:

"γ-ray spectroscopy can yield site-independent predictions of soil status, at scales exceeding the farm scale"

2.6.1 Chapter 3 Aims

With the objective of determining whether γ-ray spectroscopy is an effective soil monitoring technique at the regional (Chapter 3) and national (Chapter 4) scale. Chapter 3 therefore explores whether γ-ray spectroscopy can predict an exemplar soil property, cation-exchange capacity (CEC), which is a useful indicator of fertility in agriculture at the national scale. CEC is largely a function of soil texture and OM content, which have been well characterised by γ-ray signals at the within field scale. Petersen *et al.* (2012) also present good site-independent predictions of CEC (using MLR of ROIs), which may suggest that a relationship exists between CEC and γ-ray activity, which extends beyond the field scale. CEC therefore seems to be an appropriate soil characteristic to evaluate the potential of γ-ray spectroscopy to model soil variation, at scales exceeding the within-field scale. In this chapter, PLSR will be used calibrate soil γ-signals, to see if useful predictions of CEC can be made from contrasting parent materials, landuses and landforms.

Chapter aims:

- Determine the full γ-ray spectrometry signals for soil's in North Hertfordshire and South-Mid Bedfordshire
- Apply chemometrics to the soils' γ-ray signals, in order to predict CEC.

2.6.2 Chapter 4 Aims

Chapter 4 explores whether it is possible to characterise soils at a national scale using γ-ray spectroscopy. γ-ray signals will be acquired for a section of the soils in the NSI and PLS applied to establish whether soils can be characterised over differences in land-use, geology and landforms. The National Soils Inventory is a collection of over 5,000 samples, which represents a 5km orthogonal grid of

England and Wales. The NSI dataset also contains a greater proportion of analysed soil properties than those presented in Chapter 3.

Chapter aims:

- Determine the full γ-ray spectrometry signals for an array of soil's in the NSI
- Apply chemometrics to the soils' γ-ray signals, in order to predict soil properties at the national scale.

Chapter 3 - Determination of CEC Through γ-ray Spectroscopy at the Regional Scale.

3.1 Introduction

Cation exchange capacity (CEC) is the measure of a soil's total capacity to hold exchangeable cations, expressed in centimoles per kilogram ($cmol_c\ kg^{-1}$). It is an important property for agriculture, as it serves as an indicator of a soil's ability to supply essential nutrients such as K^+, Ca^{2+} and Mg^{2+}. In addition to it being a useful indicator of fertility, it may also dictate how much fertilizer should be applied to a soil. Soils with a higher CEC tend to be more fertile, as they are capable of retaining larger quantities of cations and act as a reservoir of nutrients. To ensure healthy plant growth, it is therefore imperative that CEC is taken into consideration in the application of fertilizer. Soils with high CEC are capable of adsorbing larger amounts of fertilizer and are less susceptible to leaching than soils with low CEC. Equally soils with low CEC require smaller quantities of fertilizer, which need to be applied more frequently. Factors affecting CEC include soil texture, organic matter (OM) content, pH and the nature of the clay itself.

In general, CEC increases as a soil becomes heavier in texture (more clayey); this relationship exists because clays are aluminosilicate minerals, where the aluminium and silicate ions have been replaced by elements of a lower valance. For example, Al^{3+} may be replaced by Fe^{2+} or Mg^{2+} and subsequently produce a net negative charge. Clays are the most reactive aluminosilicate in soil; clays usually consist of alternating sheets of Si (tetrahedral coordination) and sheets of Al (octahedral coordination). Most commonly, Mg^{2+} will replace Al^{3+} in the octahedral sheets, or else Al^{3+} will replace Si^{4+} to produce the net negative charge (Peveril *et al.,* 1999). The type of clay can also impact CEC; 2:1 clays (such as montmorillonite and vermiculite) contain two tertrahedral sheets per octahedral sheets and normally produce more negative charge than the 1:1 clays (such as Kaolinite).

The OM content of a soil also influences soil CEC; for soils that are low in clay, OM may be responsible for the vast majority of its CEC. OM can also contribute

significantly to the CEC of clayey soils. For example, illitic and cholritic clays have an approximate CEC of 20 $cmol_c\ kg^{-1}$ and a soil that is composed of half of these clays and contains 5 % OM will exhibit a similar CEC (Magdoff and Weil, 2004). In contrast to clays, the source of negative charge from OM is a result of the dissociation of organic acids. The CEC of OM is more pH dependant than clay, with decreases in pH typically corresponding to reduced CEC.

Several attempts have been made to measure CEC in-situ, using proximal sensors. Kweon *et al.* (2013) predicted CEC using the commercially available OpticMapper (Veris Technologies, Salina, KS), which collects measurements in the red (660 nm) and infrared (990 nm) wavelengths and also measures ECa. Their results indicated that good cross-validated MLR predictions ($R^2 \geq 0.86$) could be made in-situ. However, out of the nine fields tested, they were only able to achieve good predictions for six fields. They suggested that soil moisture affected the sensor response, making the comparison between fields very difficult and subsequently meant different combinations of the OpticMapper response had to be used to calibrate each field independently.

In-situ CEC characterisations have been successfully made at the farm-scale by Sudduth and Hummel (1993), using a portable NIR spectrometer. Cross-validated PLSR predictions of CEC produced standard errors as low as 3.59 $cmol_c\ kg^{-1}$. To acquire the NIR signals however, the field surface had to be de-vegetated and modified in order ensure a uniform surface texture.

CEC has also been characterised for agricultural soils in five U.S. states by Lee *et al.* (2009), using a laboratory based VNIR sensor. Their PLS model with leave-ten-out cross-validation had an RMSECV of 3.43 $cmol_c\ kg^{-1}$ and was very strongly correlated to the observed values (R^2 of 0.83). These signals were collected from a laboratory-based sensor however, so the relationship may become masked with moisture content for in-situ applications, as with the findings presented by Kweon *et al.* (2013).

γ-ray spectrometers have also been used to predict CEC in situ, a study by Petersen *et al.* (2012) considered whether γ-ray spectroscopy could be used effectively to

predict CEC from sites of a similar parent material in Middle Europe. Their study used multiple linear regression analysis to estimate CEC based on the ratio of Th and K; the R^2 of all four sites combined was 0.82, demonstrating the potential for regional calibrations. A study by Taylor *et al.* (2010) compared the use of an EC_a sensor (EM88DD, Geonics) to a γ-ray spectrometer (SAIC Exploranium GRS320), for mapping CEC at Stenton farm near Pittenween, Fife, Scotland. They produced a generalised-linear regression model of both the EC_a data and the total counts from the γ-radiometer. Their results showed the γ-ray sensor to outperform the EC_a model in terms of R^2, which were 0.48 and 0.09 respectively. Taylor *et al.* (2010) suggest that whilst the results indicate γ-radiometric data to have some relevance in the mapping and management of CEC, their predictions may be improved through multivariate calibrations, to utilise the full spectra. This chapter aims to establish whether, using the soils' full γ–ray response, it is possible to make predictions at a regional scale. The use of PLSR in previous studies (Van Egmond *et al.,* 2010) has demonstrated that the use of the full γ-ray signal can yield better results than using estimates of K, Th and U. In this study a diverse range of agricultural soils from Northern Hertfordshire and Bedfordshire will be scanned using a laboratory based γ-ray spectrum analyser. PLSR will then be applied to the soils' γ-ray responses, in order to establish whether CEC predictions can be made.

The objective of this chapter is therefore to establish whether regional predictions of CEC can be made and to identify the impact variations in soil type have on these predictions.

3.2 Materials and methods

3.2.1 Study region and sampling scheme

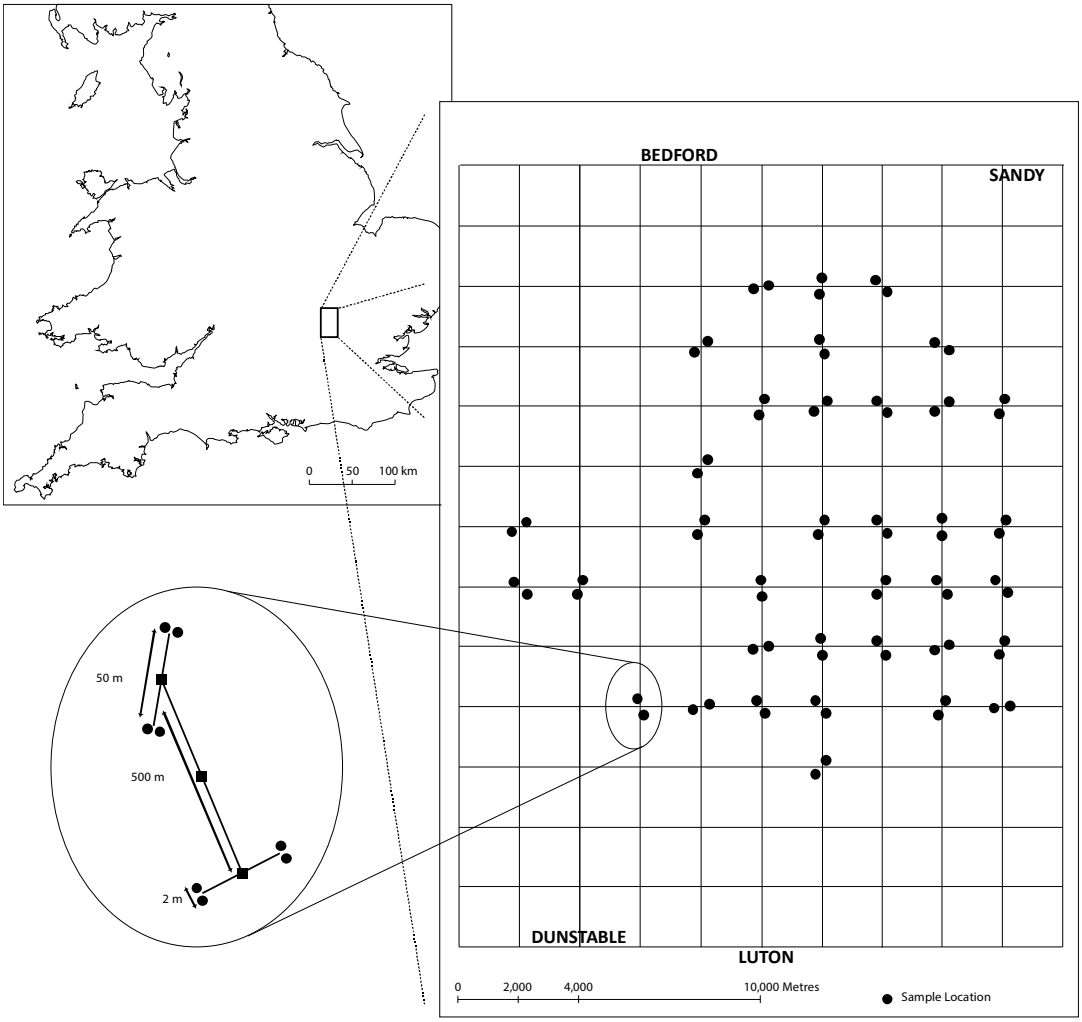

Figure 2 - Nested sampling strategy applied to a 16km x 16km region of North Hertfordshire and Bedfordshire, adapted from Corstanje *et al.* (2008).

The study region lies between the towns of Luton (south) and Bedford (north) in central England. A detailed account of the study region is given by Corstanje *et al.* (2008). The region is approximately 16 km × 16 km, with the majority of soils lying over the Cretaceous formations: Chalk, Gault Clay and Lower Greensand and also contains areas of older Jurassic Oxford Clay to the north. Much of the region is overlain by superficial material, including chalky boulder clay and other glacial drift of variable texture. A balanced nested sampling design (Figure 2; details of

which are found in Corstanje *et al.,* 2008) was used to collect 288 soil samples from 36 main-stations. The main-stations were placed on nodes of a 2,000 m grid, and were selected based on available soil data. The main stations were then subdivided into substations, separated from one another by consecutive vectors of 500 m, 50 m and 2 m (the orientation of which was selected at random). Topsoil samples (depth approximately 0 to 15 cm) were then taken from the last nodes, giving a total of eight samples per main station. The samples were gathered during September to December 2005 and came from sites associated with agricultural land use (predominantly arable but with areas of grassland also) (Corstanje *et al.* 2008).

3.2.2 Sample Preparation

The samples were air-dried and large plant fragments removed prior to being passed through a 0.5 mm sieve. In this study, 276 of the 288 samples collected were used, due to the availability of the samples and corresponding geochemical information.

3.2.3 CEC determination

As described in Corstanje *et al.* (2008), exchangeable Ca, Mg and K ions were extracted from a weighed, air-dried soil sample into 1 M ammonium ethanoate buffer (pH 7.0). This was then displaced with ethanol and the concentrations of the three extracted ions were determined by flame photometry. Ammonium was then extracted from the soil with 1 M KCl, acidified to stop volatilization, and determined by steam distillation and titration. The CEC was then expressed as $cmol_c\ kg^{-1}$.

3.2.4 Measurement of gamma-ray spectra

Soil samples were scanned using an RT-50 lead-shielded laboratory γ-ray spectrometer (Georadis Ltd., 2010), with a 3”× 3” NaI (Sodium Iodide) scintillation detector. The spectrometer records the energy in the range 0 to 3,069+ KeV, over 1024 channels, with cosmic γ-rays (3,066+ KeV) being measured in the last few channels. To ensure the instrument was running under optimal conditions, it was

calibrated with a 9 Bq kg^{-1} reference source of ^{137}Cs twice daily. Calibrations from the ^{137}Cs source were then processed using LabCentre v2.9.8 (Georadis Ltd., 2010) to avoid spectral drift and minimize the impact of external variability such as temperature. A 400 g subsample of the air-dried soil was placed in a Polyethylene container and measured once, over a measurement period of 10 min.

3.2.5 Pre-processing of γ-ray spectra

The spectra acquired from the RT-50 gamma ray analyser contain background information and noise, in addition to the useful analytical information. In order to obtain stable, reliable and robust calibration models, it is necessary to pre-process the spectra prior to chemometric modelling. Pre-processing of the spectra is performed to reduce the irrelevant information contained within the spectra and maximise the signal-to-noise ratio (SNR). In this study a number of pre-processing methods were compared: the Savitzky-Golay filter, loess regression and wavelet-analysis. All pre-processing techniques were carried out in Matlab v7.14 (Mathworks, Massachusetts, 2012).

Savitzky-Golay filter - The Savitzky-Golay filter (Savitzky and Golay, 1964) was applied to smooth the spectra, in order to improve the signal-to-noise ratio. The Savitzky-Golay filter used a moving polynomial fit of a given order (k), across a filter width (F) of (2n+1), where n represents half the width of the smoothing window. The central point of each window was interpolated by the polynomial fit.

Loess Regression - Loess is a nonparametric technique for estimating local regression, proposed by Cleveland (1979). The loess method employs weighted least squares to fit a 2^{nd}-degree polynomial to a subset of the data, in order to estimate each point in the spectra. The weight allocated to each point corresponds to the distance between it and the point that is being estimated, with greater weights being assigned to the points that are proximate. The degree, to which the data is smoothed, is determined by the "smoothing parameter" (α), which is proportional to the data considered in each fit, expressed as a percentage of the total population. When more points are considered (α increases), the spectra

become smoother. The loess method is very flexible, as it is not based on assumptions about the parametric form of the spectra.

Wavelet Analysis - It has been suggested (e.g. Gang *et al.,* 2004) that the use of techniques such as the Savitzky-Golay filter, which only smooth out statistical-fluctuations in the energy domain may distort the data and subsequently reduce its predictive capabilities. For example, by smoothing the spectra in this manner, high-frequency peaks are often lost and equally false low-frequency peaks are regularly produced. Techniques such as wavelet analysis, which incorporate the spectral information of both the energy and frequency space are increasingly being applied to hyperspectral γ-ray signals, to overcome the shortcomings of traditional smoothing techniques and uncover the analytically useful information contained in the spectra (e.g. Gang *et al.,* 2004; Viscarra Rossel *et al.,* 2007). The theoretical background of wavelets in soil science can be found in Lark and Webster (1999) and Viscarra Rossel and Lark (2009), in this study we aim to present the salient principles of wavelet analysis for de-noising γ-ray spectra.

In this study, the spectra were decomposed using a discrete wavelet transform (DWT) with Daubechies' wavelet of four-vanishing moments as the 'mother-wavelet' (Daubechies, 1991). As with all wavelets, Daubechies' wavelet is a local oscillation, which rapidly damps down to zero either side of its centre. The aim of wavelet analysis is to separate 'noisy', high frequency components of the spectra from the low frequency, high-scale components associated with the peaks of radionuclides. Multiplying the 'mother-wavelet' by the γ-ray spectrum, and integrating the result in terms of the energy-domain returns wavelet coefficients. These resulting wavelet coefficients reflect the variation of the signal within the interval where the mother-wavelet is not at zero. The wavelet is successively shifted to generate coefficients that explain the variation across the entire energy range. The process is then iterated, with the wavelet function being dilated, so the interval at which it responds to variation in the spectra is increased. Wavelet coefficients are then returned for successive translations (shifts) and scales of the wavelet up to a coarse scale, by sequentially applying a high pass filter obtained from the wavelet function (referred to as detailed coefficients) and a low pass filter

given by the scaling function (approximation coefficient), which returns a smoothed version of the γ-ray spectrum.

In this study, the spectra were reconstructed based on the approximation coefficients and setting the detailed coefficients to zero. However, by discarding all the high frequency, low-scale components some of the analytically significant peaks may be lost, in order to address this, wavelet thresholding is used. Wavelet thresholding discards only the detailed coefficients, which exceed or fall below a chosen limit. Thresholding therefore allows certain high-frequency peaks in the spectra to be preserved, whilst eliminating certain components that fall outside of the threshold. The approximate coefficients and remaining details are then used to reconstruct the spectra. In this study we have used several techniques to find an appropriate threshold value. The first of which is the universal threshold method (details of which can be found in Donoho and Johnstone, 1994), which is a simple entropy measure based on the number of γ-ray channels included. The threshold value is given by:

$$Thresh = \sqrt{2 \times \log n} \qquad \text{[Eq. 5]}$$

Where: n is the number of γ-ray channels and $Thresh$ is the threshold value. Stein's unbiased risk estimate (SURE) (Donoho, 1995) was also used, where the threshold value is dictated by the variance of the detailed coefficients at each wavelet scale. Thirdly the threshold values were set manually to penalise high and low components of noise.

3.2.6 Partial Least Squares Regression (PLSR)

The partial-least-squares one (PLS1) algorithm (Wold *et al.,* 1983) with LOOCV was used to calibrate the hyperspectral γ-ray information to the reference (lab-analysed) CEC data. The analysis was carried out in the R environment (R Core Team, 2012), using the 'pls' package (Mevik and Wehrens, 2007).

Prior to PLS, the pre-processed spectra were split into a calibration ($n = 239$) and an independent validation dataset ($n = 36$). Corstanje *et al.* (2008) note that the largest variation of CEC in this study area, reflected changes in parent material (at

scales > 2,000 m). In order to capture this variation in the independent validation set, one sample from each of the 36 main-stations was included. Table 1 shows the sample statistics for the calibration and independent validation dataset. The independent set includes at least one sample from the different soil types present in the calibration set. The observed values in the independent set fall within the range of the calibration set for each soil type (with the exception of the single 'freely draining lime rich loamy clay' sample, which had the highest CEC for its soil series, but falls well within the range of the other soil types in the calibration set).

Table 1 - Sample statistics for laboratory analysed CEC, for the calibration and independent datasets with regards to the soil-type.

Soil Type	Dataset	n	Mean	SD	Min.	Median	Max.
Freely draining slightly acid but base-rich soils	Cal.	7	15.6	5.5	10.3	13.1	22.0
	Ind.	1	23.9	N/A	23.9	23.9	23.9
Freely draining slightly acid loamy soils	Cal.	19	9.8	5.8	4.0	8.2	29.7
	Ind.	2	10.5	0.2	10.4	10.5	10.6
Lime-rich loamy and clayey soils with impeded drainage	Cal.	131	20.4	8.5	3.2	18.9	45.6
	Ind.	18	20.9	8.2	3.2	20.5	36.4
Shallow lime-rich soils over chalk or limestone	Cal.	57	16.9	6.5	4.2	18.4	26.9
	Ind.	8	18.3	6.3	7.1	21.1	23.9
Slightly acid loamy and clayey soils with impeded drainage	Cal.	25	12.5	5.5	1.9	12.1	25.8
	Ind.	6	10.7	4.8	5.8	9.6	18.5

The spectra and CEC values of the calibration set were used to develop a PLSR model. LOOCV was applied to avoid over-fitting and the model was then assessed in terms of the RMSECV (Eq. 4). The number of LVs to include was selected based on the RMSECV, with lower values indicating more accurate models. Once the number of LVs had been selected, independent predictions were then made from the spectra in the independent validation set and were compared to those determined through laboratory analysis to calculate the coefficient of determination (R^2, Eq. 9).

The performance of each model was evaluated in terms of accuracy, precision (SDE) and bias (ME). The accuracy was assessed by the root mean-square error of independent predictions (Eq. 4), the ratio of performance to deviation (RPD, Eq.7)

of the independent predictions and the residuals produced (Eq. 10). Chang and Laird (2002) outlined three categories of RPD for soil spectroscopy: category A (RPD > 2) are models that provide accurate predictions of a given soil property, category B (1.4 ≤ RPD ≥ 2) is indicative of models that can be possibly improved, and models which fall into category C (RPD < 1.4) are unsuccessful at prediction. The model bias is given by the mean error (ME, Eq. 6) and the precision of the models was expressed by the standard deviation of the error (SDE, Eq. 8).

$$\boldsymbol{ME} = \frac{\sum_{i=1}^{n}(\hat{y}_i - y_i)}{n} \quad \textbf{[Eq. 6]}$$

$$\boldsymbol{RPD} = \frac{\sigma_{y_{i-n}}}{\boldsymbol{RMSE}} \quad \textbf{[Eq. 7]}$$

$$\boldsymbol{SDE} = \sqrt{\frac{\sum_{i=1}^{n}(\hat{y}_i - y_i - \boldsymbol{ME})^2}{n-1}} \quad \textbf{[Eq. 8]}$$

$$\boldsymbol{R^2} = \frac{\sum_{i=1}^{n}(y_i - \bar{y})^2}{\sum_{i=1}^{n}(y_i - \hat{y}_i)^2} \quad \textbf{[Eq. 9]}$$

$$\boldsymbol{e_i} = y_i - \hat{y}_i \quad \textbf{[Eq. 10]}$$

Where: $y_i$is the ith observed value, $\hat{y}_i$ is the ith predicted value, $\bar{y}$ is the mean of $y_{i\ldots n}$, $\sigma_{y_{i-n}}$is the standard deviation of $\boldsymbol{Y}$ and RMSE is the root mean-square error (Eq. 4) of the independent predictions.

3.3 Results

A statistical description of the samples' CEC and soil series is presented in Table 1. It reveals that the majority (81 %) of the soils were lime-rich, with the remainder (19 %) being slightly acidic. The soil CEC of the study site ranged from 1.9 to 45.6 $cmol_c$ kg^{-1}. The comparison of the PCA scores (Figure 3a), revealed a positive correlation between CEC and the first principal component of the γ-ray signals. No clear anomalies were revealed in the score plot between the samples' spectral responses and CEC; therefore all samples were included in PLSR. The PCA loading plot (Figure 3b) showed channel 1,023 (cosmic γ-rays with energies >3,066 KeV) to be divergent to the rest of the channels, the removal of this channel led to an increase in RMSECV (6.3 $cmol_c$ kg^{-1} for 1 component, Table A-1), this channel was therefore included and contributed considerably to the loadings of PC2 (Figure 3b).

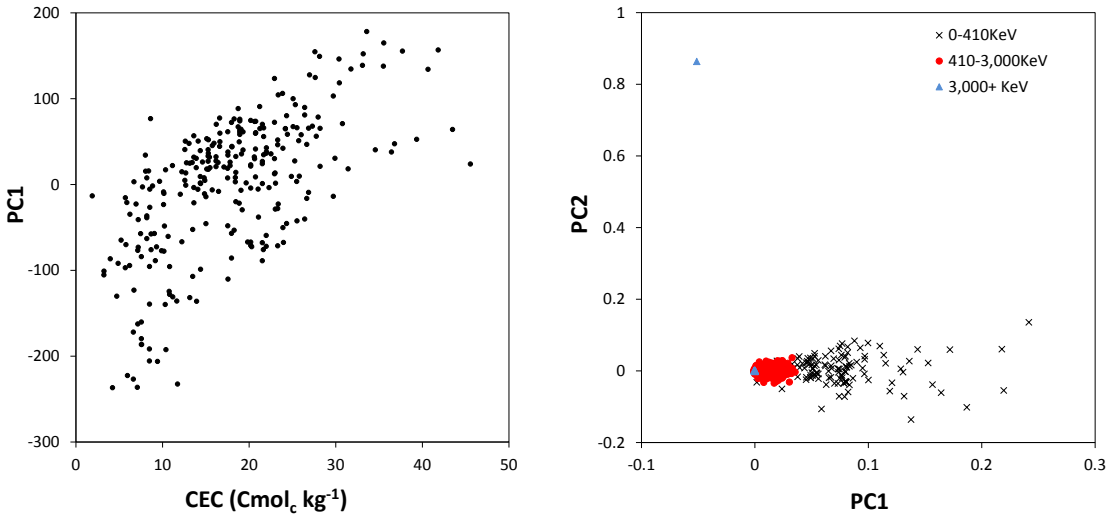

Figure 3 –PCA plots of the unprocessed spectra. (a) provides a comparison between CEC and the scores from PC1 and (b) shows the channel loadings of PC1 and PC2.

A comparison between the spectral pre-processing techniques producing the lowest RMSECV is presented in Table 2 (Appendix A provides a full comparison of the pre-processing techniques). The results in Table 2 show that all of the pre-processing methods reduce the RMSECV when compared to the unprocessed spectra. Thresholding the detailed coefficients at level 3 by universal thresholding

produced the lowest RMSECV (5.18 $cmol_c\ kg^{-1}$). Despite all of the pre-processing techniques (presented in Table 2) lowering the RMSECV, the correlation (R^2) of the observed and predicted CEC in the calibration models was also decreased, with the unprocessed spectra producing the best correlation to the reference CECs.

Table 2 - A comparison between spectral pre-processing techniques, in terms of PLSR statistics of the CEC calibration model.

Pre-processing technique		[a]LV	R^2	[b]RMSECV ($cmol_c\ kg^{-1}$)	[c]RMSE ($cmol_c\ kg^{-1}$)
Unprocessed	-	2	0.70	5.310	4.47
[1]Approx. Coefficient	Level 3	3	0.67	5.308	4.67
[2]Rigorous SURE	Level 3	2	0.67	5.201	4.72
[3]Universal Threshold	Level 3	2	0.66	5.183	4.79
[4]Penalise ≤ 1	Level 3	2	0.67	5.223	4.68
[5]Penalise ≤ 2	Level 3	2	0.67	5.201	4.72
[6]Penalise ≥ 5	Level 3	2	0.66	5.186	4.79
[7]Loess	α 3%	3	0.67	5.298	4.73
[8]Savitzky-Golay	k 3, F 5	2	0.67	5.270	4.69

[a]LV – Number of latent variables

[b]RMSECV – Cross validated root mean-square-error (accuracy).

[c]RMSE - root mean-square-error of calibration.

[1] Spectra reconstructed from the approximation coefficients at level 3.

[2-6] Spectra reconstructed from approximations and details, thresholded by [2] SURE, [3]universal threshold and manual thresholding [4]penalising details ≤ 1, [5] ≤ 2 and [6] ≥ 5.

[7]Loess – Spectra processed using local regression using weighted linear least squares and a 2nd degree polynomial model, with a neighborhood of 3% of the spectral channels.

[8]Savitzky-Golay – Spectra processed with the Savitzky-Golay filter, with a 3rd degree polynomial and a filter width of 5.

Table 3 - Independent validation statistics of the PLSR models of CEC.

Pre-processing Technique	Filter Description	[a]NF	R^2	[b]ME ($cmol_c\ kg^{-1}$)	[c]SDE ($cmol_c$ kg-1)	[d]RMSE ($cmol_c\ kg^{-1}$)	[e]RPD
Unprocessed	-	2	0.58	0.28	5.11	5.05	1.56
Approx.	Level 3	3	0.61	0.04	4.98	4.91	1.60
Rigorous SURE	Level 4	2	0.59	0.12	5.07	5.00	1.57
Fixed Thresh	Level 5	2	0.59	0.07	5.06	4.99	1.57
Penalise ≤ 1	Level 6	2	0.59	0.15	5.08	5.01	1.57
Penalise ≤ 2	Level 7	2	0.59	0.12	5.07	5.00	1.57
Penalise ≥ 5	Level 8	2	0.59	0.08	5.06	4.99	1.57
Loess	α 3%	3	0.62	0.24	4.88	4.81	1.63
Savitzk-Golay	k 3, F 5	2	0.57	0.09	5.19	5.12	1.54

[a]LV – number of PLSR factors
[b]ME – mean error (bias)
[c]SDE – standard deviation of error
[d]RMSE – root mean-squared error
[e]RPD – ratio of prediction deviation

The results from the independent predictions are presented in Table 3. The models are consistently producing positive bias (ME of 0.20-0.28 $cmol_c\ kg^{-1}$), representing the over-prediction of CEC. In terms of accuracy, the RPD of each model falls into the intermediate category proposed by Chang and Laird (2002) ($1.4 < RPD < 2$), these are models that are capable of making fair predictions of **Y**. The spectra processed by Loess produced the most accurate predictions, with an RMSE of 4.81 $cmol_c\ kg^{-1}$. This technique also produced the highest RPD and R^2 and was therefore selected for model interpretation.

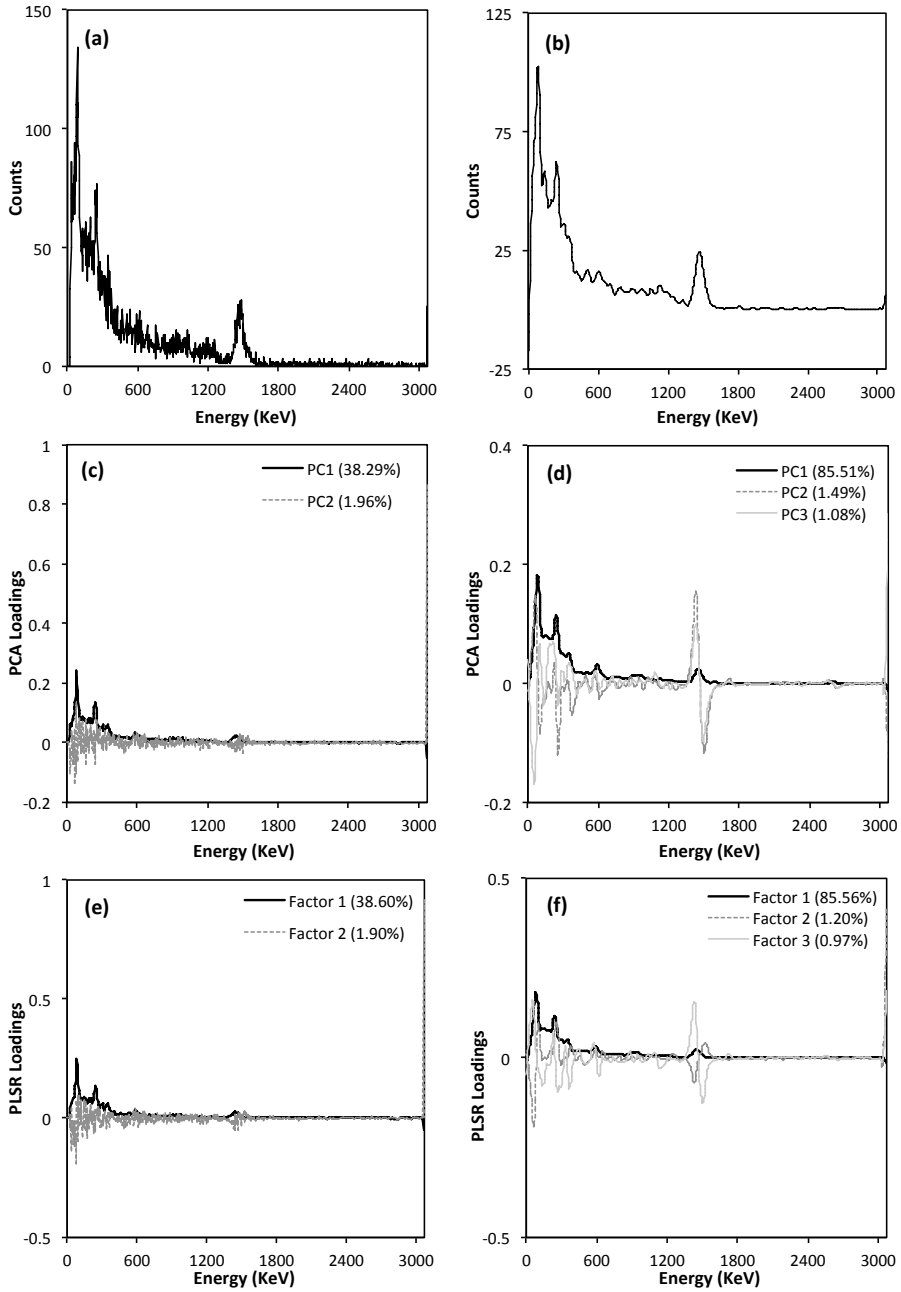

Figure 4 - Examples of (a) the raw spectra, (b) the Loess smoothed spectra. Corresponding principle component loading plots are given in (c) and (d) respectively and PLSR loading plots in (e) and (f).

The raw spectra contained a considerable amount of noise (Figure 4a), making it difficult to establish the peaks associated with CEC. As mentioned in section 2.4.1, loading plots can be an important diagnostic tool to establish the contribution each energy channel has on the prediction of **Y** (in this case CEC). The loadings of the raw spectra reflect the spectral noise, particularly in PC2 (Figure 4c) and factor 2

(Figure 4e). Both PLSR loading plots (Figure 4e, f) show the high positive loadings, which were assigned to energies in excess of 3,066 KeV, for the prediction of CEC. In contrast to the raw spectra, the processed spectra (Figure 4b) display clear peaks of K^{40} (ca. 1,470 KeV), Bi^{214} (daughter of Th, ca. 600 and 1,120 KeV) and the less prominent peaks of Tl^{208} in PC2 (daughter of U, ca. 580 and 2,600 KeV). Positive loadings are visible for the peaks associated with K and Th (Figure 4e, f).

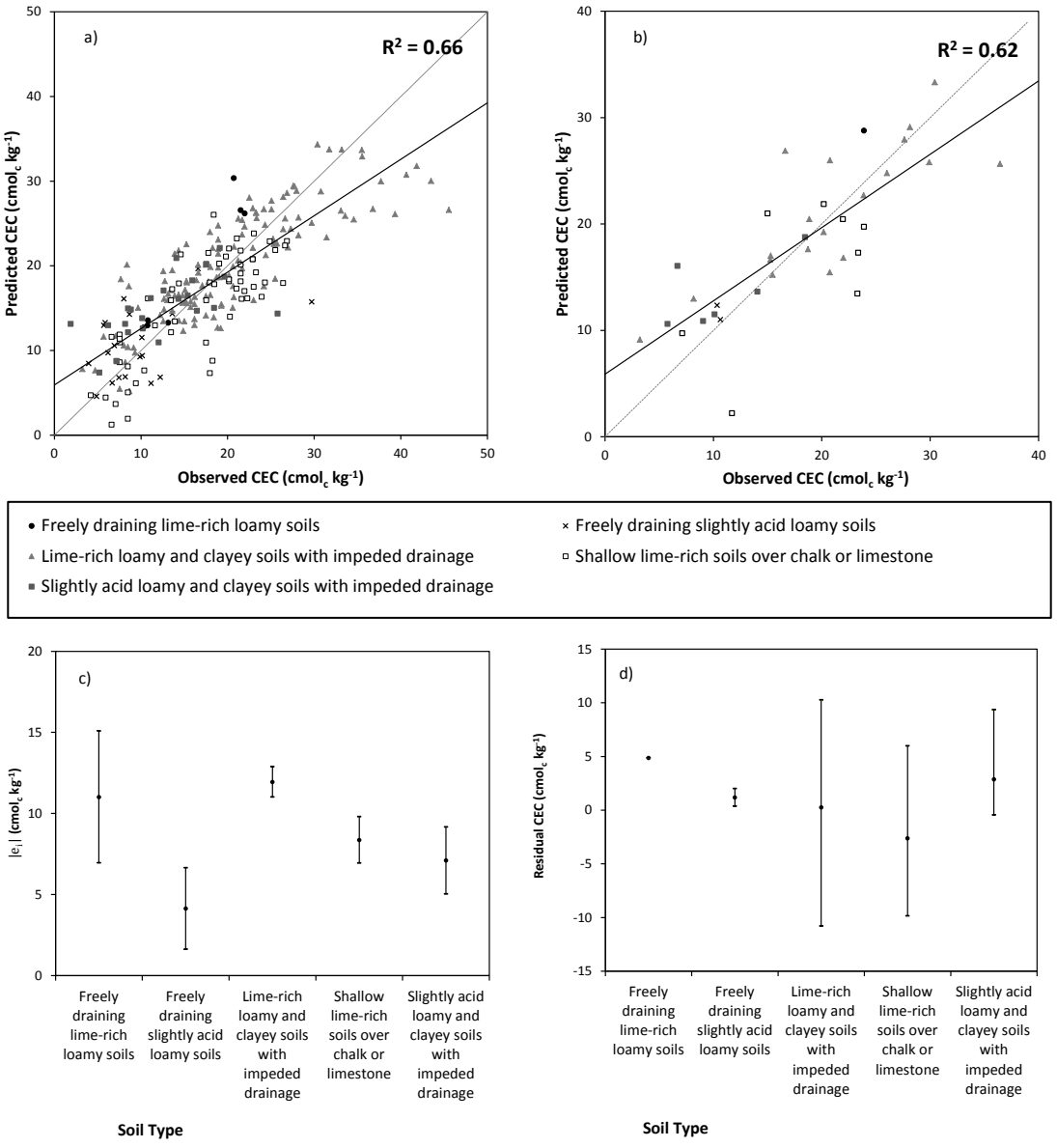

Figure 5 - Observed versus predicted CEC, with regard to soil type, for (a) Calibration dataset and (b) the independent validation set. (c) Shows the absolute residual ($|e_i|$, Eq. 10) CEC for each soil type at 95% significance level for entire dataset and (d) presents the residual CEC of the independent predictions.

A comparison between the observed and predicted CEC values from the Loess processed spectra is presented in Figure 5. It is apparent from Figure 5a that the shallow lime-rich soils over chalk and lime, which have a low CEC, are consistently being under-predicted in the calibration model. The lime-rich loamy and clayey soils with impeded drainage produced significantly higher residuals (deviation from observed value) than all other soil types (Figure 5c), with the exception of the freely draining lime-rich soils. The residuals in the calibration models are largely reproduced in the independent predictions (Figure 5b), with the shallow lime-rich soils and lime-rich loamy and clayey soils with impeded drainage producing the largest residuals. The residual plot (Figure 5d) further emphases the high degree of deviation from observed values in these soils, with the shallow lime rich soils displaying residuals of -9.8 to 6.0 $cmol_c\ kg^{-1}$ and the residuals of the lime-rich soils with impeded drainage being in the range -10.8 to 10.3 $cmol_c\ kg^{-1}$. These values are considerably higher than the SDE of 4.88 $cmol_c\ kg^{-1}$.

3.4 Discussion

3.4.1 Spectral pre-processing

The results have shown that using chemometrics, it is possible to make fair predictions of soil fertility (CEC) from a soil γ-radiometric response, at scales exceeding the within-field scale previously studied. Smoothing of the spectra improved the accuracy (RMSE) and precision (SDE) of independent predictions. The Savitzky-Golay pre-processing was the least effective smoothing technique, as although RMSECV was reduced in comparison to the unprocessed data, the correlation was also decreased in both the calibration and independent predictions. These findings seem to reinforce the concerns raised by Gang *et al.* (2004) who suggest the smoothing of a γ-ray signal in the energy domain alone may lead to the loss of analytically significant peaks and therefore impede predictions. The results from Table 3 suggest that using techniques which smooth the spectra in both the energy and frequency domains (loess and wavelet transform) it is possible to reduce noise, whilst preserving sharp peaks in the spectra, which appear critical in the prediction of CEC. Reconstructing the spectra

from approximation coefficients at level 3 produced similar results to loess smoothing (α = 3 %) in terms of R^2 and RMSE of independent predictions. Whilst both techniques out-perform the raw spectra, in terms of independent predictions, the loess method explains more of the variation in the γ-ray spectra (88.1 %) than the approximation coefficients (85.05 %) and also produces less error (SDE = 4.88 $cmol_c\ kg^{-1}$ compared with 4.98 $cmol_c\ kg^{-1}$). Loess was therefore considered to be the preferred smoothing technique.

3.4.2 Analysis of loading plots

Positive PLSR loading weights for CEC prediction (Figure 4f) correspond to the spectral peaks associated with the elements K and Th. Comparable results are presented in Viscarra Rossel *et al.* (2007), for the prediction of clay. As higher CEC values tend to correspond with increases in clay content, the positive loadings may signify that elevated K and Th concentrations are indicative of clay content. High positive loadings were also found for energies <400 KeV, in this energy range the photoelectric effect is predominant. The photoelectric effect occurs when a γ-ray photon undergoes an interaction with an absorber atom in the soil, resulting in the disappearance of the γ-ray photon, in its place a photoelectron is produced from one of the electron shells of the absorbing atom and possesses kinetic energy equal to the gamma-ray photon minus the binding energy of the liberated electron. An X-ray characteristic of the binding energy is also released, typically between a few to tens of KeVs (Knoll, 2010; IAEA, 2003). Viscarra Rossel *et al.* (2007) suggested that high loadings in this region are difficult to interpret, given that they are not explicitly linked to the environmental radioisotopes and may be attributed to the photoelectric effect.

At the high-energy end of the spectrum, cosmic γ-rays (energy > 3,066 KeV) were also a major contribution to the PLSR loadings of factor 2 (Figure 4f). The high counts in the cosmic channel appeared to cluster in the south of the study site (Figure 6) in an area dominated by lime-rich loamy and clayey soils with impeded drainage and shallow lime-rich soils over chalk and lime. The distribution of counts in the 'cosmic' channel over the study site may have been beneficial in

differentiating different soil types, hence their high loadings. Further study is required to establish whether this association could lead to favourable results for other regions, or whether these findings are coincidental.

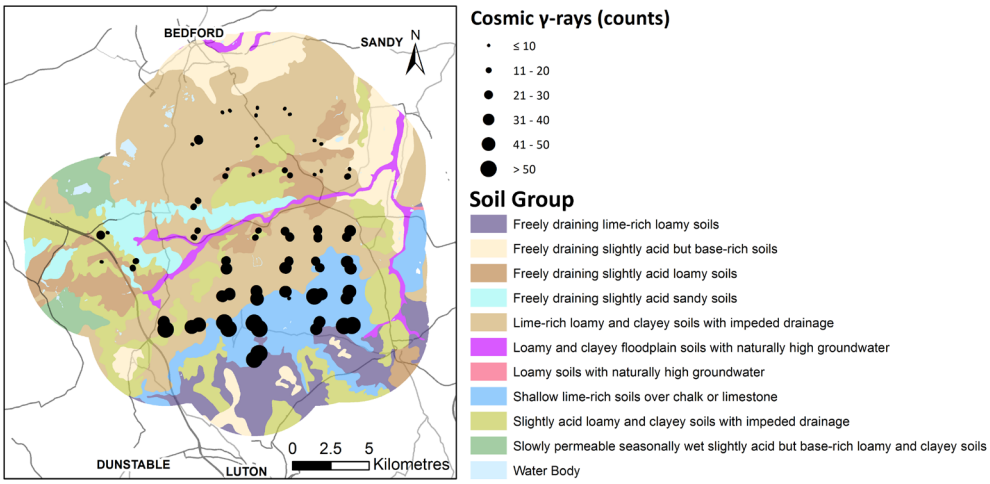

Figure 6 - Spatial representation of cosmic γ-ray intensity (energy >3,066 KeV), shown as γ-ray counts of the unprocessed spectra (10 min measurement period).

3.4.3 Comparisons to other studies

Calibrating soil γ-ray responses using PLS, produced fair predictions of CEC at the regional scale. The results presented, are an improvement (in terms of R^2) to previous farm-scale predictions of CEC from γ–ray spectroscopy presented by Taylor *et al.* (2010), who used a univariate approach (general least squares; R^2 of 0.48). The independent predictions of this study are closer to field-scale clay predictions made by Viscarra Rossel *et al.* (2007), from full γ-ray signals (R^2s of 0.63-0.76). This may therefore suggest that the relationship between γ-ray activity and CEC exists beyond the within-field scale.

Petersen *et al.* (2012) also observed a strong relationship (R^2 of 0.82) between CEC and radiometric K and Th using MLR, for four fields in Middle Europe of comparable parent material. They also report that predictions made from the quantitative response of the detector (using MLR), yielded significantly worse results (R^2 -0.42 to 0.22), which appears to support the idea that using stripping

factors to acquire estimates of radionuclide concentrations introduces uncertainty into the model relative to full spectrum multivariate methods, such as PLS, however further study is required to confirm this.

Savvides *et al.* (2010) tested the relationship between CEC and VNIR spectra, for the soils used in this study. Using PLS they obtained similar predictions of CEC in their calibration model to this study (R^2 of 0.71, RMSECV of 4.8 $cmol_c\ kg^{-1}$), however their randomly selected validation samples ($n = 56$) produced inferior results (R^2 of 0.24, RMSE of 5.6 $cmol_c\ kg^{-1}$). By analysing the covariance between predicted and observed they found that the relationship was scale dependent with improved results at scales of 50 m (R^2 of 0.82) and 500 m (R^2 of 0.73). The variation in the γ-ray signals of this study may therefore reflect changes in parent material, in addition to soil texture; further study is required to establish at what scale the majority of the variation in γ-ray signals occur.

Lee *et al.* (1999) report stronger relationships using VNIR spectra. They calibrated 165 soil samples from five U.S. states, using PLSR with leave-ten-out cross-validation, which produced RMSE of 3.43 $cmol_c\ kg^{-1}$ and an R^2 of 0.83. Whilst the results of Lee *et al.* (1999) may indicate that VNIR sensors are more appropriate predictors of CEC than γ-ray spectroscopy, it is important to remember that vegetation cover unless thick has little impact on the γ-ray response, making them more suited for in-situ measurements. Moreover Kweon *et al.* (2013) emphasise the difficulty of calibrating VNIR data, with soil moisture affecting their response and subsequently having to calibrate each field individually.

3.4.4 Sources of Inaccuracy

Five of the independent predictions (36 in total) had residuals greater than 1.5 SDE. These samples were a consistent source of inaccuracy in all of the independent predictions. A comparison between the outlying spectra and representative spectra (producing accurate predictions for similar CEC values) is presented in Figure 7. Figure 7a, b show the two samples that produced over-predictions of CEC. It is apparent from these plots that the outlying spectra produced more pronounced peaks at energies <410 KeV compared with the

representative spectra. Whilst there seems to be a good relationship between soil CEC and its γ-ray response, it would appear that certain features in the spectrum particularly at low energies (<200 KeV) do not always correspond well with CEC. These peaks are not directly associated with the environmental radioisotopes and are likely to be attributed to photoelectric absorption, making them much harder to interpret. These peaks were allocated high positive loadings; hence a slight difference between the spectra has led to relatively high discrepancies in predictions. However, the removal of these peaks from the spectra led to an increase in RMSECV in the calibration models and so was therefore included. The unprocessed spectra also displays comparatively low peaks in these areas, therefore the inaccuracy of these samples is unlikely to be a consequence of the pre-processing technique.

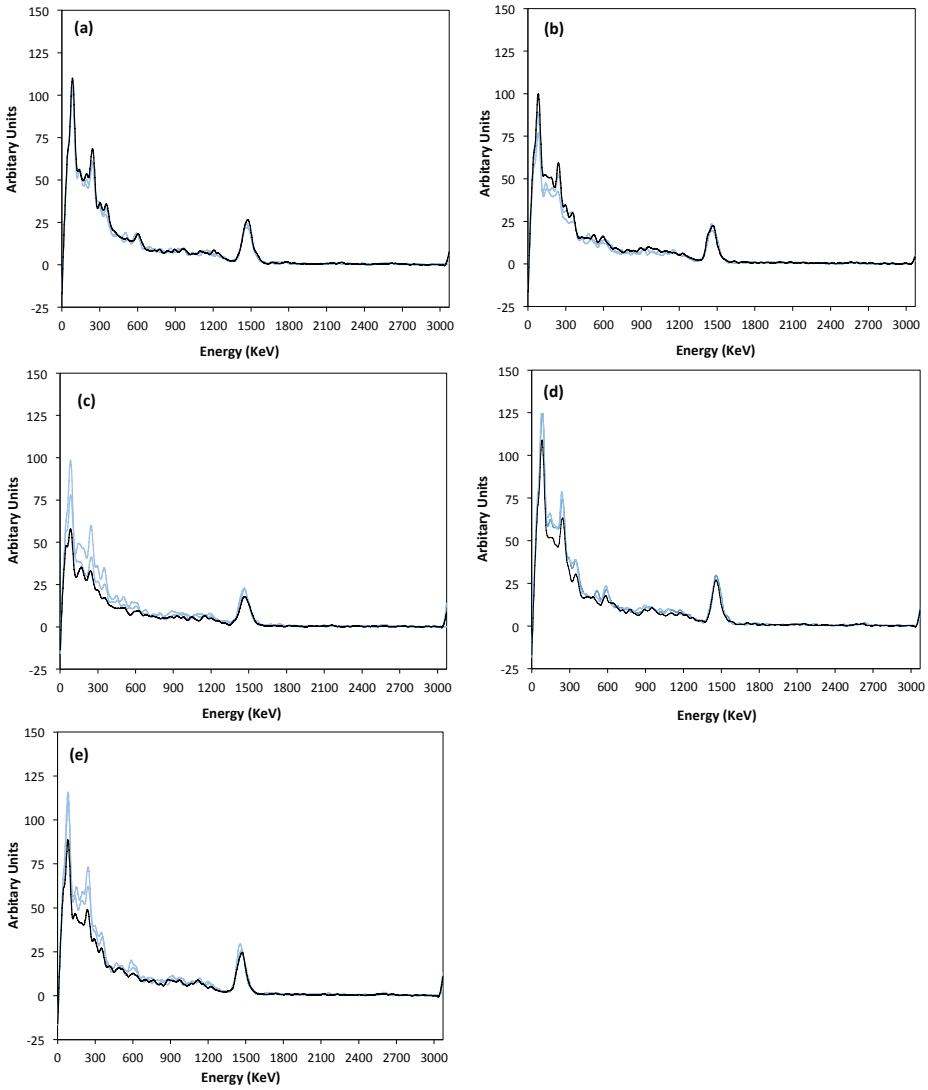

Figure 7 - A comparison between spectral responses of samples; indicative spectra are presented in blue, and outlying spectra shown in black. Corresponding descriptive statistics are presented in Table 4.

Table 4 - Descriptive statistics of absolute residual error.

	Outlying Sample			Comparitive Samples		
Sample	Soil Group	CEC	Error	CEC (lower)	CEC (upper)	Mean Error
a)	Lime-rich loamy and clayey soils with impeded drainage	16.63	10.26	16.18	17.09	0.64
b)	Slightly acid loamy and clayey soils with impeded drainage	6.70	9.35	6.70	7.47	0.61
c)	Shallow lime-rich soils over chalk or limestone	11.73	9.53	11.64	12.05	1.21
d)	Lime-rich loamy and clayey soils with impeded drainage	36.43	10.79	35.50	35.54	2.23
e)	Shallow lime-rich soils over chalk or limestone	23.30	9.85	23.30	23.36	2.61

For the three samples which significantly under-predicted CEC (Figure 7c, d and e), the most noticeable differences between the outlying and the representative spectra also occurred at lower energies (<410 KeV). The disparities between the peaks associated with K, U and Th were however much more pronounced (than Figure 7a,b). These samples were lime-rich and such soils generally have low radioelement concentrations, Dickson and Scott (1997) note typical concentrations of K, U and Th in Calcrete can be as low as 0.3 %, 1.2 mg kg^{-1} and 3.2 mg kg^{-1} respectively (in comparison to the global average of 2.5 %, 3 mg kg^{-1} and 15 mg kg^{-1}). Sample (c) produced the second lowest $\boldsymbol{\gamma_{TC}}$ in the entire dataset, which may indicate a greater $CaCO_3$ content than the representative spectra. However, with limited chemical and physical information about the samples, this is merely conjecture; what is apparent is that the peaks at ~600 KeV associated with ^{214}Bi (a daughter of Th) are significantly lower in the outlying spectra. Th content is seen to be a good indicator of clay content (e.g. Pracilio *et al.,* 2006; Van Egmond *et al.,* 2010), which may indicate that these soils are relatively deficient in Clay. A significant constraint on interpreting inaccuracies in the model was the lack of physical and chemical information available for each sample. As CEC is not purely a function of properties that have been successfully characterised by γ-ray spectroscopy, additional factors (such as pH), which influence CEC, may not be

reflected in the γ-ray response. Conversely factors such as a change in parent material, which can heavily impact the γ-rays response, may not have such a bearing on CEC.

In this study a single γ-ray response was measured for each sample, forcing the assumption that each γ-ray response was representative and accurate. In situ γ-ray studies typically record one γ-ray response every second, usually at 3 m intervals (e.g. Van Egmond *et al.,* 2008; Viscarra Rossel *et al.,* 2007), this allows for the spectra to be spatially aggregated. Recent work by Viscarra Rossel *et al.* (2007) and Taylor J.A. *et al.* (2010) has shown the spatial aggregation of spectra by kriging to improve the signal-to-noise ratio. The technique may also help to highlight areas of spectral variation, which would be beneficial for the selection of reference samples. As the sample locations in this study were sporadic and spanned different soil types, spatial aggregating of the spectra would have been inappropriate.

Although it is unclear from the limited information available, exactly why the five samples reported have produced unsatisfactory predictions of CEC, if these are a consequence of erroneous measurements of the γ-ray signal or CEC determination, the relationship is much better than reported. The removal of the five samples with residuals >1.5 SDE resulted in an increased R^2 of 0.80 of the independent predictions for the loess model and an RPD of 2.2, which places it in the top tier of predictions (RPD >2, Chang and Laird, 2002).

3.4.5 Applications and further work

Although Petersen *et al.* (2012) report the response of a laboratory based Ge γ-ray sensor to be comparable to mobile sensors in their study; they also note that absolute values of dried laboratory samples are systematically higher than in-situ measurements. Dierke *et al.* (2011) suggest that this difference is a result of soil moisture, which attenuates γ-ray activity in the field. It would therefore be important to establish whether the measurements from the RT-50 NaI sensor produce similar rises in spectral peaks, if calibrations of γ-ray signal acquired in-situ were to be made at a regional level. Further work is also required to determine precisely how texture and OM content correspond with the γ-ray signals at these

scales, as although the results seem to indicate they do, without adequate reference information this is simply speculation.

3.5 Conclusion

Fair predictions of CEC were made at the regional scale, through the calibration of γ-ray signals using PLSR. It would appear from the results that γ-ray spectroscopy could be a useful indicator of CEC and in comparison to VNIR and EC_a sensors offers a greater potential for in-situ measurement. The limited chemical and physical information about the soils restricted the interpretation of model inaccuracies, but variations in certain parts of the γ-ray signal generally seem to reflect variations in CEC. Further study is required to establish whether this relationship exists at larger scales or whether certain aspects of the spectra (particularly the 'cosmic channel') were associated to CEC coincidentally. Additional study is also required to determine which other soil properties can be characterised through γ-ray spectroscopy and how the laboratory based spectra compare to those acquired in-situ.

Chapter 4 - National scale calibrations of γ-ray signals for England and Wales

4.1 Introduction

During the 20th century, the majority of European countries produced nationwide soil surveys, primarily in an effort to support agricultural development (Vitharana *et al.,* 2007). These surveys were typically produced at coarse scales, for reasons of cost (McGrath and Loveland, 1992). The current demand for sustainable land-management calls for timely, soil data at resolutions finer than these data datasets can provide. Timely soil information is required for a variety of purposes including: climate change modelling, flood plain management, precision agriculture and identifying sources of pollution. The traditional way to update a soil map is to obtain further samples from subsequent surveys, which can be extremely costly, considering the associated fieldwork and laboratory analysis required. The European Commission (EC) acknowledges that at present, little is known about the status and quality of European soils (EC, 2012). The Soil Thematic Strategy (EC, 2012) intends to address this lack of knowledge, by monitoring the soil at regular intervals (5-10 years). The EC proposes adopting remote sensing techniques to achieve a harmonised approach of soil monitoring (EC, 2012). A recent study by Vitharana *et al.* (2008) has demonstrated the potential benefits of combining proximal soil sensors with existing soil maps, in order to update national datasets.

The previous chapters suggest that γ-ray spectroscopy offers a rapid and relatively inexpensive alternative to conventional laboratory analyses, for the determination of physical soil properties and stable geochemical properties. This chapter aims to establish whether accurate calibrations of γ-ray signals can be made at a national scale, from soils in the National Soil Inventory (NSI) of England and Wales.

At the field-scale, strong correlations have been shown to exist between the distribution of radionuclides and physical soil properties such as soil texture and OM content, as well as stable soil characteristics such as potassium (K), Iron (Fe), pH and phosphates (e.g. Viscarra Rossel *et al.,* 2007; Pracilio *et al.,* 2006; Loonstra,

2011). The relationship between soil texture and γ-radiometrics is based on the preferential adsorption of K, U and Th onto clay colloids. Soil texture is an important indicator of a soil's ability to retain water and nutrients and therefore is indicative of many physical and chemical properties of soil, which include: leaching and erosion potential, bulk density and water and nutrient retention (Shahid *et al.,* 2013). It is difficult to map the spatial distribution of soil texture, through conventional techniques as a large proportion of textural variations occur at small scales between 20 and 200 m (McBratney and Pringle, 1999). Soil texture is classified in terms of the size and proportions of soil particles, with clay particles being <2 μm in diameter, silts >2 to 60 μm and sand fractions being >60 μm. Accurate information about soil texture can also help establish areas at risk of soil erosion. A study by Brazier *et al.,* (2001) aimed to quantify the rate of hillslope erosion in the UK, using a minimum information required approach. They found a strong association between soil texture and erosion risk in the Great Ouse catchment, Cambridgeshire and showed increases in sand content corresponded to an increased risk of erosion. As fertile soils are in increasing demand, accurate mapping assessments of the risk of erosion are fundamental to mitigating the loss of valuable arable land and thus ensuring global food demands are met.

High clay content is typically indicative of elevated soil OM content, with clays providing chemical protection of soil OM through its adsorption on to clay colloids (Huang *et al.,* 2012). Soil OM plays a vital role in maintaining soil health and productivity, however agricultural practices such as tillage accelerate the decomposition of soil OM, therefore leading to its depletion (West and Post, 2002). Soil OM is a significant source of organic carbon (OC), comprising approximately 50 to 60 % of OM (Kutsch *et al.,* 2009). Since preserving soil carbon stocks is an essential part of the commitments made by the EU to the Kyoto protocol, it is essential that soils be regularly monitored, to mitigate further loss of soil OM through intensive and sustained agricultural practices. Bellamy *et al.* (2005) report that an average of 0.6 % carbon was lost from soils in England and Wales per year, for the period 1978 to 2003. A study by Martz and Jong (1990) found a positive correlation at the regional scale, between OC and clay content for Seymor Basin

soils, Canadian prairie catchment. If this apparent relationship between OC and clay content exists beyond the regional scale, γ-ray spectroscopy may provide a relatively inexpensive tool for the monitoring of terrestrial carbon stocks.

In addition to being considered a direct measurement of a soils mineralogical and textural composition, γ-ray spectrometers also have the potential to predict certain soil chemical properties. Viscarra Rossel *et al.* (2007) found a strong relationship (R^2 of 0.87) between soil γ-ray response and Fe, for three fields in New South Wales, Australia. Their results indicated that the relationship was similar to clay, with positive PLSR loadings being allocated to the peaks associated with K, Th and U. Fe is principally associated with the silt-clay fraction, as clay minerals carry more Fe than sand grains (Saccà *et al.,* 2011). Fe^{3+} generated during chemical weathering is typically adsorbed onto layers of secondary clay minerals or combined with OM. A study by Zhu *et al.* (2011) demonstrated the ability to predict clay content using Fe concentrations from a portable X-ray florescence spectrometer. Their findings reveal a strong correlation (R^2 of 0.97) between Fe and clay content in Louisiana soils. Similarly, essential nutrients such as P are much less susceptible to leaching in clayey soils. This association is supported by Mahmood *et al.* (2011), who found strong correlations between total P and the radiometric concentrations of U in an organically managed field (R^2 of 0.91) and ^{137}Cs in a conventionally managed field (R^2 of 0.94). Their results however were not consistent between management zones, with unsuccessful predictions (R^2 of 0.29) being made from U in the conventionally managed field. Additionally, as the radioisotope ^{40}K is the only radioisotope of K and exists as a fixed proportion (c. 0.012%) of natural K, good predictions of total K from γ-ray signals are well documented (e.g. Mahmood *et al.,* 2011; Wong and Harper, 1999).

Good relationships (R^2 of 0.75) between γ-ray signals and the pH of deep soil horizons (15 to 50 cm) have been reported by Viscarra Rossel *et al.* (2007). Their predictions were made for a 202 ha field in New South Wales, Australia and showed an inverse relationship between sand content and pH. However, Taylor *et al.* (2010) found the association between pH and γ-ray total counts to be relatively poor at the farm scale (R^2 of 0.05 for topsoil and 0.48 for subsoil). As soil pH at the

field scale is dependent on lime application, crop rotations and management history between fields, Taylor *et al.* (2010) suggested that prediction at the farm scale might be optimistic. Soil pH unlike clay, is also not directly associated with the concentration of terrestrial radioisotopes, however as soil pH is influenced by factors such as parent material, which γ-ray signals are sensitive to, it might be possible to predict soil pH at scales greater than the farm-scale, where pH variation is governed to a lesser extent by management practices.

Rawlins *et al.* (2007) assessed the potential of airborne γ-radiometric surveys to assist in mapping soil texture and parent materials in Eastern England. By assessing the coregionalisation of radiometric concentrations, they were able to establish that a third of the variation of ^{40}K could be attributed to changes in parent material, while a substantial proportion of the variation within the geological subclasses could be attributed to changes in geochemistry. Wilford and Minty (2007) state that soil radiometric signatures from airborne sensors are not unique and thus are unable differentiate between characteristics of geologically dissimilar soils. Bierwirth (1996b) further suggests that it is naïve to assume that maps of pH and soil texture may be generated from γ-ray imagery alone, as K and Th can behave different over geomorphic and geological terrain, thus geology should be taken into account in analysis. Surface and laboratory γ-ray spectrometers have a greater spectral resolution in comparison to airborne sensors (Petersen *et al.,* 2012) and therefore may be able to detect certain features of the γ-ray spectrum, which correspond to coarse-scale variations in soil characteristics.

As discussed in Chapter 2, laboratory spectrum analysers measure γ-ray activity at finer spectral resolutions than in-situ sensors, therefore making the distinction between spectral peaks easier. Noise associated with environmental conditions is also eliminated, thus offering the potential to compare responses between sites. In this chapter the ability of γ-ray spectroscopy to supplement conventional laboratory analysis, in national soil monitoring is assessed. Full γ-ray signals are to be obtained from samples in the National Soil Inventory (NSI) using a laboratory-based γ-ray spectrometer, in order to make calibrations of physical and chemical

soil properties at the national scale. As the results from Chapter 3 suggest, it may be possible to extract analytically important information from γ-ray signals, which pertains to coarse-scale variation in soil characteristics. The models produced will then be assessed to establish the impact geology and soil type have on the PLSR predictions.

4.2 Materials and Methods

4.2.1 Study area and sampling scheme

The soil samples used in this study were from the NSI, which contains topsoil information for England and Wales. The NSI was commissioned in the late 1970s and at the time of sampling (1982), only about 25 % of England and Wales was mapped at resolutions finer than 1:125,000 (McGrath and Loveland, 1992). The NSI aimed to acquire an unbiased and representative selection of topsoils (0 to 15 cm) for England and Wales, to map their physical and geochemical properties. The interval between soil samples was set at 5 km, for reasons of cost. The NSI is the most comprehensive account of soils in England and Wales and is the only dataset of its kind to be resampled (Bellamy *et al.,* 2005).

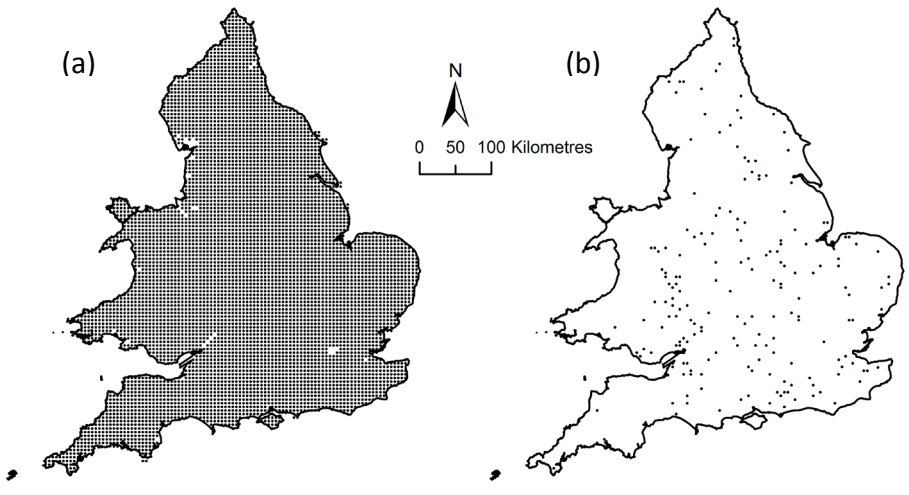

Figure 8 - (a) Sample locations of the NSI and (b) the samples used in this study.

As described in McGrath & Loveland (1992), the samples were collected from an orthogonal grid to avoid sample bias. A total of 6,127 sites were visited, from which, 5,692 samples were obtained. At each site 25 cores were collected, at 4 m

intervals from a 20 m × 20 m square centred on the grid intersection. The cores were taken from a maximum depth of 15 cm and were bulked in the field. From the 5,692 samples collected, 196 samples were used in this study (Figure 8b). Sample characteristics are presented in Table 5 and clearly show the comprehensive range of soil textures, pHs and geochemical concentrations represented and reflect the extensive variations in parent material of the study area. The samples were selected purely based on mass, with the sample mass needing to exceed 190 g in order to be effectively detected by the γ-ray spectrometer.

Table 5 – NSI Sample statistics.

Property	n	Min.	Max.	Mean	SD
Clay (%)	196	0.0	67.3	23.8	11.5
Silt (%)	196	0.1	76.9	36.7	16.4
Sand (%)	196	2.3	99.1	39.6	22.4
pH	192	3.8	9.2	6.2	1.2
OC (%)	196	0.7	11.0	3.2	1.7
Fe (g kg^{-1})	196	0.61	235.79	30.49	21.99
K (g kg^{-1})	196	0.08	13.97	4.95	2.57
P_{tot} (g kg^{-1})	196	0.04	4.54	0.83	0.50
P_{ext} (mg l^{-1})	196	0.0	149.0	26.2	24.1

$P_{tot.}$ – Total P
$P_{ext.}$ – Extractable P

4.2.2 Sample preparation and analyses

The reference soil data used in this chapter comes from the NSI, the methods for which are outlined in Avery & Bascomb (1982). The samples were air-dried in the laboratory at 25 to 30°C and milled in a mild-steel roller mill to pass a 2 mm sieve. All analyses except for totals were carried out on this material.

Particle size distribution was determined by the pipette method and was inclusive of $CaCO_3$. The fractions determined were clays (<2 μm), silts (2-60 μm) and sands (>60 μm). pH was measured at ADAS laboratories and was measured using a pH meter after shaking 10 ml of soil with 25 ml of water for 15 min. Organic Carbon (OC) was measured either by loss-on-ignition for soils estimated to contain more

than about 20% OC or by dichromate digestion. Total K, Fe and P (P_{tot}) were measured on a 25 g subsample of the soil, ground to <150 μm in an all-agate planetary ball. The total concentrations were determined by Inductively Coupled Plasma Emission Spectrometry (ICP) in an aqua regia digest and expressed as g kg^{-1}. Extractable Phosphorus ($P_{ext.}$) concentration (mg l^{-1}) was determined by shaking 5 ml of air dry soil with 100 ml of 0.5 M sodium bicarbonate for 30 min at 20°C, filtering and then measuring the absorbance at 880 nm colorimetrically with acid ammonium molybdate solution.

4.2.3 γ-ray Spectral Acquisition

As with Chapter 3, the γ-ray spectra were acquired using an RT-50 lead based gamma-ray spectrum analyser, calibrated with a 9 Bq kg^{-1} source of ^{137}Cs to prevent spectral drift. The NSI samples used had to remain in their archive bags, to avoid cross-contamination. Consequently, the 196 samples analysed varied in mass between 190-390 g. The samples were measured over a 10 min measurement period and their variances in mass accounted for, following measurement.

To account for the influence of mass on the γ-ray response, a representative sample from Chapter 3 was scanned at 10 g intervals over the range 190-390 g. The relationship between the γ-ray total counts and mass was linear and thus can be expressed by:

$$\boldsymbol{\gamma_{TC} = d \times m + c} \qquad \textbf{[Eq. 11]}$$

Where: γ_{TC}, is the total γ-ray count, d is the line gradient, m is the sample mass and c is the y-intercept, associated with the background response of the sensor. The adjusted γ-ray response of a soil at channel i (adj γ_i) was then given by:

$$\boldsymbol{adj\ \gamma_i = \frac{\gamma_i}{(d \times m) + c} \times (d \times \bar{m}) + c} \qquad \textbf{[Eq. 12]}$$

Where: γ_i is the γ-ray response of a soil for ith channel and $\bar{m}$ is the mean mass of the samples. Adjusting the spectra in this manner, forces the assumption that the γ-ray sources are equally affected by changes in mass. A comparison between mass adjustment techniques is presented in Appendix B.

4.2.4 Pre-processing the γ-ray signals

As in Chapter 3, the γ-ray signals were pre-processed prior to PLSR calibration, in order to improve the signal to noise ratio. All pre-processing was carried out Matlab v7.14 (Mathworks, Massachusetts, 2012). In this chapter the wavelet transform is again used to denoise the signals and the thresholding techniques are also the same as Chapter 3. Local weighted regression (loess) was also used to smooth the spectra.

4.2.5 Partial Least Squares Regression

Principle component analysis (PCA) was used to identify any irregular γ-ray responses that can influence PLSR calibration. Following PCA, PLSR was again carried out in the R statistical environment (R Core Team, 2012), using the PLS1 algorithm in the 'pls' package (Mevik and Wehrens, 2007). PLSR was used to develop calibrations between the laboratory analysed soil properties and corresponding γ-ray signals. As the NSI samples were spatially independent and derived from a variety of parent materials, dividing the data into an independent and calibration dataset was deemed inappropriate, therefore internal validation was used. In order to mitigate over-fitting of the data, a leave-10-out CV was used to select the optimum number of latent variables. As with Chapter 3, the number of LVs was chosen based upon the lowest RMSECV (Eq. 4, page 10) and the precision and accuracy of the models was inferred from descriptive statistics. Accuracy was deduced by the coefficient of determination (R^2, Eq. 9, page 26) and the RPD (Eq. 7, page 26). As what constitutes a good model is somewhat subjective, the categories of RPD values outlined by Chang and Laird (2002) are referred to. A model that is capable of discriminating between high and low values, are those, which have an RPD between 1.4 and 2.0, whilst models exceeding 2.0 are seen as being capable of providing approximate quantitative predictions. A Principal component analysis of the data was conducted prior to modelling, in order to establish any outlying samples, which may weaken the PLSR predictions.

4.2.6 One-way ANOVA

To assess whether variations in soil-type and lithology have significant bearings on the precision of the PLSR models, a one-way ANOVA was performed in JMP 4.0.4. (SAS Institute Inc., Cary, 2001). Three factors were compared, the major soil group, the maximum geological period and parent material. The major soil group is a classification of soil characteristics that occur as a result of changes in parent material, through pedogenic processes (the classification criteria are presented in Avery, 1980). Each sample in the NSI has been classified and this information should help establish whether model inaccuracy is associated to particular soil groups. In airborne gamma-radiometric surveys, geological information is typically referred to in the analyses, in order to establish a radiometric baseline for a particular rock-type and subsequently assess the variation within each major geological unit. As soil characteristics are partly attributed to the lithology of the parent material, from which they have formed comparing impressions in the model to geological information should help in the identification of model error associated to differences in geology. The geological information referenced came from the British Geological Survey 1:625,000 geological map (BGS, 2008). The absolute residuals of the models were compared to these three factors using JMP 4.0.4. and R^2s were calculated by the following equation:

$$\boldsymbol{R^2} = \frac{\boldsymbol{Explained\ Variabilty\ of\ |e_i|}}{\boldsymbol{Total\ Variabilty\ of\ |e_i|}} \qquad \textbf{[Eq. 13]}$$

Where: $|e_i|$ are absolute values of the residuals produced by the model (Eq. 10), i.e. imprecisions to be explained.

4.3 Results

Sample statistics are presented in Table 5; the samples represent a broad range of soil textures and geochemical concentrations, reflecting the variations in parent material, land use and topography at the national scale. Sample distribution maps are presented in Figure 9, the predominant major soil groups are brown soils ($n = 102$) and surface water gleysols ($n = 43$), and the host geology is primarily mudstone ($n = 96$). A comparison between sample characteristics and the first principal component of their corresponding γ-ray signals are presented in Figure 10.

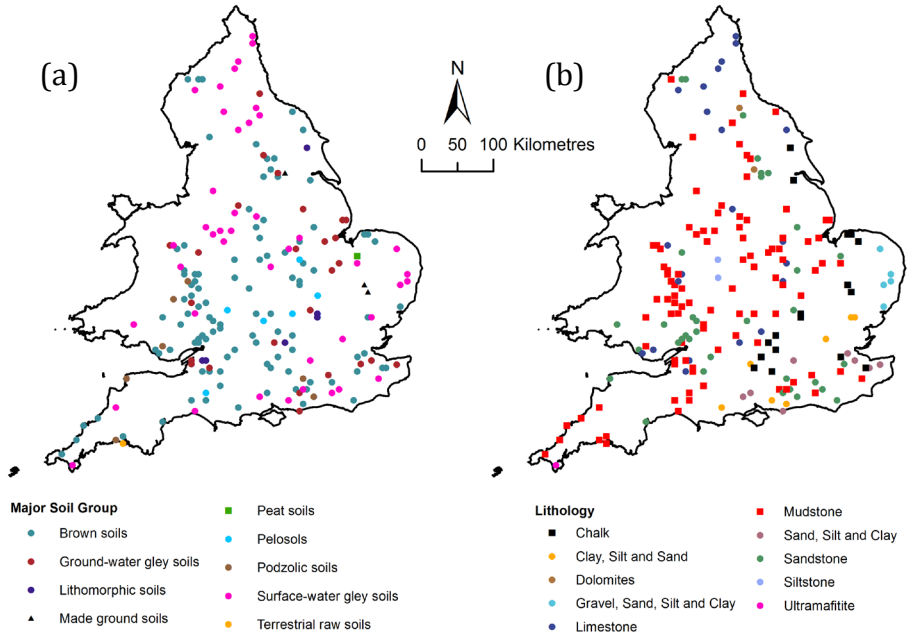

Figure 9 - Distribution of NSI samples and their corresponding (a) major soil group and (b) lithology. (Lithology's are presented in order of dominance, i.e. for 'Clay, Silt and Sand', clay is the dominant particle size)

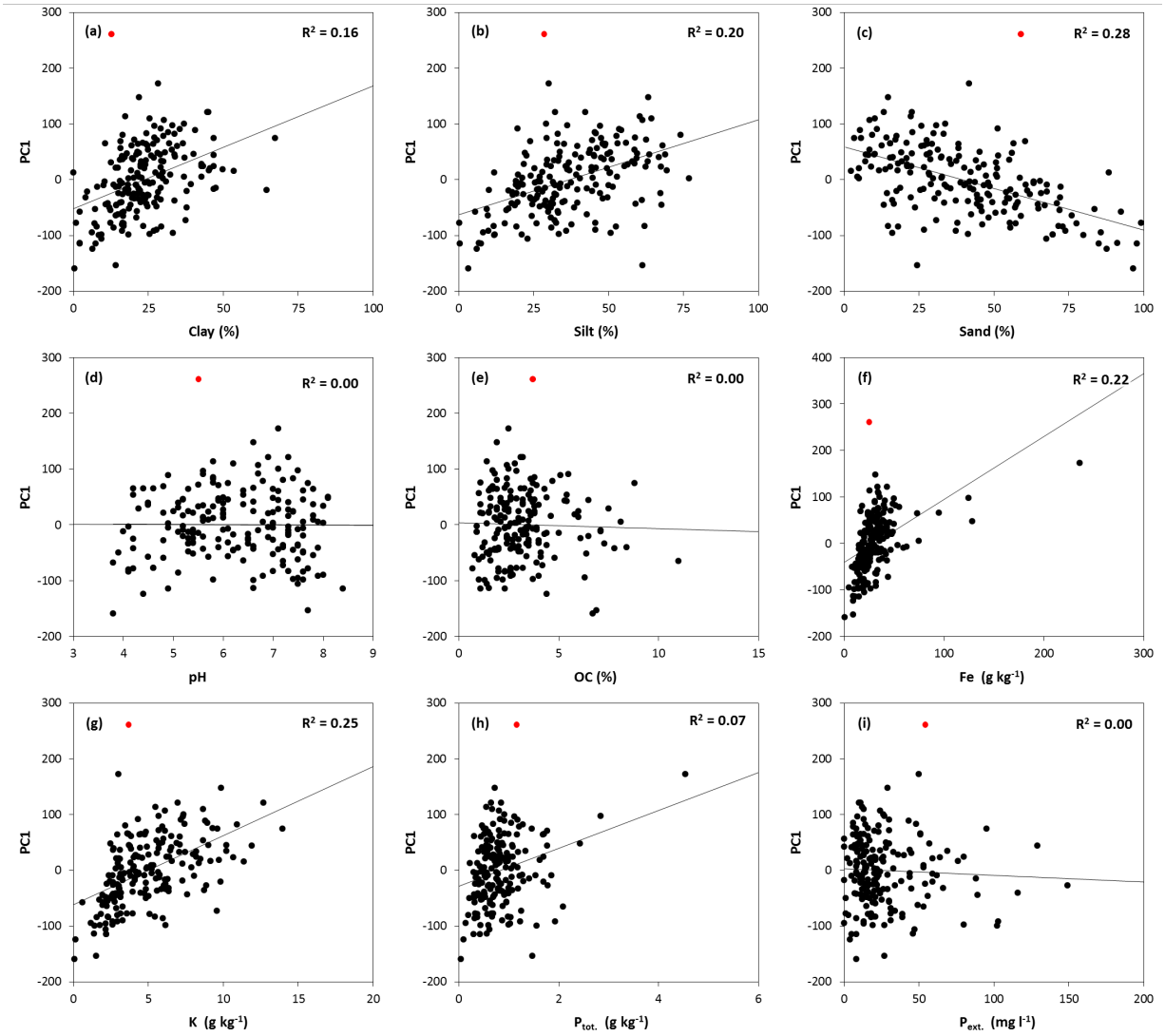

Figure 10 - Principal component score plots. PC1 versus (a) Clay, (b) Silt, (c) Sand, (d) pH, (e) OC, (f) Fe, (g) K, (h) $P_{tot.}$ and (i) $P_{ext.}$

The PCA score plots suggest a trend between the variation in the γ-ray signals and soil texture, with low γ-ray activity corresponding to elevated sand content. The relationship between total K concentration and γ-ray activity is also apparent (Figure 10g). It is apparent from the score plot that one sample (highlighted in red in all figures), is divergent from the rest of the samples, with a much higher score given. This sample was therefore removed, as it may provide unrepresentative associations in PLSR modelling. The spectral loadings of PC1 and PC2 are presented in Figure 11 (page 52); the loading plots show that the variation in the γ-ray response at energies <410KeV (largely attributed to the photoelectric effect)

are allocated considerably higher loadings than those attributed to terrestrial radionuclide activity (410 to 3,000 KeV). The high-energy cosmic γ-rays (3,000+ KeV) are a significant source of the variation in PC2. This variation between energies was therefore taken into consideration before constructing PLSR calibrations; with the models being constructed over three energy bands: the full spectrum (0 to 3,069 KeV), the energy range corresponding to terrestrial radioactivity (410 to 3,000 KeV) and the full spectrum minus low level energies (410 to 3069+ KeV).

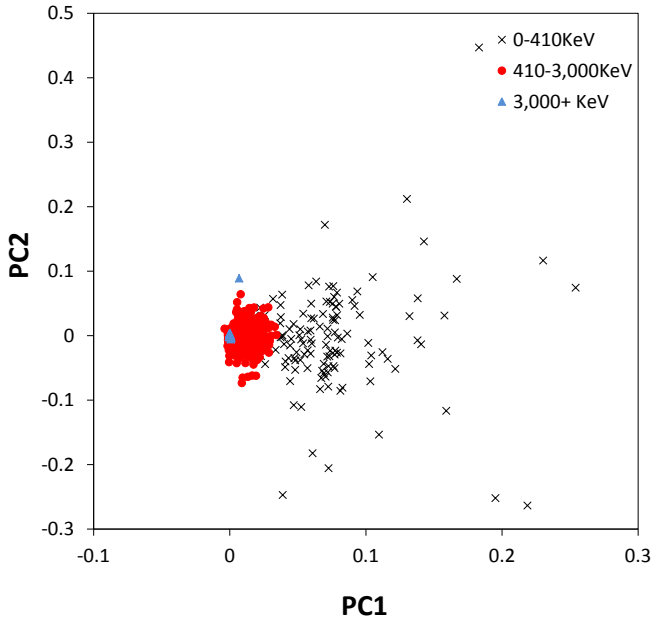

Figure 11 - Channel loadings, for principal components 1 and 2.

A comparison between PLSR models is presented in Table 6. Pre-processing the spectra by Loess and wavelet reconstruction from approximation coefficients produced models with the lowest RMSECV. Models were selected based on their RMSECV, as it is indicative of the prediction accuracy of the samples that were 'left-out' during cross-validation and therefore is suggestive of how well a model will perform on new spectra. The inclusion of all 195 samples into the PLSR models produced unsuccessful predictions for each soil property calibrated (with RPDs <1.4). The Fe and K model demonstrate the most significant relationships, both with R^2s of 0.48 and RPDs close to Chang & Laird's threshold of 1.4, which signifies a model capable of discriminating between high and low values.

Table 6 –PLSR statistics of the NSI calibration models.

Soil Property	[a]NF	[b]RMSECV	R^2	[c]RMSE	[d]RPD	[e]Energy range (KeV)	[f]Pre-processing Technique	
Clay (%)	1	10.26	0.22	10.11	1.1	410-3,000	Loess	α 4.00%
Silt (%)	2	14.31	0.31	13.60	1.2	410-3,000	Approx	Level 4
Sand (%)	1	18.44	0.34	18.13	1.2	410-3,000	Approx	Level 4
pH	2	1.12	0.16	1.06	1.1	Full	Approx	Level 5
OC (%)	3	1.70	0.14	1.59	1.1	410-3,000	Approx	Level 5
Total Fe (g kg^{-1})	2	18.15	0.48	15.88	1.4	Full	Loess	α 2.50%
Total K (g kg^{-1})	2	1.90	0.48	1.84	1.4	410-3,000	Approx	Level 6
$P_{tot.}$ (g kg^{-1})	11	0.47	0.08	0.41	1.2	410-3,069	Approx	Level 3
$P_{ext.}$ (mg/l^{-1})	1	24.22	0.01	23.90	1.0	Full	Approx	Level 2

[a]NF – Number of PLSR factors.
[b]RMSECV – leave-10-out cross-validated root mean-squared error
[c]RMSE – Root mean-squared error of predicted values
[d]RPD – Ration of prediction to deviation
[e]Energy Range – Energy range used in the PLSR model
[f]Pre-processing Technique – Where Approx is spectra reconstructed from the approximate coefficient and its corresponding level.

Loading weights for the PLSR models are presented in Figure 12 (page 54). The loading-weights of the particle size distribution models (Figure 12a,b,c) demonstrate the inverse relationship between sand fractions and the γ-ray activity associated with the decay of K, Th and U. Negative loadings are evident at the peaks related to the decay of Th (^{208}Tl peaks at c. 580 and 2,600KeV), K (^{40}K at c. 1,460KeV) and U (^{214}Bi at c. 609 and 1,120KeV). Conversely Clay, Silt, total P and K loading plots (Figure 12a,b,g,f), show positive loadings given to those peaks in the first principal components. The second principal component of K shows high loadings for the peak associated with ^{40}K, thus emphasising the fixed proportion between total K and its radioisotope ^{40}K. The models of pH, OC and extractable P models, which produced large high residuals and poor predictions, are less easily interpreted by their loading-weights, with high frequency fluctuations not attributed to the decay of the terrestrial radionuclides. High loadings in the pH and extractable P models are allocated to the low energy γ-rays (<410KeV), typically attributed to the photoelectric effect. In the OC model, high loadings are also found at the peak associated with the decay of U (^{214}Bi c. 609KeV). This degree of noise is

also reflected in the corresponding RMSECVs (Table 6), which were similar to 1 SD of the reference values; thus indicating a poor relationship.

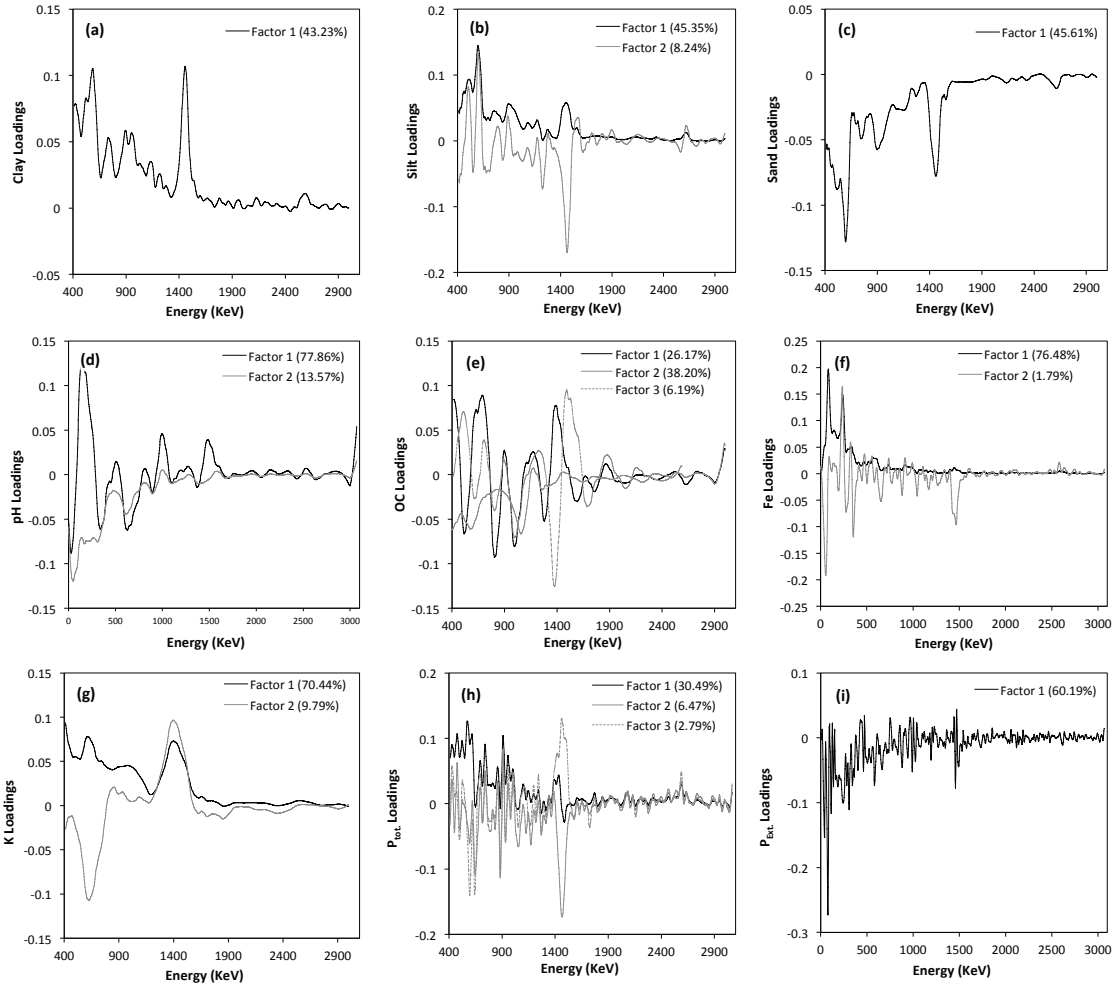

Figure 12 – PLSR model loading weights for for (a) Clay, (b) Silt, (c) Sand, (d) pH, (e) OC, (f) Fe, (g) K, (h) Ptot. and (i) Pext. The explained variance of each factor is presented in brackets.

Figure 13 provides a comparison between the laboratory analysed soil properties and their corresponding PLSR predictions. The PLSR predictions of K were able to effectively differentiate between high and low values more successfully than the other models. The correlation of the Fe model despite showing a similar correlation (R^2 of 0.48) to K, is principally driven by high concentrations, while low concentrations are predicted with poor precision. The particle size distribution plots also fail to reflect sample variation, with a significant proportion producing

erroneous results. A one-way ANOVA was used to assess how soil-type and geological differences contributed to model imprecision.

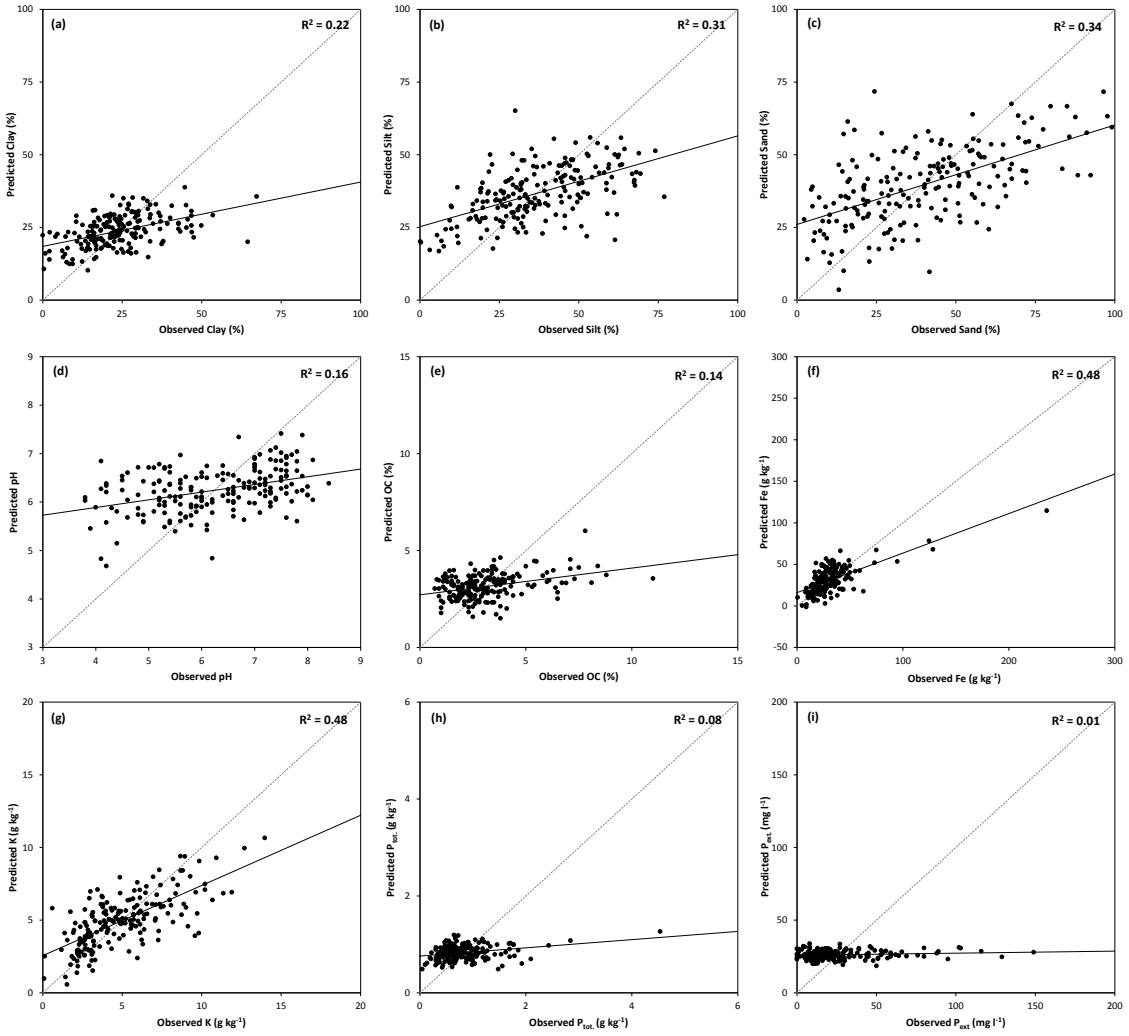

Figure 13 - Observed versus predicted plots of (a) Clay, (b) Silt, (c) Sand, (d) pH, (e) OC, (f) Fe, (g) K, (h) $P_{tot.}$ and (i) $P_{ext.}$

Figure 9a (page 50) shows the distribution of major soil groups represented in this study, it is apparent the selected samples are predominantly brown soils. Brown soils are widespread, mainly found on permeable materials, at elevations below about 300 m and are mostly located in agricultural areas (Avery, 1980). The ANOVA results show that the absolute mean residual ($|\bar{e}|$) of clay for brown soils was 6.5 %, which is considerably lower than the combined RMSECV of 10.3 %. The $|\bar{e}|$ of the surface-water gley soils was also lower at 6.1 %. At the 95 % significance level these soils groups produced significantly more accurate predictions than

ground-water gley soils. The brown soils and surface water gley $|\bar{e}|$ are also lower than the rest of the major groups (with the exception of peat soils, 2.1 %); however, given the limited number of samples in the rest of the major soil groups, these differences are not significant (at the 95 % confidence level). The geological factors used, do not appear to have a significant bearing on model precision, with R^2s <0.13 between these variables and $|e_i|$, for all soil characteristics tested (Table 7). Sand however, was significantly over-predicted in areas of chalk parent material (at the 95 % confidence level for limestone, mudstone and the areas of clay, silt and sand deposits).

Table 7 - Significance of Soil Group and Geological factors on the precision of the NSI calibration models, expressed in terms of R^2

Soil Property	Major Soil Group	Geological Period	Parent material
Clay	0.13	0.03	0.03
Silt	0.02	0.05	0.03
Sand	0.09	0.13	0.13
pH	0.10	0.11	0.08
OC	0.13	0.05	0.05
Fe	0.03	0.07	0.03
K	0.11	0.12	0.05
$P_{tot.}$	0.05	0.02	0.03
$P_{ext.}$	0.03	0.04	0.03

4.4 Discussion

4.4.1 Accounting for variations in mass

Accounting for variations in sample mass by examining the linear relationship between the mass of a representative sample and its corresponding total γ-ray counts, produced the most consistently low RMSECV (when compared with other techniques; results presented in Appendix B). Calculating this linear relationship meant that an estimation of the degree of background noise produced by the spectrometer could be made. Accounting for this constant source of radiation helped prevent unbalanced scaling, where low-mass samples would be given

disproportionally high counts and equally high-mass samples given unreasonably low-counts. It is important to acknowledge that by scaling the samples based on total counts forces the assumption that γ-rays over the entire energy range are equally affected by variations in mass. This assumption however, may not be accurate considering the majority of the variation in the spectra corresponds to the decay of K, Th and U. Further work is therefore required to verify this and establish whether the relationship between mass and radioactivity is consistently linear. If this technique does prove to be accurate, it may support other studies wishing to produce spectral libraries from samples of varying masses (or where cross-contamination of samples is a concern).

4.4.2 Model Selection

As with Viscarra Rossel *et al.,* (2006), the PLSR models were selected based on the lowest RMSECV. This indicator was used to determine the most effective technique of spectral denoising and how many LVs should be included in the PLSR calibration. The RMSECV values remained relatively consistent throughout pre-processing, with the differences in RMSECV between the un-processed spectra and the selected model generally being <4 % of 1 SD of the soil property of interest (8.8% pH and 5.6% OC). Despite the RMSECV remaining relatively constant, the R^2s between predicted and reference values were diminished with pre-processing in certain PLSR models (e.g. pH and OC), with strongly correlated associations being made from the unprocessed spectra (R^2 = 0.8 for pH and 0.7 for OC). However, on closer inspection it is apparent these models are based on a small fraction of the variation in the γ-ray spectra (<8.5 %) and are produced from high frequency fluctuations in the spectra (loading plots presented in Figure 14, page 58), which are more likely to be attributed to spectral noise rather than the decay of K, Th and U as illustrated by Figure 1 (page 9).

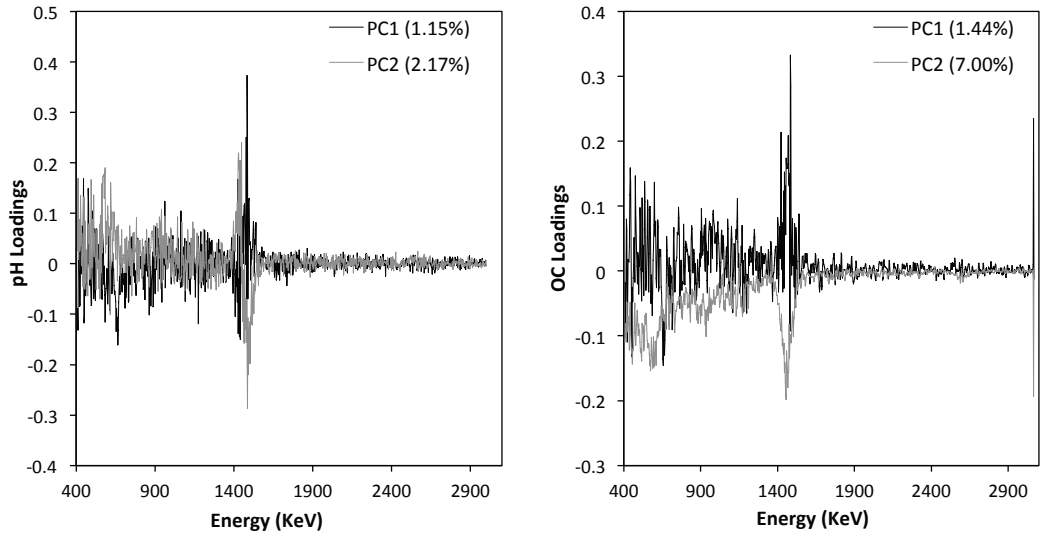

Figure 14 - Loading plots of pH and OC from unprocessed spectra

This therefore emphasises the importance of appropriate model selection and the removal of background 'noise' from the spectra, to mitigate false associations to soil properties from being made.

The RMSECVs of the models were typically high and comparative to one SD of the corresponding soil property; CV relies on the assumption that PLSR model performance is not sensitive to changes in the size of the calibration data (Dietterich, 1997), which given the broad array of land uses, topographies and geologies assessed in this study, may be false. To verify that the leave-10-out cross-validation was producing realistic indications of model precision, PLSR was re-run using LOOCV (Appendix B, Table B-5). The RMSECVs of the LOOCV were similar to the original models (leave-10-out CV), therefore suggesting that the original CV was providing a reasonable indication of model precision.

4.4.3 Model Interpretation

Particle Size Distribution Despite unsuccessful predictions of soil texture being made at the national scale, the corresponding PLSR loading weights indicate the association between γ-ray activity (associated with the decay of K, Th and U) and clay content. The ANOVA results (presented in full in Appendix C) indicate that soil group and geology are largely independent of model inaccuracies, however, as an

unbalanced sampling design was used (due to limitations of sample mass); certain groups contained a limited number of samples, thus making the differences insignificant at the 95 % confidence level. In spite of this, certain trends can be seen in the ANOVA, sand content for example, was typically over predicted in areas of chalk parent material, which considering the negative loadings in the sand PLSR model may be attributed to chalk deposits being associated with low γ-ray activity (Dickson & Scott, 1997). This notion is further supported in the clay and silt models, with inaccuracies being linked to areas of chalk (though to a lesser extent). The ANOVA results also show that model imprecision tended to be associated with soil groups containing fewer samples (in comparison to those with numerous samples), indicating model bias toward the groups that represent the majority of the dataset. Predictions of clay for example were significantly more accurate (95 % confidence level) in areas of brown soils compared with ground water gleys. A comparison between clay content (observed) and residual clay is presented in Figure 15a and reveals that the model is failing to reflect the extremes of the clay distribution; with over-predictions being found for low levels of clay and equally high clay content is being under-predicted.

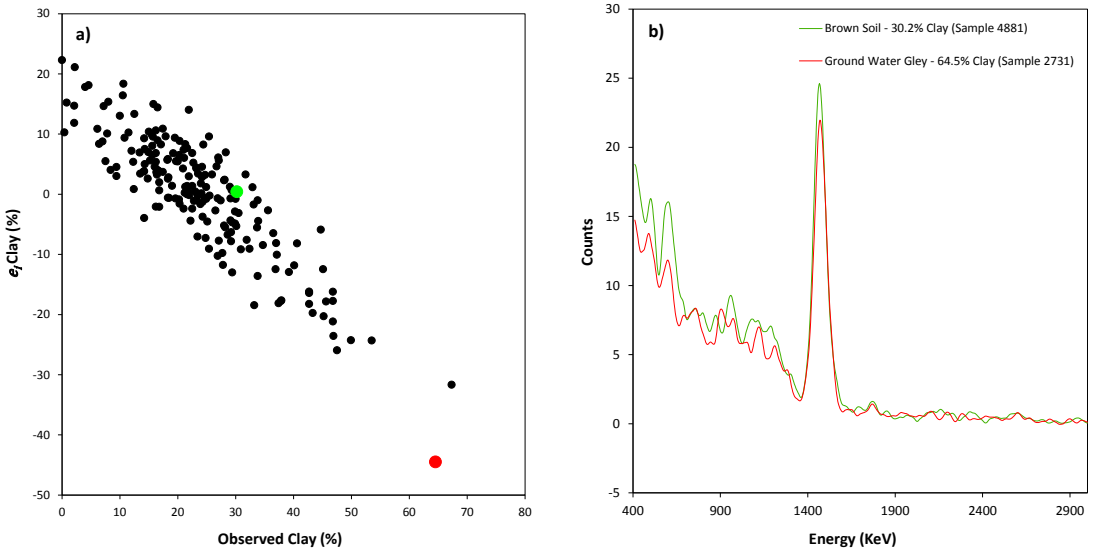

Figure 15 - (a) Comparison between Observed and Residual Clay and (b) example spectral responses of different soil groups, with corresponding samples highlighted in (a).

A comparison between a spectral response of a ground-water gley soil producing an inaccurate estimate of clay (under-prediction of -44 % clay) and an accurately predicted brown soil (over prediction of 0.4 % clay) is presented in Figure 15b. It is apparent from the spectral comparison that despite having twice the clay content of the brown soil sample, the surface water gley emitted less γ-ray counts associated with the decay of ^{40}K (1,460 KeV) and the daughter products of Th and U (580, 1,120 KeV respectively). The difference in accuracy (in terms of absolute residuals,$|e_i|$) between brown soils and ground water gleys was statistically significant, which may indicate that the radionuclide concentrations of these soils are dissimilar to one another and therefore should be classified separately in future studies. The majority of samples in this model were brown soils ($n = 102$) and a large proportion of samples had clay content between 15 and 40 %, for effective analysis a greater number of samples from other soil types and a larger array of clay content is required, to verify the trends observed.

Previous studies (e.g. Van Egmond *et al.,* 2008; Viscarra Rossel *et al.,* 2007) have demonstrated that at the within-field scale, γ-ray activity can offer a useful surrogate for mapping soil texture, with accurate predictions being made (R^2s >0.75). The results from this study however, are much weaker, which suggests that variation in γ-ray activity at the national scale is not entirely reflective of particle-size but rather a function of additional factors such as land-use and geology. At the within-field scale these coarse-scale factors remain relatively constant and variation in γ-ray activity is primarily indicative of geochemical differences. Rawlins *et al.* (2007) for example reported that much of the variation in Th in Eastern England is driven by changes in parent material and therefore may largely be irrespective of soil textural variations. Similarly, whilst Rawlins *et al.* (2007) report that a substantial proportion of the variance in K can be accounted for by variations in geochemistry, a study by Boukhenfouf and Boucenna (2011) demonstrates that the application of K bearing fertilizers may lead to elevated concentrations of K. Although in their study the ^{40}K concentration of fertilized soils was within the world average range, they found phosphate fertilizers (NPK fertilizers) to contain between 14 and 31 times as much ^{40}K as the world average

and therefore suggested that the use of such fertilizers is likely to result in increased ^{40}K activity in the soils over time. As high positive loadings were given to K and Th in the soil texture models, factors such as this may have contributed to poor model performance. For γ-ray spectroscopy to successfully increase the spatial resolution of traditional soil surveys, factors such as this need to be considered in the sampling design.

pH Predictions of pH in this study are similar to those reported by Taylor *et al.,* (2010) who reported an R^2 of 0.05 for within-field pH predictions from a portable γ-ray spectrometer. The pH loading plot indicates an inverse relationship to sand content (Figure 12d), an association also observed by Viscarra Rossel *et al.,* (2007) and possibly suggestive of increased pH buffer capacity being associated with elevated CEC. Whilst pH is governed by factors such as parent material and CEC that are reflected by γ-ray activity, management practices such as lime-application and crop rotation can also impact pH (Taylor J.A. *et al.,* 2010). Although soil pH is sensitive to such management practices, the γ-ray signals may be less responsive, which would also support the findings by Viscarra Rossel *et al.,* (2007), who found variations in subsoil pH to be predicted to a higher degree of accuracy (R^2 of 0.62) than topsoil samples (R^2 of 0.4), which are more susceptible to the application of liming materials (Brady and Weil, 2008).

Organic Carbon The OC model shares similar loadings to that of the clay model and CEC, reflective of the similar ability of OC and clay to adsorb radionuclides. Martz and de Jong (1999) found OC and clay to be related in a small agricultural catchment of Canada (where parent material remained constant); the relationship between (standardised) OC and Clay for the samples in this study however, was not significant (R^2 of 0.05) and may help to explain the poor precision of the predictions.

Total Fe Positive loadings in the Fe model were found at the peaks associated with K, Th and U, supporting findings by Saccà *et al.* (2011), whose findings suggest that Fe is principally associated with clay content. Positive loadings were also found at energies <410 KeV similar to the CEC model presented in Chapter 3,

which may indicate that elevated Fe concentrations (e.g. Fe^{3+} and Fe^{2+}) are associated to areas of high CEC. Fe concentrations were relatively well predicted by PLSR (R^2 of 0.48), however the inclusion of all 195 samples meant that this relationship was principally driven by one high concentration sample (235.8 g kg^{-1}), with this sample removed the association was weaker (R^2 of 0.39), suggesting that whilst the model could distinguish between high and low concentrations, it was less suited to predicting lower concentrations.

Total K Of the soil characteristics modelled by PLSR, predictions of total K were the most accurate (R^2 of 0.48). Positive loadings in both PLSR factors were found at the peak associated with the decay of ^{40}K. Despite isotopic K occurring as a fixed ratio of natural K (0.012 %, IAEA, 2003) the model was ineffective at predicting the distribution of total K (RPD of 1.39). Wong and Harper (1999) report strong predictions (R^2 of 0.90) of total K in topsoils of Jerramungup, Western Australia using ^{40}K measurements taken from an Exploranium GR 256 portable γ-ray spectrometer. They also state that ^{40}K occurs as a direct measure of total K, irrespective of the form in which the K fractions occur. The inaccuracy of the predictions in this paper may be therefore likely to be a result of imprecision in γ-spectral acquisition (such as spectral drift), spectral processing (mass correction and denoising) or total K determination.

Phosphorus (total and extractable) The results indicate that γ-ray signals are an ineffective surrogate for the prediction of phosphorus at the national scale. Both $P_{tot.}$ and $P_{ext.}$ models had loading plots with high-frequency components, unlike the original spectra and thus are indicative of over-fitting. Mahmood *et al.* (2011) used the windows method to predict $P_{tot.}$ from γ-ray activity associated with the decay of U and also report unsuccessful P_{tot}. predictions between management zones (R^2 of -0.12). An inverse relationship between U and P_{tot}, is also inferred by the loading plots in this study, however given the high-frequency components, this association may not be significant.

4.4.4 - Recalibration of a single soil type.

Table 8 – PLSR statistics of brown soil calibration models.

Soil Property	n	[a]NF	[b]RMSECV	R^2	[c]RMSE	[d]RPD	[e]Energy Range (KeV)	[f]Pre-processing Technique	
Clay (%)	102	1	7.96	0.26	7.73	1.2	410-3,000	Loess	4.00%
Silt (%)	102	1	15.41	0.23	14.89	1.1	410-3,000	Approx	Level 4
Sand (%)	102	1	18.79	0.31	18.17	1.2	410-3,000	Approx	Level 4
pH	99	2	1.07	0.21	0.97	1.1	Full	Approx	Level 5
OC (%)	102	3	1.57	0.20	1.35	1.1	410-3,000	Approx	Level 5
Fe (g kg^{-1})	101	2	17.38	0.50	14.16	1.4	Full	Loess	2.50%
K (g kg^{-1})	102	2	1.94	0.41	1.84	1.4	410-3,000	Approx	Level 6
$P_{tot.}$ (g kg^{-1})	101	1	0.45	0.10	0.42	1.1	410-3,069	Approx	Level 3
$P_{ext.}$ (mg l^{-1})	102	1	22.27	0.04	21.69	1.0	Full	Approx	Level 2

[a]NF – Number of PLSR factors.
[b]RMSECV – leave-10-out cross-validated root mean-squared error
[c]RMSE – Root mean-squared error of predicted values
[d]RPD – Ration of prediction to deviation
[e]Energy Range – Range of energy channels used in the PLSR model
[f]Pre-processing Technique – Where Approx is spectra reconstructed from the approximate coefficient and its corresponding level.

The majority of the samples in this study were classified as brown soils; in order to determine whether model performance could be improved by calibrating a particular soil group, the PLSR model was rerun on brown soils alone. The same pre-processing techniques as before (Table 6) were used for calibration and the models were validated using a LOOCV (as used in Chapter 3). The elevated Fe sample (discussed in section 4.4.3) was removed from the Fe model, to avoid an unrepresentative R^2. There was also an extreme and potentially influential sample of P_{tot} that was removed, which had a sample with a concentration of 4.5 g kg^{-1}, with the next largest recorded value at 2.8 g kg^{-1}. Developing a model based on the brown soils reduced the RMSECV of clay from 10.26 % to 7.96 % and increased the R^2 from 0.22 to 0.26, suggesting that the inclusion of dissimilar soil groups influenced model performance. Predictions of Fe and K were also improved, with RPDs indicating that they are capable of distinguishing between high and low concentrations (Chang and Laird, 2002). Silt and sand predictions were weaker in comparison to the calibration of the entire sample population; as brown-soils are

typically associated with agricultural land use, differences in land management practices such as the application of K-bearing fertilizers may have contributed to the masking of these relationships.

4.4.5 Suggestions for further work

The unbalanced sampling design and limited number of samples used in this study meant it was difficult to determine trends between major soil groups and their corresponding γ-ray response. Whilst the results indicate that certain host geologies and soil groups produced higher degrees of inaccuracy than others, these trends were typically insignificant (at the 95 % confidence level) given the limited samples used. For future national scale calibrations to be constructive, a balanced sampling design that comprises numerous samples in each soil group is recommended. This would allow an assessment of how changes in soil type and parent material affect prediction accuracy.

In future studies on the NSI or other datasets where mass correction of γ-ray spectra is required, subsequent analysis is required to determine whether the relationship between γ-ray activity and sample mass is always linear and whether the influence of mass on the γ-ray spectrum is uniform over the entire energy range. In order to do this numerous samples would need to be collected for each lithology tested and each sample would need to be measured in the γ-ray spectrum analyser over different increments of sample mass.

It is also important to recognise that the samples in this study were taken prior to the Chernobyl disaster and therefore precede the associated ^{137}Cs fallout. This fallout would therefore need to be considered for samples acquired after 1986, as peaks in the spectra corresponding to the decay of ^{137}Cs (660 KeV) may be indicative of ^{137}Cs precipitation following the event, rather than being linked to any soil characteristics. Historic rainfall data should therefore be consulted to mitigate false associations being made from γ-ray peaks at 662 KeV.

4.5 Conclusion

The results suggest that the distribution of radionuclides at the national scale is not principally associated to variations in soil texture, with inadequate predictions being made from full γ-ray signals. Although the relationship between γ-ray activity and clay content at the within-field scale is widely reported (e.g. Viscarra Rossel *et al.,* 2007; Van Egmond *et al.,* 2010), this association does not appear to hold between different host geologies and soil-groups. Subsampling of the NSI was dictated by sample mass, which forced the adoption of an unbalanced sampling design. In this study the limited distribution of samples prevented any conclusive trends between soil type and γ-ray activity from being made. For γ-ray spectroscopy to be a practical tool for updating national soil datasets, further work is required to establish whether the trends observed in this study are accurate.

Chapter 5 - General Discussion

This objective of this study was to establish whether γ-ray spectroscopy could provide valuable information about soil status, beyond the farm scale. The results indicate that whilst fair predictions of soil properties may be achieved at a regional scale, variations in soil type and lithology can influence γ-ray signals and impair predictions. The findings from Chapter 3 suggest that laboratory acquired γ-ray signals are capable of providing site-independent predictions of CEC at a regional scale. At the national scale however, the relationship between γ-ray activity and soil texture was more tenuous and produced imprecise predictions. Whilst previous site-specific studies have demonstrated that γ-ray spectroscopy can be a useful surrogate for soil texture, the majority of soil texture variation occurs at fine-scales (20 to 200 m; McBratney and Pringle, 1999), which therefore may make it an unsuitable property for modelling at coarser scales. For instance at the national scale, the distribution of radionuclides may principally reflect factors such as parent material and therefore mask local relationships between γ-ray activity and soil texture.

The mixed results of this study indicate that further topics need to be considered, for γ-ray spectroscopy to become a viable technique for monitoring soil at coarse scales. The purpose of this chapter is to discuss the implications of this study and propose how subsequent research could follow on from this study. Firstly, a short overview is given as to the effect different spectral pre-processing techniques had on model performance and provides recommendations for future applications (Section 5.1). Section 5.2 discusses the effect scale has on the use of γ-ray spectroscopy and proposes further studies to attain a greater understanding of how coarse scale factors may influence a soil's γ-ray response. Section 5.3 discusses how supplementary data may help to develop our understanding of radionuclide distributions.

5.1 Spectral pre-processing

The results have shown that robust PLSR calibrations can be formed from pre-processed γ-ray spectra, with lower RMSECV values produced in comparison to models formed from unprocessed spectra. The results further suggest that calibrating unprocessed γ-ray signals can produce misleading results, by utilising high-frequency components in the spectra, which explain little of the variation in the γ-ray response. Pre-processing the γ-ray spectra allowed more of the spectral variation to be explained and models were typically based on the energy channels of the spectra related to the decay of K, Th, and U. Spectral pre-processing therefore appears essential to producing robust and reliable predictions of soil characteristics.

The pre-processing techniques that take into account the frequency of the γ-ray response, in addition to the intensity of the response appear to outperform methods such as the Savitzky-Golay filter, which smooth the spectra in the energy domain alone. The findings therefore seem to support Gang *et al.,* (2004) who suggest that methods such as the Savitzky-Golay filter may distort γ-ray responses, through the loss of analytically significant peaks. Additionally, the results also indicate that wavelet thresholding leads to higher model imprecision than reconstructing the spectra from the approximation coefficients alone. This may be because the peaks produced from the decay of K, Th and U are low frequency, high-scale components and are therefore largely returned by the approximation coefficients. For future PLSR calibrations of γ-ray spectra techniques such as the wavelet transform and loess, appear to be more effective than traditional techniques such as the Savitzky-Golay filter.

5.2 Effects of Scale

The results from Chapter 4 support the work of Bierwirth (1996b), who suggests that relationships between soil characteristics and the distribution of radionuclides do not necessarily hold over different soil types and host geologies. Whilst a comparison between lithology and soil type is given in Chapter 4, the sample size and geological factors considered are not sufficient to draw any firm

conclusions. Subsequent studies will therefore need to be conducted, to both establish how baseline radionuclide concentrations vary over England and Wales and how they relate to differences in geology. In addition, further research is also required to understand how geological events such as the Devensian glaciation may have redistributed radionuclide concentrations and the subsequent affects this may have on the relationships to soil properties.

A greater understanding of the general distribution of radionuclides is critical to the development of soil monitoring through γ-ray spectroscopy, as it will assist in distinguishing between trends in γ-ray activity within geological subclasses (that are potentially associated with soil properties) and coarser variations that may correspond to geology. The poor overall correlation between soil texture and γ-ray activity at the national scale, may therefore be a result of differences in geology being more dominant in γ-ray activity than the local differences in soil texture. These coarse scale differences in γ-ray activity would therefore need to be accounted for, in order to uncover the fine-scale variations in soil texture. It is also essential that land-management history be incorporated in to the interpretation of future studies, as studies have shown that the application of K-bearing fertilisers may also affect ^{40}K activity.

Savvides *et al.,* (2010) used geostatistics to demonstrate that the relationship between VNIR spectra and CEC is scale dependent, with relationships being masked at fine (2 to 50 m) and coarse (>2,000 m) scales. A similar geostatistical approach would be advantageous in the development of γ-ray spectroscopy as a soil-monitoring tool, to establish to what extent the variation in γ-ray activity is attributed to coarse scale factors. For example, whilst the results of Chapter 3 suggest there is a relationship between γ-ray activity and CEC at a regional scale, without evaluating at what scale variations in the γ-ray signals occur, it is difficult to establish whether the signals relate to fine-scale variations in soil texture or coarse scale factors such as soil type. The study by Savvides *et al.,* (2010), show that the variation of CEC in Chapter 3, was primarily found at coarse scales (>2,000 m), which may suggest that γ-ray activity reflected these coarse scale variations. If this is the case, then calibrations of γ-ray signals at the regional and national scale

may be more suited to the prediction of soil properties, which vary over wider distances rather than characteristics such as soil texture that vary over fine scales.

5.3 Data fusion

Results presented by Taylor *at al.* (2010) and Piikki *et al.* (2013) have shown there is no significant benefit to sensor coupling (such as the inclusion of EC_a data) in the prediction of clay from γ-ray data at the within-field scale. At the regional and national scale however, the results presented in this study and former airborne studies (Bierwirth, 1996b) indicate that the distribution of radionuclides is influenced by changes in geology and soil type and thus for reliable predictions to be made at these scales, it is essential these factors are considered during calibration and interpretation. In this study the effects of lithology and soil type were considered, however additional factors may also be need to be considered, such as the presence of superficial material, which may differ from the underlying lithology.

A recent study by Dent *et al.* (2013) showed that the distribution of radionuclides in the Cariboo Region, British Columbia reflected differences in mineralogy and lithology. Using ternary airborne radiometric images, they showed that variations in K, U and Th corresponded to differences in soil type of the area. However, they also report that they were unable to establish a consistent relationship between γ-ray activity and soil texture, despite certain trends being apparent in particular regions. They note that in Australia coarse textured soil is typically associated with low γ-ray activity because it is derived from the weathering of siliceous material (which has low γ-ray activity), whilst in British Columbia high γ-ray activity is linked to coarse, recently eroded and deposited materials (with higher γ-ray activity). For future studies on the association between γ-ray activity and soil texture, an initial assessment of ternary airborne radiometric images and geomorphological information may help to establish a better understanding of the relationship to soil texture, for a given area.

In summary then, the findings suggest that given the present knowledge about the distribution of radionuclides in England and Wales, γ-ray spectroscopy is an

inappropriate technique for soil sensing at the national scale. Further work is needed to establish geological baselines of radioactivity for this technique is to be viable at these coarse scales.

Chapter 6 - Conclusion

The findings of this study show that γ-ray spectroscopy can provide useful predictions of soil status at the regional scale, whilst at the national scale, variations in γ-ray activity appear to largely reflect differences in soil type and host geology. Using a laboratory-based γ-ray spectrum analyser, it was possible to eliminate environmental noise associated with measuring γ-ray activity in situ. PLSR was then used to calibrate these γ-ray responses and proved to be a useful technique of predicting CEC at the regional scale. Reasonable independent predictions of CEC (R^2 of 0.62) were made for an expansive agricultural region in Eastern England. The results therefore signify an improvement on previous CEC predictions in the area from VNIR spectra (R^2 of 0.24, Savvides *et al.,* 2010) and offer a greater potential for in situ applications. High values of CEC were associated with the decay of K, Th and U, potentially reflecting the positive relationship between clay content and CEC. Additional research is required to establish whether γ-ray activity at the regional scale primarily reflects fine-scale variations such as soil texture, or conversely are dominated by aspects such as parent material that relate to soil composition.

More tenuous results were found at the national scale, indicating that local relationships between γ-ray activity and soil properties (such as soil texture) may not necessarily hold at coarse scales. The results indicate that radiometric baselines vary between soil types and subsequently mask any localised variations in physical and chemical soil properties. The findings suggest certain trends between soil type and the level of γ-ray activity, samples taken from areas of chalk for instance appear to be associated with lower γ-ray activity. The samples used in this national scale study, varied in mass, which prevented the adoption of a stratified sampling scheme and also meant sample mass had to be accounted for prior to calibration. Employing an unstratified sampling scheme had implications on the study; for example, it was difficult to acquire a representative variation of γ-ray signals from different soil types, which in turn prevented any firm conclusions about radiometric baselines from being made. In order for γ-ray spectroscopy to be an effective tool for supplementing national soil surveys these coarse variations

would need to be considered and accounted for, to expose the local variations in soil properties that are of interest. In order to account for such regional trends, a greater number of samples from each soil type and underlying geology would need to be considered, to establish the significance of these variations in γ-ray activity. The use of the NSI sample also forced an assumption about the influence mass has on the γ-ray response; the results of the national scale study rely on the assumption that all aspects of the measured spectra to respond equally to changes in sample mass. This may not be the case, however as the majority of the variation in the γ-ray spectrum is found at the peaks attributed to the decay of K, Th and U, further research is therefore required to establish whether this assumption is reasonable.

In summary, this study has demonstrated that γ-ray spectroscopy may be a useful alternative to conventional soil sampling at the regional scale, by showing fair predictions of CEC. At the national scale however, it appears that coarse trends in γ-ray activity need to be accounted for, in order to examine finer-scale variations that may pertain to differences in soil characteristics. Currently, there is limited information available about these coarse scale variations in γ-ray activity for England and Wales, further study is therefore critical to the development of γ-ray spectroscopy as a soil monitoring technique. Given the present lack of this coarse scale data, it was not possible to account for these coarse trends and therefore no significant relationships between γ-ray activity and soil properties were found at the national scale.

References

Adamchuk, V.I., Hummel, J.W., Morgan, M.T., Upadhyaya, S.K., 2004. On-the-go soil sensors for precision agriculture. Computers and Electronics in Agriculture 44, 71-91.

Anjos, R.M., Okuno, E., Gomes, P.R.S., Veiga, R., Estellita, L., Mangia, L., Uzeda, D., Soares, T., Facure, A., Brage, J.A.P., Mosquera, B., Carvalho, C., Santos, A.M.A., 2004. Radioecology teaching: evaluation of the background radiation levels from areas with high concentrations of radionuclides in soil. European Journal of Physics 25, 133-144.

Avery, B.W., 1980. Soil Classification for England and Wales (Higher Categories). Soil Survey Technical Monograph No. 14. Soil Survey of England & Wales, Harpenden.

Avery, B.W., Bascomb, C.L., 1982. Soil survey laboratory methods. Soil Survey of England and Wales, Harpenden.

Beebe, K.R., Pell, R.J., Seasholtz, M.B., 1998. Chemometrics: A Practical Guide. John Wiley & Sons, New York.

Bellamy, P.H., Loveland, P.J., Bradley, R.I., Lark, R.M., Kirk, G.J.D. 2005. Carbon losses from all soils across England and Wales 1978-2003. Nature 437, 245-248.

Bierwirth, P.N., Gessler, P.E., McKane, D., 1996a. Empirical investigation of airborne gamma-ray images as an indicator of soil properties - Wagga Wagga, NSW. In: 8th Australasian Remote Sensing Conference Proceedings, Canberra, Australia.

Bierwith, P.N. 1996b. Gamma-Radiometrics: A Remote Sensing Tool for Understanding Soils. Australian Collaborative Land Evaluation Project Newsletter 5, 12-14.

Boukhenfouf, W., Boucenna, A., 2011. The radioactivity measurements in soils and fertilizers using gamma spectrometry technique. Journal of Environmental

Radioactivity 102, 336–339.

Brady, N.C., Weil, R.R., 2008. The Nature and Properties of Soils, fourteenth international ed. Prentice Hall, New Jersey.

Brazier, R.E., Rowan, J.S., Anthony, S.G., Quinn, P.F., 2004. "MIRSED" towards an MIR approach to modelling hillslope soil erosion at the national scale. Catena 42, 59-79.

Brenchley, P.J., Rawson, P.F., 2006. The Geology of England & Wales, second ed. Geological Society Publishing House, Bath.

British Geological Survey, 2008. Digital Geological Map of Great Britain 1:625 000 scale (DiGMapGB-625), bedrock data [CD-Rom]. Version 5.17. Keyworth, Nottingham: British Geological Survey. Release date 11-2-2008.

Carrier, F., Bourdon, B., Pili, E., Truffert, C., Wyns, R., 2006. Airborne gamma-ray spectrometry to quantify chemical erosion processes. Journal of Geochemical Exploration 88, 266-270.

Chang, C.W., Laird, D.A., 2002. Near-infrared reflectance spectroscopy analysis of soil C and N. Soil Science 167, 110–116.

Chapman, H.D., 1965. Cation-exchange capacity. In: C.A. Black (Ed.). Methods of soil analysis - Chemical and microbiological properties. Monographs on Agronomy 9, 891-901.

Cleveland, W.S., 1979. Robust Locally Weighted Regression and Smoothing Scatterplots. Journal of the American Statistical Association 74, 829–836.

Corstanje, R., Kirk, G.J.D., Pawlett, M., Read, R., Lark, R.M., 2008. Spatial variation of ammonia volatilization from soil and its scale-dependent correlation with soil properties. European Journal of Soil Science 59, 1260-127.

Daubechies, I. 1991. Ten Lectures on Wavelets. Society for Industrial and Applied Mathematics, Philadelphia.

Dent, D.L., MacMillan, R.A., Mayr, T.L., Chapman, W.K., Berch, S.M., 2013. Use of Airborne Gamma Radiometrics to Infer Soil Properties for a Forested Area in British Columbia, Canada. Journal of Ecosystems and Management 14, 1-10.

Dickson, B.L., Scott K.M. (1997) Interpretation of aerial gamma-ray surveys – adding the geochemical factors. Journal of Australia Geology & Geophysics 17, 187-200.

Dierke, C., Werban, U., Dietrich, P., 2011. Towards a better understanding of γ-ray for soil mapping - analysis of γ-ray measurements at field sites across Europe Proceedings of the Second Global Workshop on Proximal Soil Sensing, 15-18 May, Montreal, Contribution in proceedings. 128 – 131

Dietterich, T.G., 1997. Machine Learning Research: Four Current Directions. Artificial Intelligence Magazine 18, 97-136.

Donoho, D.L., Johnstone, I., 1994. Ideal Spatial Adaptation by Wavelet Shrinkage. Biometrika 81, 425-455.

Donoho, D.L., 1995. De-noising by soft-thresholding. IEEE Transactions on Information Theory 41, 613-627.

European Comission (EC), 2012. The implementation of the Soil Thematic Strategy and on-going activities. Report From The Commission To The European Parliament, The Council, The European Economic And Social Committee And The Committee Of The Regions, Brussels. URL: http://eur-lex.europa.eu/LexUriServ/LexUriServ.do?uri=COM:2012:0046:FIN:EN:PDF

Gang, X., Li, D., Benai, Z., Jianshi, Z., 2004. A Nonlinear Wavelet Method for Data Smoothing of Low-level Gamma-ray Spectra. Journal of Nuclear Science and Technology 41, 73-76.

Godfray, H.C., Beddington, J.R., Crute, I.R., Haddad, L., Lawrence, D., Muir, J.F., Pretty, J., Robinson, S., Thomas, S.M., Toulmin, C., 2010. Food Security: The Challenge of Feeding 9 Billion People. Science 327, 812-818.

Georadis, 2010. Laboratory Gamma Ray Spectrum Analyser – RT-50 User Manual, eighth ed. Georadis, Brno.

Hendriks, P.H., Limburg, J., de Meijer, R.J., 2001. Full-spectrum analysis of natural gamma-ray spectra. Journal of Environmental Radioactivity 53, 365-380.

Hendriks, P.H., Maucec, M., de Meijer, R.J., 2002. MCNP modelling of scintillation-detector gamma-ray spectra from natural radionuclides. Applied Radiation and Isotopes 57, 449-457.

Horng, M.C., Jiang, S.H., 2004. In situ measurements of gamma-ray intensity from radon progeny in rainwater. Radiation Measurements 38, 23-30.

Huang, P.M., Li, Y., Sumner, M., 2012. Handbook of Soil Sciences: Principles and Processes. CRC Press, Boca Raton.

Hyvönen, E., Turunen, P., Vanhanen, E., Arkimaa, H., Sutinen, R., 2005. Airborne Gamma-ray Surveys in Finland. Geological Survey of Finland 39, 119-134.

International Atomic Energy Agency (IAEA) 2003. Guidelines for Radioelement Mapping Using Gamma Ray Spectrometry Data. IAEA-Technical Document 1363, International Atomic Energy Agency, Vienna.

Knoll, G.F., 2010. Radiation Detection and Measurement, fourth ed. John Wiley & Sons, New York.

Kutsch, W.L., Bahn M., Heinemeyer, A., 2009. Soil Carbon Dynamics: An Intergrated Methodology. Cambridge University Press, Cambridge.

Kweon, G., Lund, E., Maxton, C., 2013. Soil organic matter and cation-exchange capacity sensing with on-the-go electrical conductivity and optical sensors. Geoderma 199, 80-89.

Lal, R., 1991. Soil structure and sustainability. Journal of Sustainable Agriculture 4, 67–92.

Lark, R.M., Webster, R., 1999. Analysis and elucidation of soil variation using wavelets. European Journal of Soil Science 50, 185–206.

Larson, W.E., Robert, P.C., 1991. Farming by Soil. In: Lal, R., Pierce, F.J. (Eds.), Soil Management for Sustainability. Soil and Water Conservation Society, Ankeny, 103–120.

Lee, K.S., Lee, D.H., Sudduth, K.A., Chung, S.O., Kitchen, N.R., Drummond, S.T., 2009. Wavelength identification and diffuse reflectance estimation for surface and profile soil properties. Transactions of the American Society of Agricultural and Biological Engineers 52, 683–695.

Loonstra, E. H., 2010. Mapping Clay Content in Northwest Europe with a Mole -A First Attempt towards Universal Calibration Models. The Soil Company, Groningen.

Loonstra, E.H., Van Egmond, F.M., 2009. On-the-go Measurement of soil Gamma Radiation. The Soil Company, Groningen.

McGrath, S.P., Loveland, P.J., 1992. The Soil Geochemical Atlas of England and Wales. Blackie Academic & Professional, London.

Magdoff, F., Weil, R.R. 2004. Soil organic matter in sustainable agriculture. CRC Press, Boca Raton, 1-43.

Mahmood, H.S., Hoogmoed, W.B., Henten, E.J.V., 2011. Estimating soil properties with a proximal gamma-ray spectrometer using windows and full-spectrum analysis methods. Proceedings of the Second Global Workshop on Proximal Soil Sensing, 15-18 May, Montreal, Canada, Contribution in proceedings, 132-135.

Martz, L.W., de Jong E., 1990. Natural radionuclides in the soils of a small agricultural basin in the Canadian prairies and their association with topography. Soil properties and erosion. Catena 17, 85–96.

Matlab, 2012. Version v7.14 2012. The Mathworks Inc. Natick.

McBratney, A.B., Pringle, M.J., 1999. Estimating Average and Proportional Variograms of Soil Properties and Their Potential Use in Precision Agriculture. Precision Agriculture 1, 125-152.

McGrath, S.P., Loveland, P.J., 1992. The Soil Geochemical Atlas of England and Wales. Kluwer Academic Publishers, Glasgow.

Mevik, B.H., Wehrens, R., 2007. The pls Package: Principal Component and Partial Least Squares Regression in R. Journal of statistical software 18, 1-24.

Minty, B.R.S., 1997. Fundamentals of Airborne Gamm-ray Spectroscopy. Journal of Australian Geology and Geophysics 17, 39-50.

Mouazen, A.M., De Baerdemaeker, J., Ramon, H., 2005. Towards development of on-line soil moisture content sensor using a fibre-type NIR spectrophotometer. Soil and Tillage Research 80, 171-183.

Navas, A., Soto, J., Machin, J., 2002. ^{238}U, ^{226}Ra, ^{210}Pb, ^{232}Th and ^{40}K activities in soil profiles of the Flysch sector. Applied Radiation and Isotopes 57, 579-589.

Petersen, H., Wunderlich, T., Attia al Hagrey S., Rabbel, W., 2012. Characterization of some Middle European soil textures by gamma-spectrometry. Journal of Plant Nutrition and Soil Science 175, 651–660.

Peveril, K.I., Sparrow, L.A., Reuter, D.J., 1999. Soil Analysis: An Interpretation manual. CSIRO, Melbourne.

Piikki, K., Söderström, M., Stenberg, B., 2013. Sensor data fusion for topsoil clay mapping. Geoderma 199, 106-116.

Pracilio, G., Adams, M.L., Smettem, K.R.J., Harper, R.J., 2006. Determination of spatial distribution patterns of clay and plant available potassium contents in surface soils at the farm scale using high resolution gamma ray spectrometry. Plant and Soil 282, 67-82.

Pretty, J., 2008. Agricultural sustainability: concepts, principles and evidence. Philosophical Transactions of the Royal Society B. 363, 447-465.

R Development Core Team, 2010. R: A language and environment for statistical computing. R Foundation for Statistical Computing, Vienna. URL: http://www.R-project.org/

Rawlins, B.G., Lark, R.M., Webster, R., 2007. Understanding airborne radiometric survey signals across part of eastern England. Earth Surface Processes and Landforms 32, 1503–1515.

Ritchie, J.C., McHenry, J.R., 1990. Application of radioactive fallout Cesium-137 for measuring soil erosion and sediment accumulation rates and patterns: a review. Journal of Environ- mental Quality 19, 215-233.

Saccà, C., Saccà, D., Nucera, P., de Fazio, A., 2011. Composition and geochemistry of clay sediments offshore the northeastern Sicilian coast (Southeastern Tyrrhenian Sea, Italy). Estuarine, Coastal and Shelf Science 92, 564-572.

Savitzky, M., Golay, M.J.E., 1964. Smoothing and Differentiation of Data by Simplified Least Squares Procedure. Analytical Chemistry 36, 1627–1639.

Savvides, A., Corstanje, R., Baxter, S.J., Rawlins, B.G., Lark, R.M. 2010. The relationship between diffuse spectral reflectance of the soil and its cation exchange capacity is scale-dependent. Geoderma 154, 353-358.

Shahid, S.A., Taha, F.K., Abdelfattah, M.A., 2013. Developments in Soil Classification, Land Use Planning and Policy Implications. Springer, New York.

Shonk, G.A., Gaultney, L.D., Schulze, D.G., Van Scoyoc, G.E., 1991. Spectroscopic sensing of soil organic matter content. Transactions of the American Society of Agricultural and Biological Engineers 34, 1978–1984

Stafford, J.V., 2000. Implementing Precision Agriculture in the 21st Century. Journal of Agricultural Engineering Research 76, 267-275.

Sudduth, K.A., Hummel, J.W., 1993. Soil organic matter, CEC, and moisture sensing with a portable NIR spectrophotometer. Transactions of the American Society of Agricultural and Biological Engineers 36, 1571-1582.

Sudduth, K.A., Kitchen, R.A., Sadler, E.J., Drummond, S.T., Myers, D.B., 2010. VNIR spectroscopy of within-field variability in soil properties. In: Viscarra Rossel, R.A., McBratney, A.B., Minasny, B. (Eds.), Proximal Soil Sensing: Progress in Soil Science, Springer Science and Business Media B.V., Netherlands, 387–396.

Taylor, J.A., Short, M., McBratney, A.B., Wilson, J., 2010. Comparing the ability of multiple soil sensors to predict soil properties in a Scottish potato production system. In: Viscarra Rossel, R.A., McBratney, A.B., Minasny, B. (Eds.), Proximal Soil Sensing: Progress in Soil Science, Springer Science and Business Media B.V., Netherlands, 387–396.

Taylor, M.J., Smettem, K., Pracilio, G., Verboom, W., 2002. Relationships between soil properties and high-resolution radiometrics, central eastern Wheatbelt, Western Australia. Exploration Geophysics 33, 95-102.

United Nations (UN), 2009. World Population to Exceed 9 Billion by 2050: Developing Countries to Add 2.3 Billion Inhabitants with 1.1 Billion Aged Over 60 and 1.2 Billion of Working Age. UN Press Release, URL: http://www.un.org/esa/population/publications/wpp2008/pressrelease.pdf

Van Egmond, F.M, Loonstra, E.H., Limburg, J., 2008. Gamma ray sensor for topsoil mapping the Mole. 1st Global Workshop on High Resolution Digital Soil Sensing and Mapping, Sydney.

Van Egmond, F.M., Viscarra Rossel, R.A., Loonstra, E.H., 2010. Comparison Of Gamma Ray Analysis Methodologies For High Resolution Digital Soil Mapping. The Soil Company, Groningen.

Viscarra Rossel, R.A., Walvoort, D.J.J., McBratney, A.B., Janik, L.J., Skjemstad, J.O., 2006. Visible, near infrared, mid infrared or combined diffuse reflectance spectroscopy for simultaneous assessment of various soil properties. Geoderma 131, 59-75.

Viscarra Rossel, R.A., Taylor, H.J., McBratney, A.B., 2007. Multivariate calibration of hyperspectral γ-ray energy spectra for proximal soil sensing. European Journal of Soil Science 58, 343-353.

Viscarra Rossel, R.A., Lark, R.M., 2009. Improved analysis and modelling of soil diffuse reflectance spectra using wavelets. European Journal of Soil Science 60, 453–464.

Viscarra Rossel, R.A., Adamchuck, V.I., Sudduth, K.A., McKenzie, N.J., Lobsey, C., 2011. Proximal Soil Sensing: An Effective Approach for Soil Measurements in Space and Time. In: Sparks, D.L. (Eds), Advances in Agronomy, Academic Press 113, 237-282.

Vitharana, U.W.A., Van Meirvenne, M., Amakor, X.N.C., Saey T., Simpson. D., 2007. Potency of proximal soil sensing to upgrade the soil map of Belgium: test case UGent experimental farm at Melle. Thematic Day: Soil resources in Belgium - Current and future issues Soil Science Society of Belgium, Brussels, 10.

Vukašinović, I., Dorđević, A., Rajković, M.B., Todorović, D. and Pavlović, V.B., 2010. Distribution of natural radionuclides in anthrosol-type soil. Turkish Journal of Agriculture and Forestry 34, 539-546.

Ward, S.H., 1981. Gamma-ray spectrometry in geological mapping and uranium exploration. Economic Geology, 75th Anniversary Volume, 840-849.

West, T.O., Post, W.M., 2002. Soil organic carbon sequestration rates by tillage and crop rotation: a global data analysis. Soil Science Society of America Journal 66, 1930–1946.

Wilford, J., 2002. Airborne Gamma-ray Spectroscopy. In: Papp, E. (Ed.), Geophysical and Remote Sensing Methods for Regolith Exploration. CRC LEME Open File Report, 144, 46–52.

Wilford, J., Minty, B., 2007. The use of airborne gamma-ray imagery for mapping soils and understanding landscape processes. In: Lagacherie, P., McBratney, A.B., Voltz, M., (Eds.), Digital Soil Mapping – An Introductory Perspective. Developments in Soil Science 31, 207-218.

Wold, S., Martens, H., Wold, H. 1983. The multivariate calibration method in chemistry solved by the PLS method. In: Ruhe, A., Kågstrom, B., (Eds.), Proceedings of the Conference on Matrix Pencils. Lecture Notes in Mathematics. Springer, Heidelberg.

Wold, S., Sjostrom, M., Eriksson L., 2001. PLS-regression: a basic tool of chemometrics. Chemometrics and Intelligent Laboratory Systems 58, 109-130.

Wong, M.T.F., Harper, R.J., 1999. Use of on-ground gamma-ray spectrometry to measure plant-available potassium and other topsoil attributes. Australian Journal of Soil Research 37, 267–277.

Zhu, Y., Weindorf, D.C, Zhang, W., 2011. Characterising soils using a portable X-ray fluorescence spectrometer: 1. Soil texture. Geoderma 167–168, 167-177.

Appendices

Appendix A Comparison of Pre-processing Methods (Chapter 3)

Appendix A provides a comparison between PLSR summary statistics of the unprocessed and pre-processed spectra of Chapter 3. Table A.1. provides a comparison of PLSR summary statistics of unprocessed spectra, with a reduced energy range, in order to establish whether all energy channels should be included in the PLSR models of Chapter 3. The lowest error (RMSECV) was found for the full γ-ray spectra (values in bold) so all channels were therefore included and used in the analysis of Chapter 3. Pre-processing techniques are then compared in Tables A.2 through to A.5, in terms of PLSR summary statistics.

Table A-1- Statistics for PLSR models with reduced spectral range.

Energy Range (KeV)	Calibration					Independent		
	[a]NF	R^2	[b]RMSECV ($cmol_c\ kg^{-1}$)	[c]RMSE ($cmol_c\ kg^{-1}$)	[d]RPD	R^2	[e]RMSE ($cmol_c\ kg^{-1}$)	[f]RPD
Full Spectra	**2**	**0.70**	**5.31**	**4.47**	**1.84**	**0.58**	**5.05**	**1.56**
410-3069KeV	2	0.64	5.62	4.92	1.67	0.56	5.23	1.50
410-3000KeV	1	0.44	6.43	6.12	1.34	0.34	6.38	1.23
0-300KeV	1	0.43	6.26	6.17	1.33	0.56	5.23	1.50

[a]LV – Number of Latent Variables used in PLSR model.
[b]RMSECV– Cross-validated root mean-squared-error of calibration.
[c]RMSE – Root mean-squared-error of calibration
[d]RPD – The relative prediction deviation of calibration.
[e]RMSE – Root mean-squared-error of independent predictions.
[f]RPD – The relative prediction deviation of independent predictions

Table A-2 - Statistics for the PLSR models, pre-processed with the Savitzky-Golay Filter

[a]k	[b]F	Calibration					Independent		
		[c]NF	R^2	[d]RMSECV ($cmol_c\ kg^{-1}$)	[e]RMSE ($cmol_c\ kg^{-1}$)	[f]RPD	R^2	[g]RMSE ($cmol_c\ kg^{-1}$)	[h]RPD
Unprocessed	-	2	0.70	5.31	4.47	1.84	0.58	5.05	1.56
	3	2	0.68	5.35	4.65	1.77	0.55	5.25	1.5
	5	2	0.65	5.3	4.82	1.7	0.56	5.19	1.52
	7	2	0.64	5.29	4.89	1.68	0.56	5.2	1.51
1	9	2	0.64	5.29	4.94	1.66	0.55	5.24	1.5
	11	2	0.63	5.31	4.98	1.65	0.54	5.29	1.49
	13	3	0.67	5.33	4.74	1.73	0.62	4.82	1.63
	15	3	0.66	5.36	4.79	1.71	0.62	4.82	1.63
	5	2	0.70	5.42	4.5	1.82	0.53	5.36	1.47
	7	2	0.68	5.42	4.67	1.76	0.54	5.32	1.48
	9	2	0.66	5.37	4.77	1.72	0.55	5.28	1.49
2	11	2	0.65	5.36	4.84	1.7	0.55	5.24	1.5
	13	2	0.65	5.34	4.88	1.68	0.55	5.24	1.5
	15	2	0.64	5.32	4.9	1.68	0.55	5.25	1.5
	17	2	0.64	5.31	4.92	1.67	0.55	5.27	1.49
	5	2	0.67	5.27	4.69	1.75	0.57	5.12	1.54
	7	2	0.67	5.32	4.7	1.75	0.56	5.19	1.52
	9	2	0.66	5.35	4.77	1.72	0.55	5.25	1.5
3	11	2	0.65	5.36	4.84	1.7	0.55	5.25	1.5
	13	2	0.65	5.34	4.88	1.68	0.55	5.24	1.5
	15	2	0.64	5.31	4.89	1.68	0.55	5.23	1.5
	17	2	0.64	5.29	4.91	1.67	0.55	5.24	1.5

[a]k – Polynomial degree of the filter.
[b]F – Filter width.
[c]NF – Number of PLSR factors.
[d]RMSECV – Cross-validated root mean-squared-error of calibration.
[e]RMSE – Root mean-squared-error of calibration
[f]RPD – The relative prediction deviation of calibration.
[g]RMSE – Root mean-squared-error of independent predictions.
[h]RPD – The relative prediction deviation of independent predictions.

Table A-3 - Statistics for the PLSR models, pre-processed with the Loess Filter

[a]α	Calibration					Independent		
	[b]NF	R^2	[c]RMSECV ($cmol_c\ kg^{-1}$)	[d]RMSE ($cmol_c\ kg^{-1}$)	[e]RPD	R^2	[f]RMSE ($cmol_c\ kg^{-1}$)	[g]RPD
Unprocessed	2	0.7	5.31	4.47	1.84	0.58	5.05	1.56
1.00%	2	0.66	5.41	4.74	1.73	0.54	5.32	1.48
1.50%	2	0.65	5.35	4.83	1.7	0.55	5.25	1.50
2.00%	2	0.65	5.32	4.85	1.69	0.55	5.23	1.50
2.25%	2	0.65	5.3	4.86	1.69	0.55	5.22	1.51
2.50%	2	0.65	5.3	4.87	1.68	0.55	5.22	1.51
2.75%	2	0.64	5.3	4.89	1.68	0.55	5.22	1.51
2.80%	2	0.64	5.3	4.89	1.68	0.55	5.22	1.51
2.90%	3	0.67	5.3	4.73	1.74	0.62	4.81	1.63
3.00%	**3**	**0.67**	**5.3**	**4.73**	**1.74**	**0.62**	**4.81**	**1.63**
3.10%	3	0.66	5.3	4.75	1.73	0.62	4.83	1.63
3.25%	3	0.66	5.31	4.78	1.72	0.62	4.85	1.62
3.50%	3	0.66	5.32	4.81	1.71	0.61	4.87	1.62

[a]α – Smoothing parameter, expressed as a percentage.
[b]NF – Number of PLSR factors.
[c]RMSECV– Cross-validated root mean-squared-error of calibration.
[d]RMSE – Root mean-squared-error of calibration
[e]RPD – The relative prediction deviation of calibration.
[f]RMSE – Root mean-squared-error of independent predictions.
[g]RPD – The relative prediction deviation of independent predictions.

Table A-4 - Statistics for the PLSR models with spectra reconstructed from the approximate coefficients of the discrete wavelet transform (DWT), using Daubechies wavelet with four vanishing movements.

Approximation Coefficient Level	Calibration					Independent		
	[a]NF	R^2	[b]RMSECV ($cmol_c\ kg^{-1}$)	[c]RMSE ($cmol_c\ kg^{-1}$)	[d]RPD	R^2	[e]RMSE ($cmol_c\ kg^{-1}$)	[f]RPD
Unprocessed	2	0.7	5.31	4.47	1.84	0.58	5.05	1.56
1	2	0.68	5.38	4.64	1.77	0.55	5.20	1.51
2	2	0.66	5.44	4.80	1.71	0.53	5.40	1.45
3	3	0.67	5.31	4.67	1.76	0.61	4.91	1.6
4	4	0.63	5.59	4.99	1.64	0.6	4.92	1.6
5	2	0.59	5.43	5.26	1.56	0.53	5.33	1.47
6	2	0.58	5.4	5.32	1.54	0.54	5.27	1.49

[a]NF – Number of PLSR factors.
[b]RMSECV– Cross-validated root mean-squared-error of calibration.
[c]RMSE – Root mean-squared-error of calibration
[d]RPD – The relative prediction deviation of calibration.
[e]RMSE – Root mean-squared-error of independent predictions.
[f]RPD – The relative prediction deviation of independent predictions.

Table A-5 - Statistics for the PLSR models, pre-processed with the DWT and wavelet thresholding. As with Appendix A.4 the spectra were decomposed using Daubechies wavelet with four vanishing movements.

Thresholding technique		Calibration					Independent		
		[a]NF	R^2	[b]RMSECV ($cmol_c\ kg^{-1}$)	[c]RMSE ($cmol_c\ kg^{-1}$)	RPD	R^2	[d]RMSE ($cmol_c\ kg^{-1}$)	RPD
Approx. Coefficient	Level 3	3	0.67	5.31	4.67	1.76	0.61	4.91	1.60
Rigorous SURE	Level 3	2	0.67	5.20	4.72	1.74	0.59	5.00	1.57
Fixed Thresh	Level 3	2	0.66	5.18	4.79	1.71	0.59	4.99	1.57
Penalise ≤ 1	Level 3	2	0.67	5.22	4.68	1.76	0.59	5.01	1.57
Penalise ≤ 2	Level 3	2	0.67	5.20	4.72	1.74	0.59	5.00	1.57
Penalise ≥ 5	Level 3	2	0.66	5.19	4.79	1.71	0.59	4.99	1.57

[a]NF – Number of PLSR factors.
[b]RMSECV – Cross-validated root mean-squared-error of calibration.
[c]RMSE – root mean-squared-error of calibration.
[d]RMSE – root mean-squared-error of prediction.

Appendix B – Comparison of mass-correction techniques.

Appendix B provides a comparison of techniques used to account for variations in mass of the samples used in Chapter 4. The PLSR results from the uncorrected spectra are presented in Table B-1. Table B-2 to Table B-4 provide a comparison of PLSR results between mass correction techniques and Table B-5 compares CV methods.

Table B-1 - Descriptive statistics for PLSR models produced from raw/uncorrected spectra

Soil Property	Energy Range (KeV)	[1]NF	[2]RMSECV	R^2	[3]RMSE	[4]RPD
Clay (%)	0 - 3,069	1	10.62	0.18	10.37	1.11
	410-3,069	1	10.74	0.29	9.66	1.19
	410-3,000	1	10.72	0.29	9.67	1.19
Silt (%)	0 - 3,069	1	15.01	0.2	14.70	1.12
	410-3,069	1	19.57	0.36	17.81	1.26
	410-3,000	1	15.12	0.31	13.67	1.2
Sand (%)	0 - 3,069	1	19.44	0.28	19.01	1.18
	410-3,069	1	19.57	0.36	17.81	1.26
	410-3,000	1	19.56	0.36	17.84	1.26
pH	0 - 3,069	2	1.24	0.63	0.70	1.64
	410-3,069	2	1.29	0.68	0.65	1.78
	410-3,000	2	1.29	0.69	0.65	1.79
OC (%)	0 - 3,069	1	1.73	0.05	1.67	1.03
	410-3,069	2	1.78	0.68	0.97	1.77
	410-3,000	2	1.77	0.69	0.95	1.8
Fe (g kg^{-1})	0 - 3,069	1	19.74	0.25	19.02	1.16
	410-3,069	1	20.41	0.34	17.75	1.24
	410-3,000	1	20.38	0.35	17.75	1.24
K (g kg^{-1})	0 - 3,069	1	2.29	0.25	2.22	1.16
	410-3,069	2	2.07	0.77	1.23	2.09
	410-3,000	2	2.07	0.78	1.20	2.14
$P_{tot.}$ (g kg^{-1})	0 - 3,069	1	0.49	0.09	0.47	1.05
	410-3,069	1	0.51	0.27	0.43	1.17
	410-3,000	1	0.51	0.27	0.43	1.17
$P_{ext.}$ (mg l^{-1})	0 - 3,069	1	25.00	0.07	23.16	1.04
	410-3,069	2	25.32	0.7	13.21	1.83
	410-3,000	2	25.15	0.7	13.15	1.84

[1]NF – Number of PLSR factors; [2]RMSECV – Cross-validated root mean-squared-error of calibration; [3]RMSE – Root mean square error of calibration; [4]RPD – Relative prediction deviation of calibration.

Table B-2 Descriptive statistics for PLSR models produced from spectra corrected by the following:

$$adj\ \gamma_i = \frac{\gamma_i}{m} \times \overline{m}$$

Where: adjγ_i is the adjusted γ-ray response of a soil at channel i, $\boldsymbol{\gamma_i}$ is the corresponding uncorrected response, m is the mass of the sample and $\overline{m}$ is the mean mass of the samples.

Soil Property	Energy Range (KeV)	[1]NF	[2]RMSECV	R^2	[3]RMSE	[4]RPD
	0-3,069+	1	10.84	0.13	10.71	1.1
Clay (%)	410-3,069+	1	11.07	0.12	10.77	1.1
	410-3,000	1	10.84	0.13	10.71	1.1
	0-3,069+	2	15.14	0.48	11.78	1.4
Silt (%)	410-3,069+	2	15.30	0.59	10.55	1.6
	410-3,000	2	15.14	0.48	11.78	1.4
	0-3,069+	2	19.67	0.50	15.86	1.4
Sand (%)	410-3,069+	1	20.77	0.18	20.22	1.1
	410-3,000	2	19.67	0.50	15.86	1.4
	0-3,069+	1	1.20	0.02	1.14	1.0
pH	410-3,069+	1	1.20	0.11	1.09	1.1
	410-3,000	1	1.20	0.02	1.14	1.0
	0-3,069+	1	1.72	0.02	1.69	1.0
OC (%)	410-3,069+	2	1.71	0.60	1.09	1.6
	410-3,000	1	1.72	0.02	1.69	1.0
	0-3,069+	2	19.10	0.57	14.38	1.5
Fe (g kg^{-1})	410-3,069+	2	20.36	0.67	12.62	1.7
	410-3,000	2	19.10	0.57	14.38	1.5
	0-3,069+	1	2.35	0.19	2.30	1.1
K (g kg^{-1})	410-3,069+	1	2.37	0.20	2.29	1.1
	410-3,000	1	2.35	0.19	2.30	1.1
	0-3,069+	1	0.50	0.04	0.49	1.0
$P_{tot.}$ (g kg^{-1})	410-3,069+	2	0.51	0.57	0.33	1.5
	410-3,000	1	0.50	0.04	0.49	1.0
	0-3,069+	1	24.23	0.02	23.83	1.0
$P_{ext.}$ (mg l^{-1})	410-3,069+	1	24.43	0.08	23.11	1.0
	410-3,000	1	24.23	0.02	23.83	1.0

[1]NF – Number of PLSR factors.
[2]RMSECV – Cross-validated root mean-squared-error of calibration.
[3]RMSE – Root mean square error of calibration.
[4]RPD – Relative prediction deviation of calibration.

Table B-3 - Descriptive statistics for PLSR models produced from spectra corrected by the following:

$$adj\ \gamma_i = \frac{\gamma_i}{(d \times m) + c} \times (d \times \bar{m}) + c$$

Where: adj γ_i is the adjusted γ-ray response of the ith channel, γ_i is the corresponding uncorrected response, m is the mass of the sample and $\bar{m}$ is the mean mass of the samples.

Soil Property	Energy Range (KeV)	[1]NF	[2]RMSECV	R^2	[3]RMSE	[4]RPD
	0-3,069+	1	10.36	0.22	10.14	1.13
Clay (%)	410-3,069+	1	10.47	0.31	9.51	1.21
	410-3,000	1	10.45	0.31	9.51	1.21
	0-3,069+	1	14.56	0.25	14.23	1.16
Silt (%)	410-3,069+	1	14.67	0.34	13.33	1.23
	410-3,000	1	14.65	0.34	13.34	1.23
	0-3,069+	1	18.50	0.35	18.05	1.24
Sand (%)	410-3,069+	1	18.65	0.42	17.07	1.31
	410-3,000	1	18.63	0.42	17.07	1.31
	0-3,069+	2	1.24	0.62	0.71	1.62
pH	410-3,069+	2	1.23	0.76	0.56	2.06
	410-3,000	2	1.22	0.80	0.52	2.23
	0-3,069+	2	1.89	0.61	1.07	1.60
OC (%)	410-3,069+	2	1.77	0.70	0.94	1.82
	410-3,000	2	1.78	0.70	0.94	1.83
	0-3,069+	1	19.46	0.28	18.65	1.18
Fe (g kg^{-1})	410-3,069+	1	20.23	0.36	17.59	1.25
	410-3,000	1	20.21	0.36	17.61	1.25
	0-3,069+	1	2.19	0.31	2.12	1.21
K (g kg^{-1})	410-3,069+	1	1.96	0.52	1.78	1.44
	410-3,000	1	1.96	0.52	1.78	1.44
	0-3,069+	1	0.49	0.10	0.47	1.06
$P_{tot.}$ (g kg^{-1})	410-3,069+	1	0.51	0.28	0.42	1.18
	410-3,000	1	0.51	0.28	0.42	1.18
	0-3,069+	1	24.54	0.05	23.44	1.03
$P_{ext.}$ (mg l^{-1})	410-3,069+	2	25.29	0.69	13.35	1.81
	410-3,000	2	25.15	0.70	13.31	1.81

[1]NF – Number of PLSR factors.
[2]RMSECV – Cross-validated root mean-squared-error of calibration.
[3]RMSE – Root mean square error of calibration.
[4]RPD – Relative prediction deviation of calibration

Table B-4 - Descriptive statistics for PLSR models produced from spectra corrected by the following:

$$adj\ \gamma_i = \frac{\gamma_{i-^{bg}\gamma_i}}{m} \times \bar{m}$$

Where: adj γ_i is the adjusted γ-ray response of a soil at channel$i$, γ_i is the corresponding uncorrected response, ${}^{bg}\gamma_i$ is the corresponding reponse of the sensor without a sample, m is the mass of the sample and $\bar{m}$ is the mean mass of the samples.

Soil Property	Energy Range (KeV)	[1]NF	[2]RMSECV	R^2	[3]RMSE	[4]RPD
	0-3,069+	1	10.40	0.21	10.20	1.13
Clay (%)	410-3,069+	1	10.58	0.27	9.82	1.17
	410-3,000	1	10.55	0.27	9.82	1.17
	0-3,069+	1	14.54	0.24	14.26	1.15
Silt (%)	410-3,069+	1	14.89	0.29	13.83	1.19
	410-3,000	1	14.87	0.29	13.83	1.19
	0-3,069+	1	18.53	0.34	18.14	1.24
Sand (%)	410-3,069+	1	19.19	0.36	17.93	1.25
	410-3,000	1	19.15	0.36	17.93	1.25
	0-3,069+	2	1.25	0.53	0.79	1.46
pH	410-3,069+	2	1.22	0.60	0.73	1.59
	410-3,000	2	1.24	0.60	0.72	1.59
	0-3,069+	2	1.86	0.49	1.22	1.40
OC (%)	410-3,069+	2	1.75	0.59	1.09	1.57
	410-3,000	2	1.73	0.61	1.06	1.61
	0-3,069+	1	19.60	0.28	18.68	1.18
Fe (g kg^{-1})	410-3,069+	1	20.63	0.33	18.02	1.22
	410-3,000	2	20.52	0.72	11.67	1.88
	0-3,069+	1	2.20	0.31	2.13	1.20
K (g kg^{-1})	410-3,069+	1	2.11	0.42	1.95	1.32
	410-3,000	1	2.11	0.42	1.95	1.32
	0-3,069+	1	0.49	0.10	0.47	1.05
$P_{tot.}$ (g kg^{-1})	410-3,069+	1	0.50	0.25	0.43	1.16
	410-3,000	1	0.50	0.25	0.43	1.16
	0-3,069+	1	24.35	0.04	23.62	1.02
$P_{ext.}$ (mg l^{-1})	410-3,069+	2	24.83	0.64	14.55	1.66
	410-3,000	2	24.59	0.64	14.37	1.68

[1]NF – Number of PLSR factors.
[2]RMSECV – Cross-validated root mean-squared-error of calibration.
[3]RMSE – Root mean square error of calibration.
[4]RPD – Relative prediction deviation of calibration.

Table B-5 Comparison between cross-validation methods, in terms of RMSECV.

Soil Property	[a]Energy range	[b]Pre-processing Technique		[c]NF	Leave-10-Out RMSECV	Leave-One-Out RMSECV	R^2
Clay (%)	410-3,000	Loess	4.00%	1	10.26	10.29	0.22
Silt (%)	410-3,000	Approx	Level 4	2	14.31	14.33	0.31
Sand (%)	410-3,000	Approx	Level 4	1	18.44	18.45	0.34
pH	0-3,069	Approx	Level 5	2	1.12	1.11	0.16
OC (%)	410-3,000	Approx	Level 5	3	1.70	1.69	0.14
Fe (g kg^{-1})	0-3,069	Loess	2.50%	2	18.15	18.32	0.48
K (g kg^{-1})	410-3,000	Approx	Level 6	2	1.90	1.89	0.48
$P_{tot.}$ (g kg^{-1})	410-3,069	Approx	Level 3	11	0.47	0.49	0.32
$P_{ext.}$ (mg l^{-1})	0-3,069	Approx	Level 2	1	24.22	24.20	0.01

[a]Energy Range - Range of energy channels used in the PLSR model
[b]Pre-processing Technique – Where Approx is spectra reconstructed from the approximate coefficient and its corresponding level.
[c]NF Number of PLSR factors.

Appendix C - Analysis of variation (Chapter 4).

Appendix C provides a breakdown of the ANOVA results from Chapter 4. The absolute-mean residuals ($|e_i|$) were compared to soil group, geological period and lithology, in an effort to explain model imprecision.

Table C-1 – One-way ANOVA results of Clay (%) in terms of $|e_i|$.

Major Group	n	Group Mean	[a]Lower	[b]Upper
Brown soils	102	6.5	5.2	7.7
Ground-water gley soils	26	12.6	10.1	15.1
Lithomorphic soils	6	7.5	2.3	12.6
Made ground soils	3	8.6	1.3	15.9
Peat soils	1	2.1	-10.6	14.7
Pelosols	6	12.8	7.7	18.0
Podzolic soils	7	8.6	3.9	13.4
Surface-water gley soils	43	6.1	4.1	8.0
Terrestrial raw soils	1	15.2	2.6	27.9
[c]Geological Period				
Neogene	5	5.9	-0.1	11.9
Palaeogene	15	7.7	5.5	9.8
Cretaceous	38	9.5	6.7	12.3
Jurassic	23	8.7	6.6	10.9
Triassic	40	5.9	0.5	11.4
Permian	6	6.5	4.0	9.0
Carboniferous	29	6.5	3.5	9.5
Devonian	20	7.2	3.8	10.5
Silurian	16	5.4	-2.3	13.1
Ordovician	3	6.7	3.2	10.1
Lithology				
Chalk	17	9.2	5.9	12.4
Clay, Silt and Sand	7	4.4	-0.7	9.4
Dolomitised Limestone and Dolomite	2	5.6	-3.9	15.0
Gravel, Sand, Silt and Clay	5	5.9	-0.1	11.9
Limestone	22	5.3	2.5	8.1
Mudstone	96	8.0	6.7	9.4
Sand, Silt and Clay	8	8.6	3.9	13.4
Sandstone	35	7.8	5.5	10.0
Siltstone	2	8.2	-1.2	17.7
Ultramafitite	1	2.6	-10.8	15.9

[a]Lower – Lists the lower 95% confidence interval for the group means.
[b]Upper – Lists the upper 95% confidence interval for the group means.
[c]Geological Period – Maximum geological period (BGS, 2008), listed in reverse chronological order.

Table C-2 – One-way ANOVA results of Silt (%), in terms of $|e_i|$.

Major Group	n	Group Mean	[a]Lower	[b]Upper
Brown soils	102	11.2	9.6	12.8
Ground-water gley soils	26	10.5	7.3	13.7
Lithomorphic soils	6	9.2	2.5	15.9
Made ground soils	3	7.7	-1.8	17.2
Peat soils	1	13.4	-3.0	29.9
Pelosols	6	11.4	4.7	18.1
Podzolic soils	7	14.1	7.8	20.3
Surface-water gley soils	43	9.7	7.2	12.2
Terrestrial raw soils	1	20.1	3.6	36.5
[c]Geological Period				
Neogene	5	13.9	6.6	21.2
Palaeogene	15	10.3	6.1	14.5
Cretaceous	38	12.4	9.7	15.0
Jurassic	23	9.6	6.2	13.0
Triassic	40	10.9	8.3	13.5
Permian	6	11.4	4.7	18.0
Carboniferous	29	8.4	5.4	11.4
Devonian	20	11.0	7.3	14.6
Silurian	16	13.7	9.7	17.8
Ordovician	3	3.2	-6.2	12.6
Lithology				
Chalk	17	12.7	8.9	16.5
Clay, Silt and Sand	7	9.4	3.4	15.4
Dolomitised Limestone and Dolomite	2	12.6	1.5	23.8
Gravel, Sand, Silt and Clay	5	14.1	7.0	21.1
Limestone	22	9.9	6.5	13.3
Mudstone	96	10.0	8.4	11.6
Sand, Silt and Clay	8	10.2	4.6	15.7
Sandstone	35	9.8	7.1	12.5
Siltstone	2	11.0	-0.2	22.2
Ultramafitite	1	24.5	8.7	40.2

[a]Lower – Lists the lower 95% confidence interval for the group means.
[b]Upper – Lists the upper 95% confidence interval for the group means.
[c]Geological Period – Maximum geological period (BGS, 2008), listed in reverse chronological order.

Table C-3 - One-way ANOVA results of Sand (%), in terms of $|e_i|$.

Major Group	n	Group Mean	[a]Lower	[b]Upper
Brown soils	102	15.0	12.9	17.0
Ground-water gley soils	26	15.5	11.4	19.6
Lithomorphic soils	6	19.7	11.2	28.2
Made ground soils	3	23.7	11.6	35.8
Peat soils	1	10.5	-10.4	31.4
Pelosols	6	9.4	0.9	18.0
Podzolic soils	7	19.6	11.7	27.5
Surface-water gley soils	43	11.0	7.8	14.1
Terrestrial raw soils	1	39.7	18.7	60.6
[c]Geological Period				
Neogene	5	9.0	-0.2	18.2
Palaeogene	15	10.0	4.7	15.3
Cretaceous	38	19.6	16.3	22.9
Jurassic	23	15.4	11.1	19.6
Triassic	40	14.8	11.6	18.1
Permian	6	15.1	6.8	23.5
Carboniferous	29	10.3	6.5	14.1
Devonian	20	19.1	14.5	23.7
Silurian	16	9.6	4.5	14.7
Ordovician	3	6.7	-5.1	18.5
Lithology				
Chalk	17	24.1	19.1	29.0
Clay, Silt and Sand	7	8.5	0.7	16.2
Dolomitised Limestone and Dolomite	2	14.4	-0.1	28.9
Gravel, Sand, Silt and Clay	5	9.0	-0.2	18.2
Limestone	22	11.5	7.1	15.9
Mudstone	96	13.3	11.2	15.4
Sand, Silt and Clay	8	11.4	4.1	18.6
Sandstone	35	17.3	13.9	20.8
Siltstone	2	16.7	2.2	31.2
Ultramafitite	1	29.9	9.4	50.5

[a]Lower – Lists the lower 95% confidence interval for the group means.
[b]Upper – Lists the upper 95% confidence interval for the group means.
[c]Geological Period – Maximum geological period (BGS, 2008), listed in reverse chronological order.

Table C-4 - One-way ANOVA results of pH, in terms of $|e_i|$.

Major Group	n	Group Mean	[a]Lower	[b]Upper
Brown soils	99	0.80	0.69	0.92
Ground-water gley soils	25	0.85	0.62	1.08
Lithomorphic soils	6	1.26	0.79	1.74
Made ground soils	3	1.51	0.84	2.18
Peat soils	1	0.08	-1.09	1.24
Pelosols	6	0.81	0.33	1.29
Podzolic soils	7	1.23	0.79	1.67
Surface-water gley soils	43	0.83	0.66	1.01
Terrestrial raw soils	1	2.54	1.38	3.71
[c]Geological Period				
Neogene	5	0.94	0.42	1.46
Palaeogene	15	0.99	0.69	1.29
Cretaceous	37	1.05	0.86	1.24
Jurassic	23	0.91	0.67	1.16
Triassic	39	0.74	0.55	0.92
Permian	6	1.29	0.82	1.76
Carboniferous	29	0.58	0.37	0.80
Devonian	20	1.09	0.83	1.35
Silurian	15	0.62	0.32	0.92
Ordovician	2	0.43	-0.39	1.26
Lithology				
Chalk	17	1.18	0.89	1.46
Clay, Silt and Sand	7	0.97	0.52	1.41
Dolomitised Limestone and Dolomite	2	1.58	0.75	2.42
Gravel, Sand, Silt and Clay	5	0.94	0.41	1.47
Limestone	22	0.56	0.31	0.81
Mudstone	93	0.81	0.69	0.93
Sand, Silt and Clay	8	1.02	0.60	1.43
Sandstone	34	0.94	0.74	1.15
Siltstone	2	0.66	-0.18	1.50
Ultramafitite	1	0.71	-0.47	1.90

[a]Lower – Lists the lower 95% confidence interval for the group means.
[b]Upper – Lists the upper 95% confidence interval for the group means.
[c]Geological Period – Maximum geological period (BGS, 2008), listed in reverse chronological order.

Table C-5 - One-way ANOVA results of OC (%), in terms of $|e_i|$.

Major Group	n	Group Mean	[a]Lower	[b]Upper
Brown soils	102	1.18	0.98	1.37
Ground-water gley soils	26	1.43	1.04	1.82
Lithomorphic soils	6	0.66	-0.16	1.47
Made ground soils	3	3.55	2.40	4.70
Peat soils	1	0.09	-1.90	2.08
Pelosols	6	0.65	-0.16	1.46
Podzolic soils	7	1.74	0.99	2.49
Surface-water gley soils	43	1.00	0.70	1.31
Terrestrial raw soils	1	0.41	-1.58	2.39
[c]Geological Period				
Neogene	5	1.60	0.68	2.53
Palaeogene	15	1.09	0.56	1.63
Cretaceous	38	1.57	1.24	1.91
Jurassic	23	1.27	0.84	1.71
Triassic	40	0.91	0.58	1.23
Permian	6	1.13	0.28	1.97
Carboniferous	29	1.02	0.64	1.41
Devonian	20	1.15	0.69	1.61
Silurian	16	1.25	0.74	1.77
Ordovician	3	0.74	-0.45	1.94
Lithology				
Chalk	17	1.73	1.23	2.24
Clay, Silt and Sand	7	1.08	0.29	1.86
Dolomitised Limestone and Dolomite	2	0.70	-0.77	2.17
Gravel, Sand, Silt and Clay	5	1.60	0.68	2.53
Limestone	22	0.82	0.38	1.26
Mudstone	96	1.14	0.93	1.35
Sand, Silt and Clay	8	1.11	0.37	1.84
Sandstone	35	1.27	0.92	1.62
Siltstone	2	1.42	-0.05	2.88
Ultramafitite	1	1.60	-0.48	3.68

[a]Lower – Lists the lower 95% confidence interval for the group means.
[b]Upper – Lists the upper 95% confidence interval for the group means.
[c]Geological Period – Maximum geological period (BGS, 2008), listed in reverse chronological order.

Table C-6 - One-way ANOVA results of Fe (g kg^{-1}), in terms of $|e_i|$.

Major Group	n	Group Mean	[a]Lower	[b]Upper
Brown soils	101	10.85	9.02	12.68
Ground-water gley soils	26	9.25	5.65	12.85
Lithomorphic soils	6	5.53	-1.97	13.04
Made ground soils	3	10.87	0.26	21.48
Peat soils	1	7.66	-10.71	26.04
Pelosols	6	10.84	3.34	18.35
Podzolic soils	7	8.02	1.08	14.97
Surface-water gley soils	43	7.67	4.87	10.48
Terrestrial raw soils	1	2.01	-16.37	20.39
[c]Geological Period				
Neogene	5	8.56	0.47	16.64
Palaeogene	15	12.50	7.83	17.17
Cretaceous	38	9.55	6.62	12.48
Jurassic	22	13.96	10.10	17.82
Triassic	40	10.27	7.41	13.13
Permian	6	8.57	1.18	15.95
Carboniferous	29	6.02	2.67	9.38
Devonian	20	7.26	3.21	11.30
Silurian	16	10.21	5.69	14.73
Ordovician	3	5.82	-4.62	16.26
Lithology				
Chalk	17	8.40	3.93	12.87
Clay, Silt and Sand	7	14.57	7.60	21.53
Dolomitised Limestone and Dolomite	2	2.48	-10.55	15.51
Gravel, Sand, Silt and Clay	5	8.56	0.32	16.80
Limestone	21	11.71	7.69	15.73
Mudstone	96	9.51	7.63	11.39
Sand, Silt and Clay	8	10.69	4.18	17.21
Sandstone	35	8.91	5.80	12.03
Siltstone	2	6.79	-6.24	19.82
Ultramafitite	1	0.86	-17.56	19.29

[a]Lower – Lists the lower 95% confidence interval for the group means.
[b]Upper – Lists the upper 95% confidence interval for the group means.
[c]Geological Period – Maximum geological period (BGS, 2008), listed in reverse chronological order.

Table C-7 - One-way ANOVA results of K (g kg^{-1}), in terms of $|e_i|$.

Major Group	n	Group Mean	[a]Lower	[b]Upper
Brown soils	102	1.50	1.28	1.72
Ground-water gley soils	26	1.77	1.33	2.22
Lithomorphic soils	6	0.45	-0.48	1.38
Made ground soils	3	2.41	1.10	3.72
Peat soils	1	0.22	-2.04	2.49
Pelosols	6	2.32	1.40	3.25
Podzolic soils	7	1.47	0.61	2.33
Surface-water gley soils	43	0.95	0.60	1.29
Terrestrial raw soils	1	0.40	-1.87	2.67
[c]Geological Period				
Neogene	5	0.27	-0.74	1.28
Palaeogene	15	1.05	0.47	1.63
Cretaceous	38	1.27	0.91	1.64
Jurassic	23	2.32	1.85	2.79
Triassic	40	1.33	0.98	1.69
Permian	6	1.36	0.44	2.28
Carboniferous	29	1.18	0.76	1.60
Devonian	20	1.56	1.05	2.06
Silurian	16	1.67	1.11	2.24
Ordovician	3	0.70	-0.60	2.00
Lithology				
Chalk	17	1.28	0.71	1.85
Clay, Silt and Sand	7	1.04	0.16	1.93
Dolomitised Limestone and Dolomite	2	2.63	0.98	4.29
Gravel, Sand, Silt and Clay	5	0.27	-0.78	1.32
Limestone	22	1.25	0.75	1.75
Mudstone	96	1.54	1.31	1.78
Sand, Silt and Clay	8	1.06	0.23	1.88
Sandstone	35	1.46	1.06	1.86
Siltstone	2	1.42	-0.24	3.07
Ultramafitite	1	0.72	-1.63	3.06

[a]Lower – Lists the lower 95% confidence interval for the group means.
[b]Upper – Lists the upper 95% confidence interval for the group means.
[c]Geological Period – Maximum geological period (BGS, 2008), listed in reverse chronological order.

Table C-8 - One-way ANOVA results of $P_{tot.}$ (g kg^{-1}), in terms of $|e_i|$.

Major Group	n	Group Mean	[a]Lower	[b]Upper
Brown soils	101	0.31	0.25	0.36
Ground-water gley soils	26	0.27	0.16	0.38
Lithomorphic soils	6	0.28	0.06	0.50
Made ground soils	3	0.79	0.47	1.10
Peat soils	1	0.41	-0.14	0.96
Pelosols	6	0.29	0.07	0.52
Podzolic soils	7	0.26	0.05	0.47
Surface-water gley soils	43	0.32	0.23	0.40
Terrestrial raw soils	1	0.28	-0.27	0.82
[c]Geological Period				
Neogene	5	0.18	-0.07	0.43
Palaeogene	15	0.32	0.17	0.46
Cretaceous	38	0.37	0.28	0.46
Jurassic	22	0.33	0.21	0.45
Triassic	40	0.31	0.23	0.40
Permian	6	0.27	0.04	0.50
Carboniferous	29	0.29	0.19	0.39
Devonian	20	0.27	0.14	0.39
Silurian	16	0.26	0.12	0.40
Ordovician	3	0.33	0.01	0.65
Lithology				
Chalk	17	0.40	0.27	0.54
Clay, Silt and Sand	7	0.31	0.10	0.52
Dolomitised Limestone and Dolomite	2	0.17	-0.22	0.57
Gravel, Sand, Silt and Clay	5	0.18	-0.07	0.42
Limestone	21	0.24	0.12	0.36
Mudstone	96	0.32	0.27	0.38
Sand, Silt and Clay	8	0.32	0.13	0.52
Sandstone	35	0.28	0.19	0.37
Siltstone	2	0.39	0.00	0.79
Ultramafitite	1	0.47	-0.09	1.02

[a]Lower – Lists the lower 95% confidence interval for the group means.
[b]Upper – Lists the upper 95% confidence interval for the group means.
[c]Geological Period – Maximum geological period (BGS, 2008), listed in reverse chronological order.

Table C-9 - One-way ANOVA results of $P_{ext.}$ (mg l^{-1}), in terms of $|e_i|$.

Major Group	n	Group Mean	[a]Lower	[b]Upper
Brown soils	102	16.2	12.9	19.6
Ground-water gley soils	26	20.9	14.3	27.5
Lithomorphic soils	6	11.1	-2.7	24.9
Made ground soils	3	14.1	-5.4	33.6
Peat soils	1	10.3	-23.5	44.1
Pelosols	6	24.5	10.7	38.3
Podzolic soils	7	22.3	9.6	35.1
Surface-water gley soils	43	14.8	9.6	19.9
Terrestrial raw soils	1	29.0	-4.8	62.8
[c]Geological Period				
Neogene	5	13.5	-1.5	28.6
Palaeogene	15	21.9	13.3	30.6
Cretaceous	38	19.4	14.0	24.9
Jurassic	23	22.3	15.2	29.3
Triassic	40	14.7	9.4	20.0
Permian	6	14.1	0.4	27.9
Carboniferous	29	13.8	7.6	20.1
Devonian	20	16.5	9.0	24.1
Silurian	16	11.9	3.5	20.3
Ordovician	3	14.3	-5.2	33.7
Lithology				
Chalk	17	19.2	11.0	27.4
Clay, Silt and Sand	7	16.2	3.5	29.0
Dolomitised Limestone and Dolomite	2	18.1	-5.9	42.0
Gravel, Sand, Silt and Clay	5	13.5	-1.6	28.7
Limestone	22	12.7	5.5	20.0
Mudstone	96	17.5	14.1	21.0
Sand, Silt and Clay	8	26.9	15.0	38.9
Sandstone	35	15.3	9.6	21.0
Siltstone	2	8.1	-15.9	32.0
Ultramafitite	1	13.1	-20.7	47.0

[a]Lower – Lists the lower 95% confidence interval for the group means.
[b]Upper – Lists the upper 95% confidence interval for the group means.
[c]Geological Period – Maximum geological period (BGS, 2008), listed in reverse chronological order.

Appendix D - R Script

All the PLSR calculations of this study were performed in the R statistical environment, version 3.0.1 (R Core Development Team, 2010), for Mac OS X (Apple Inc., California). The 'pls' package (Mevik and Wehrens, 2007) was used to perform PLSR. Explanations of the code are given following the hash (#) symbol and are presented in bold. Two R scripts are presented, 'Script D.1' is the code used model CEC at the regional scale (Chapter 3) and 'Script D.2' is the code used to model all the soil properties presented in Chapter 4. In both scripts the unprocessed γ-ray spectra is used, however the enclosed CD-ROM contains the pre-processed spectra, which were also used in this study.

R Script D-1– Region PLSR calibration of γ-ray spectra and CEC prediction.

```
############
###CEC PLSR###
############
#Load CEC and γ-ray data
raw<-read.csv("/Users/EdCarnell/Desktop/Work/CD ROM/Luton/Data/Unprocessed_Spectra.csv")
CEC<-raw[,6]#define column containing CEC values
Spec<-raw[,17:1031]#set γ-ray energies to include
Spec<-as.matrix(Spec)#Convert spectra into matrix
fullrawdata<-data.frame(CEC=I(CEC), Spec=I(Spec))#Define new dataset
#Split data into calibration and independent dataset
calibration =fullrawdata[1:239,]
prediction=fullrawdata[240:275,]
CECpls<- plsr(CEC ~ Spec, ncomp = 25, data = calibration, validation = "LOO")#Run PLS
RMSEPCEC<-RMSEP(CECpls)#Store RMSECV values
RMSEPadjCEC<-as.matrix(RMSEPCEC$val[1,1,2:26])#Store lowest RMSECV adj value
LV=which.min(RMSEPadjCEC)#Determine number of factors to include
CECcalib<-predict(CECpls, ncomp = LV, data = calibration, type = "response")#Predict CEC for calibration dataset
CECpred<-predict(CECpls, ncomp = LV, newdata = prediction, type = "response")#Predict CEC for independent dataset
calibrationrslt<-read.csv("/Volumes/TV/Work/CD ROM/Luton/Calibblank.csv")#Open file in which to store calibration predictions
predictionrslt<-read.csv("/Volumes/TV/Work/CD ROM/Luton/Predblank.csv")#Open file in which to store independent predictions
calibrationrslt[,8]<-CECcalib#Store calibration predictions
predictionrslt[,8]<-CECpred#Store independent predictions
CEC.lm = lm(calibration[,1] ~ CECcalib[,1,1])
calibrationrslt[1,10]<-summary(CEC.lm)$r.squared#Calculate and store R2 (Calibration)
calibrationrslt[2,10]<-min(RMSEPadjCEC)#Store lowest RMSECV (Calibration)
calibrationrslt[3,10]<-which.min(RMSEPadjCEC) #Store LV (Calibration)
CEC1.lm = lm(prediction[,1] ~ CECpred[,1,1])
predictionrslt[1,10]<-summary(CEC1.lm)$r.squared#Calculate and store R2 (Independent)
predictionrslt[2,10]<-min(RMSEPadjCEC) #Store lowest RMSECV (Independent)
predictionrslt[3,10]<-which.min(RMSEPadjCEC) #Store LV(Independent)

write.table(calibrationrslt,"/Volumes/TV/Work/CD ROM/Luton/Results/Calibration/Unprocessed.txt", row.names=F,col.names=T, sep = "\t")#Save calibration results
write.table(predictionrslt,"/Volumes/TV/Work/CD ROM/Luton/Results/Independent Predictions/Unprocessed.txt", row.names=F,col.names=T, sep = "\t")#Save independent results
```

R Script D-2 National calibration of NSI samples.

```
############
#### PLSR####
############
#Load pls package
require(pls)
#Load γ-ray spectra and corresponding soil properties
data<-read.csv("/Users/EdCarnell/Desktop/NSI Data/Data/(y÷((a×z)+c))×((a×μz)+c)/(y÷((a×z)+c))×((a×μz)+c).csv")
Clay<-data[,5]#define Clay
Silt<-data[,6] #define Silt
Sand<-data[,7] #define Sand
pH<-data[,8] #define pH
Carbon<-data[,9] #define Carbon
Fe<-data[,10] #define Fe
K<-data[,11]#define K
Pacid<-data[,12]#define P (acid)
Polsen<-data[,13] #define P (olsen)
Spec<-data[,151:1037]#set γ-ray energies to include
Spec<-as.matrix(Spec)#Convert spectra to a matrix
#Create new data set
data<-data.frame(Clay=I(Clay), Silt=I(Silt), Sand=I(Sand), pH=I(pH), Carbon=I(Carbon),Fe=I(Fe),K=I(K),Pacid=I(Pacid),Polsen=I(Polsen),Spec=I(Spec))
Claypls<- plsr(Clay ~ Spec, ncomp = 25, data = data) #Clay PLS model
Siltpls<- plsr(Silt ~ Spec, ncomp = 25, data = data) #Silt PLS model
Sandpls<- plsr(Sand ~ Spec, ncomp = 25, data = data) #Sand PLS model
pHpls<- plsr(pH ~ Spec, ncomp = 25, data = data) #pH PLS model
Carbonpls<- plsr(Carbon ~ Spec, ncomp = 25, data = data) #Carbon PLS model
Fepls<- plsr(Fe ~ Spec, ncomp = 25, data = data) #Fe PLS model
Kpls<- plsr(K ~ Spec, ncomp = 25, data = data) #K PLS model
Pacidpls<- plsr(Pacid ~ Spec, ncomp = 25, data = data) #P (acid) PLS model
Polsenpls<- plsr(Polsen ~ Spec, ncomp = 25, data = data) #p (olsen) PLS model
#set segments for leave-10-out pls cross validation
Seg10<-cvsegments(195, length.seg = 10, type = "interleaved")
ClayCV<-crossval(Claypls, Seg10)# leave-10-out cross validation of Clay pls model
SiltCV<-crossval(Siltpls, Seg10) # leave-10-out cross validation of Silt pls model
SandCV<-crossval(Sandpls, Seg10) # leave-10-out cross validation of Sand pls model
pHCV<-crossval(pHpls, Seg10) # leave-10-out cross validation of pH pls model
CarbonCV<-crossval(Carbonpls, Seg10) # leave-10-out cross validation Carbon pls model
```

FeCV<-crossval(Fepls, Seg10) **# leave-10-out cross validation of Fe pls model**
KCV<-crossval(Kpls, Seg10) **# leave-10-out cross validation K pls model**
PacidCV<-crossval(Pacidpls, Seg10) **# leave-10-out cross validation of P (acid) pls model**
PolsenCV<-crossval(Polsenpls, Seg10) **# leave-10-out cross validation of P (olsen) pls model** summary(ClayCV) **#CV clay pls summary statistics**
plot(RMSEP(ClayCV)) **#CV clay plot of RMSEP**
RMSEPClay<-RMSEP(ClayCV) **#store clay RMSEP**
RMSEPadjClay<-as.matrix(RMSEPClay$val[2,1,2:26])**#store matrix of RMSEP values for clay**
summary(SiltCV) **#CV silt pls summary statistics**
plot(RMSEP(SiltCV)) **#CV silt plot of RMSEP**
RMSEPSilt<-RMSEP(SiltCV) **#store silt RMSEP**
RMSEPadjSilt<-as.matrix(RMSEPSilt$val[2,1,2:26]) **#store matrix of RMSEP values for silt**
summary(SandCV) **#CV sand pls summary statistics**
plot(RMSEP(SandCV)) **#CV sand plot of RMSEP**
RMSEPSand<-RMSEP(SandCV) #store sand RMSEP
RMSEPadjSand<-as.matrix(RMSEPSand$val[2,1,2:26]) **#store matrix of RMSEP values for sand**
summary(pHCV) **#CV pH pls summary statistics**
plot(RMSEP(pHCV)) **#CV pH plot of RMSEP**
RMSEPpH<-RMSEP(pHCV) #store pH RMSEP
RMSEPadjpH<-as.matrix(RMSEPpH$val[2,1,2:26]) **#store matrix of RMSEP values for pH**
summary(CarbonCV) **#CV carbon pls summary statistics**
plot(RMSEP(CarbonCV)) **#CV carbon plot of RMSEP**
RMSEPCarbon<-RMSEP(CarbonCV) **#store carbon RMSEP**
RMSEPadjCarbon<-as.matrix(RMSEPCarbon$val[2,1,2:26])
#store matrix of RMSEP values for carbon
summary(FeCV) **#CV Fe pls summary statistics**
plot(RMSEP(FeCV)) **#CV Fe plot of RMSEP**
RMSEPFe<-RMSEP(FeCV) #store Fe RMSEP
RMSEPadjFe<-as.matrix(RMSEPFe$val[2,1,2:26]) **#store matrix of RMSEP values for Fe**
summary(KCV) **#CV K pls summary statistics**
plot(RMSEP(KCV)) **#CV K plot of RMSEP**
RMSEPK<-RMSEP(KCV) **#store K RMSEP**
RMSEPadjK<-as.matrix(RMSEPK$val[2,1,2:26]) **#store matrix of RMSEP values for K**
summary(PacidCV) **#CV P (acid) pls summary statistics**
plot(RMSEP(PacidCV)) **#CV P (acid) plot of RMSEP**
RMSEPPacid<-RMSEP(PacidCV) **#store P (acid) RMSEP**
RMSEPadjPacid<-as.matrix(RMSEPPacid$val[2,1,2:26])
#store matrix of RMSEP values for P (acid)
summary(PolsenCV) **#CV P (olsen) pls summary statistics**

```
plot(RMSEP(PolsenCV)) #CV P (olsen) plot of RMSEP
RMSEPPolsen<-RMSEP(PolsenCV) #store P (olsen) RMSEP
RMSEPadjPolsen<-as.matrix(RMSEPPolsen$val[2,1,2:26])
#store matrix of RMSEP values for P (olsen)
LVClay=which.min(RMSEPadjClay)#Storing LV of Clay model based on lowest RMSEP CV
LVSilt=which.min(RMSEPadjSilt) #Storing LV of Silt model based on lowest RMSEP CV
LVSand= which.min(RMSEPadjSand) #Storing LV of Sand model based on lowest RMSEP CV
LVpH= which.min(RMSEPadjpH) #Storing LV of pH model based on lowest RMSEP CV
LVCarbon= which.min(RMSEPadjCarbon) #Storing LV of Carbon model based on lowest RMSEP CV
LVFe= which.min(RMSEPadjFe) #Storing LV of Fe model based on lowest RMSEP CV
LVK= which.min(RMSEPadjK) #Storing LV of K model based on lowest RMSEP CV
LVPacid= which.min(RMSEPadjPacid) #Storing LV of P (acid) model based on lowest RMSEP CV
LVPolsen= which.min(RMSEPadjPolsen) #Storing LV of P (olsen) model based on lowest RMSEP CV
#Predictions based on LV with lowest RMSEP#
ClayPrediction<-predict(Claypls, ncomp =  LVClay, data = data, type = "response")
SiltPrediction<-predict(Siltpls, ncomp =  LVSilt, data = data, type = "response")
SandPrediction<-predict(Sandpls, ncomp =  LVSand, data = data, type = "response")
pHPrediction<-predict(pHpls, ncomp =  LVpH, data = data, type = "response")
CarbonPrediction<-predict(Carbonpls, ncomp =  LVCarbon, data = data, type = "response")
FePrediction<-predict(Fepls, ncomp =  LVFe, data = data, type = "response")
KPrediction<-predict(Kpls, ncomp =  LVK, data = data, type = "response")
PacidPrediction<-predict(Pacidpls, ncomp =  LVPacid, data = data, type = "response")
PolsenPrediction<-predict(Polsenpls, ncomp =  LVPolsen, data = data, type = "response")
#Load dataset, in which to store predictions
Results<-read.csv("/Users/EdCarnell/Desktop/NSI Data/Blank_minus5466.csv")
#Store predictions in table
Results[,14]<-ClayPrediction
Results[,15]<-SiltPrediction
Results[,16]<-SandPrediction
Results[,17]<-pHPrediction
Results[,18]<-CarbonPrediction
Results[,19]<-FePrediction
Results[,20]<-KPrediction
Results[,21]<-PacidPrediction
Results[,22]<-PolsenPrediction
#Squared Residuals
for(i in 1:195)
{Results[i,23]<-((ClayPrediction[i,1,1]-Clay[i])^2);
```

```
}
for(i in 1:195)
{Results[i,24]<-((SiltPrediction[i,1,1]-Silt[i])^2);
}
for(i in 1:195)
{Results[i,25]<-((SandPrediction[i,1,1]-Sand[i])^2);
}
for(i in 1:195)
{Results[i,26]<-((pHPrediction[i,1,1]-pH[i])^2);
}
for(i in 1:195)
{Results[i,27]<-((CarbonPrediction[i,1,1]-Carbon[i])^2);
}
for(i in 1:195)
{Results[i,28]<-((FePrediction[i,1,1]-Fe[i])^2);
}
for(i in 1:195)
{Results[i,29]<-((KPrediction[i,1,1]-K[i])^2);
}
for(i in 1:195)
{Results[i,30]<-((PacidPrediction[i,1,1]-Pacid[i])^2);
}
for(i in 1:195)
{Results[i,31]<-((PolsenPrediction[i,1,1]-Polsen[i])^2);
}
#Open dataset to store summary statistics
Summary<-read.csv("/Users/EdCarnell/Desktop/NSI Data/BlankSummary.csv")
#Store number of latent variables
Summary[1,2]<-LVClay
Summary[2,2]<-LVSilt
Summary[3,2]<-LVSand
Summary[4,2]<-LVpH
Summary[5,2]<-LVCarbon
Summary[6,2]<-LVFe
Summary[7,2]<-LVK
Summary[8,2]<-LVPacid
Summary[9,2]<-LVPolsen
#Store RMSEP values
```

```
Summary[1,3]=min(RMSEPadjClay)
Summary[2,3]=min(RMSEPadjSilt)
Summary[3,3]= min(RMSEPadjSand)
Summary[4,3]= min(RMSEPadjpH)
Summary[5,3]= min(RMSEPadjCarbon)
Summary[6,3]= min(RMSEPadjFe)
Summary[7,3]= min(RMSEPadjK)
Summary[8,3]= min(RMSEPadjPacid)
Summary[9,3]= min(RMSEPadjPolsen)
```

#Calculate and store R^2s

```
Clay.lm = lm(ClayPrediction ~ Clay, data=Results)
Summary[1,4]<-summary(Clay.lm)$r.squared
Silt.lm = lm(SiltPrediction ~ Silt, data=Results)
Summary[2,4]<-summary(Silt.lm)$r.squared
Sand.lm = lm(SandPrediction ~ Sand, data=Results)
Summary[3,4]<-summary(Sand.lm)$r.squared
pH.lm = lm(pHPrediction ~ pH, data=Results)
Summary[4,4]<-summary(pH.lm)$r.squared
Carbon.lm = lm(CarbonPrediction ~ Carbon, data=Results)
Summary[5,4]<-summary(Carbon.lm)$r.squared
Fe.lm = lm(FePrediction ~ Fe, data=Results)
Summary[6,4]<-summary(Fe.lm)$r.squared
K.lm = lm(KPrediction ~ K, data=Results)
Summary[7,4]<-summary(K.lm)$r.squared
Pacid.lm = lm(PacidPrediction ~ Pacid, data=Results)
Summary[8,4]<-summary(Pacid.lm)$r.squared
Polsen.lm = lm(PolsenPrediction ~ Polsen, data=Results)
Summary[9,4]<-summary(Polsen.lm)$r.squared
```

#Calculate and store RMSE and RPD

```
Summary[1,5]<-sqrt(mean(Results[,23]))#Clay RMSE
Summary[1,6]<-(sd(Clay)/Summary[1,5])#Clay RPD
Summary[2,5]<-sqrt(mean(Results[,24]))#Silt RMSE
Summary[2,6]<-(sd(Silt)/Summary[2,5])#Silt RPD]
Summary[3,5]<-sqrt(mean(Results[,25]))#Sand RMSE
Summary[3,6]<-(sd(Sand)/Summary[3,5])#Sand RPD
Summary[4,5]<-sqrt(mean(Results[,26]))#pH RMSE
Summary[4,6]<-(sd(pH)/Summary[4,5])#pH RPD
```

```
Summary[5,5]<-sqrt(mean(Results[,27]))#Carbon RMSE
Summary[5,6]<-(sd(Carbon)/Summary[5,5])#Carbon RPD
Summary[6,5]<-sqrt(mean(Results[,28]))#Fe RMSE
Summary[6,6]<-(sd(Fe)/Summary[6,5])#Fe RPD
Summary[7,5]<-sqrt(mean(Results[,29]))#K RMSE
Summary[7,6]<-(sd(K)/Summary[7,5])#K RPD
Summary[8,5]<-sqrt(mean(Results[,30]))#Pacid RMSE
Summary[8,6]<-(sd(Pacid)/Summary[8,5])#Pacid RPD
Summary[9,5]<-sqrt(mean(Results[,31]))#Polsen RMSE
Summary[9,6]<-(sd(Polsen)/Summary[9,5])#Polsen RPD
#Save Predictions as a txt datatable
write.table(Results, "/Users/EdCarnell/Desktop/ResultsLevel1.txt", row.names=F,col.names=T, sep = "\t")
#Save Summary statistics as a txt datatable
write.table(Summary, "/Users/EdCarnell/Desktop/SummaryLevel1.txt", row.names=F,col.names=T, sep = "\t")
```